THE
PHYSICAL REVIEW
A journal of experimental and theoretical physics established by E. L. Nichols in 1893

SECOND SERIES, VOL. 67, NOS. 7 AND 8 APRIL 1 AND 15, 1945

On the Meson Charge Cloud Around a Proton*

JOHN M. BLATT†
Cornell University, Ithaca, New York
(Received August 10, 1944)

The calculations of Fröhlich, Heitler, and Kahn for the deviation from the Coulomb law for a proton owing to mesons are re-examined and extended to the scalar meson theory. A perturbation calculation is used up to terms proportional to the square of the coupling constant, including the recoil of the nucleon to first order in μ/M. The recent Dirac theory involving negative energy states of the mesons, in conjunction with the λ-limiting process due to Wentzel, makes the theory convergent. The dissociation probability P of a proton in this theory is proportional to the square of the coupling constant and to the mass ratio μ/M. P is of the order of 2 percent. The meson charge cloud produces only a slight decrease of the Coulomb force acting on a charged test-particle, not a reversal of this force. No experimentally observable effects can be expected from the processes considered. The results of Fröhlich, Heitler, and Kahn are not reproduced by the convergent theory.

INTRODUCTION

IN this paper we are going to investigate the meson charge cloud which forms around a proton caused by the protons' interaction with a meson field. It is generally admitted that mesons must be assumed to have charge. This means physically that charge is transported in a meson beam, while no charge is transported in a (neutral) light beam. The charge of the mesons gives rise to interactions between them and electromagnetic fields. This leads, for instance, to the anomalous magnetic moments of the elementary heavy particles (neutron and proton). Not only do the heavy particles themselves interact with an external magnetic field (through their spin magnetic moment), but also the mesons which they create around themselves. The experiment gathers together the contributions from the heavy particles and from the meson field, while the usual theoretical value neglects the contribution of the mesons. This effect has been discussed by Fröhlich, Heitler, and Kemmer[1] and more recently by Jauch.[2]

In this paper we calculate another effect of the charge of the mesons. The meson field which forms around the proton contains charge, and this means an effective "smearing out" of part of the charge of the proton over a region within the range of nuclear forces. This *charge cloud around the proton* is likely to change the Coulomb force on a charged test particle brought near to the proton. It is also going to influence the scattering of charged particles on the proton. These effects might be experimentally detectable. The

* This paper contains the results of a thesis presented for the degree of Doctor of Philosophy to the faculty of the Graduate School of Cornell University, Ithaca, New York.

† Now at Princeton University.

[1] Fröhlich, Heitler, and Kemmer, Proc. Roy. Soc. **A166**, 154 (1938).

[2] J. M. Jauch, Phys. Rev. **63**, 334 (1943).

change in the Coulomb law at small distances from the proton would lead to a (slight) change in the energy levels of the s states of the hydrogen atom. The anomalous scattering would be most noticeable for very high energy incident particles which can approach the nucleus closely.

Fröhlich, Heitler, and Kahn[3] have tried to calculate this change in the energy levels of hydrogen, assuming a vector meson field. They arrive at a result for the correction, but the validity of their calculation has been questioned by Lamb[4] and a controversy ensued over it.[5] The difficulty in those calculations is caused by our insufficient knowledge of field quantization. All the standard theories lead to divergencies of terms of the self-energy type. The process by which the meson charge cloud around a proton is found leads to terms of this type. Only one nuclear particle is involved, and its interaction with the meson field created by itself is considered. This is in contradistinction to the nuclear force calculations in which the interaction of a nuclear particle with the meson field created by a different nuclear particle is found.

In our case the self-energy effect gives rise to an infinite total charge in the meson charge cloud. One of the requirements of a "reasonable" theory is that, on the average, most of the time the meson field contains no mesons at all. For a relatively short fraction of each second, the meson field should contain one or more mesons in eigenstates of the field. If the meson field contains just one (positive) meson, the proton is changed into a neutron during that time. This is necessary in order to insure conservation of charge. Let ϵ be the charge of the proton, and e the total charge in the meson field. Then we define a "dissociation probability" P by $e=P\epsilon$. The failure of the usual theory appears through the fact that P not only exceeds unity, but actually diverges.

It must be emphasized that the total charge present does not diverge. Formally, at least, the usual theories conserve the charge. The total charge present consists of the charge on the heavy particle plus the charge in the meson field. Thus it is $(1-P)\epsilon+P\epsilon=\epsilon$. The equality holds formally even when P diverges.

Let U be the potential energy of a test particle of charge ϵ in the meson field. It can be shown that $\nabla^2 U=-4\pi\epsilon\rho$ where ρ is the charge density in the meson field. This is an operator equation and thus must hold for the diagonal elements (the average values). It is seen that an infinite constant in U need not bring about a divergence of ρ; but a divergence of the total charge in the meson field will make the energy U infinite. This is physically plausible since a test particle needs infinite energy to approach an infinite charge, even when that infinite charge is spread out over a small region.

Fröhlich, Heitler, and Kahn get out of this difficulty by subtracting from their calculated term the part of the term which is indistinguishable from the effect of a charge concentrated at the center (as far as the interaction energy with a test particle is concerned). The difference turns out to be convergent. Their calculations are open to grave objections, however. Both the minuend and the subtrahend are infinite, and almost anything may be considered as the difference between two infinite terms. Also, they get a strong attraction of a positive test particle at very close distances from the nucleon. This is rather hard to accept, since we would be inclined to expect only a slight decrease of the Coulomb force because of the spreading out of the charge on the nucleon, not a complete reversal of that force.

Recently Dirac[6] has proposed a theory which involves negative energy eigenstates of the meson field. Pauli[7] has discussed this theory in great detail. It turns out that if the theory is coupled with a limiting process taken over from classical physics, all the divergencies can be eliminated. This limiting process, called the λ process, was first proposed by Wentzel.[8]

It was considered worth while to test this convergent theory by application to our particular problem. If the theory is correct, then we ought to obtain a convergent total charge in the meson field, and we should be able to calculate

[3] Fröhlich, Heitler, and Kahn, Proc. Roy. Soc. **A171**, 269 (1939).
[4] W. Lamb, Phys. Rev. **56**, 384 (1939).
[5] Fröhlich, Heitler, and Kahn, Phys. Rev. **56**, 961 (1939), W. Lamb, Phys. Rev. **57**, 458 (1940).
[6] Dirac, Proc. Roy. Soc. **A180**, 1 (1942).
[7] W. Pauli, Rev. Mod. Phys. **15**, 175 (1943).
[8] G. Wentzel, Zeits. f. Physik **86**, 479 and 635 (1933); **87**, 726 (1934).

the correction to the energy levels of the hydrogen atom without recourse to any arbitrary subtraction scheme. Furthermore, this procedure might give us some additional insight into the actual workings of the Dirac theory and of the λ process. That is, we should be able to tell just how particular terms in the charge density are affected by the introduction of those modifications, and just how the new theory manages to yield a convergent result. One difficulty must be pointed out, however. It has been shown by Pauli and Jauch[9] that the Dirac theory makes the short wave-length contributions convergent, but at the expense of changing the contributions of the long wave-lengths. Practically this means a conflict with the correspondence principle and is an extremely serious objection to the whole theory.

Hence our results cannot be expected to agree with experiment, except in a qualitative way. The main object of this paper is thus a further test of the convergent meson theory of Dirac and Pauli, rather than the calculation of experimentally verifiable results.

CHARGE DENSITY CALCULATION WITH THE USUAL SCALAR THEORY

We use the Pauli-Weisskopf[10] theory in which the meson field quantity ψ is a scalar. This theory has been discussed carefully in a review paper by Pauli.[11] The main change in notation is the difference in the Fourier decomposition of the field. We set

$$\psi(\mathfrak{x})=\frac{1}{\sqrt{2}(2\pi)^{\frac{3}{2}}}\int d^3k\left(\frac{1}{k_0}\right)\times(a_k\exp(i\mathfrak{k}\cdot\mathfrak{x})-b_k^*\exp(-i\mathfrak{k}\cdot\mathfrak{x})). \quad (2.1)$$

The notation is,

$\mathfrak{x}\equiv(\mathbf{x}, ix_0)=(\mathbf{x}, ict)$, 4-position of field point,

$d^3k=dk_1dk_2dk_3$, volume element in k-space,

$k_0=+(k^2+\mu^2)^{\frac{1}{2}}$,

$\mu=\mu c/\hbar$, Compton wave number for a particle (meson) of mass μ (about 200 electron masses),

$\mathfrak{k}\cdot\mathfrak{x}=\mathbf{k}\cdot\mathbf{x}-k_0x_0$, 4-vector dot-product.

[9] W. Pauli and J. M. Jauch, Phys. Rev. **65**, 255 (1944).
[10] W. Pauli and V. Weisskopf, Helv. Phys. Acta **7**, 709 (1934).
[11] W. Pauli, Rev. Mod. Phys. **13**, 203 (1941).

The operators a_k and b_k are, in Pauli's notation,

$$a_k=(k_0)^{\frac{1}{2}}U_+(k), \quad b_k=(k_0)^{\frac{1}{2}}U_-(k). \quad (2.2)$$

This change is helpful later on in the Dirac theory, since it throws all imaginary factors into the operators; with Pauli's original notation we would encounter factors of the type $1/(k_0)^{\frac{1}{2}}$ but also of the type $1/(-k_0)^{\frac{1}{2}}$. We wrote the Fourier decomposition as an integral rather than a sum since this is the form in which it will be used. The units are the same as in Pauli's paper (i.e., c and $\hbar$ are set equal to unity).

The wave function Ψ of the nucleon is assumed to be made up of plane-wave eigenfunctions of the Dirac Hamiltonian

$$\bar{H}_n=\boldsymbol{\alpha}\cdot\mathbf{p}+M\beta=-i\boldsymbol{\alpha}\cdot\nabla_y+M\beta. \quad (2.3)$$

Here $\boldsymbol{\alpha}, \beta$ are the well-known Dirac matrices, and M is the mass of the nucleon. $\mathfrak{y}=(\mathbf{y}, iy_0)$ is the space-time position of the nucleon.

The Schrödinger equation is

$$(\bar{H}_0+\bar{H}_n+\bar{H}_i)\Omega=id\Omega/dx_0. \quad (2.4)$$

Here

$$\bar{H}_0=\int d^3k(a_k^*a_k+b_k^*b_k)=$$

Hamiltonian of free meson field, (2.5)

$\bar{H}_n=$ Hamiltonian of the free nucleon,

$$\bar{H}_i=g(4\pi)^{\frac{1}{2}}(\tau_-\psi^*(\mathfrak{y})+\tau_+\psi(\mathfrak{y}))\cdot\beta$$

$=$ Interaction Hamiltonian,[12] (2.6)

$\Omega=$ Schrödinger functional giving the state of the meson field and of the nucleon.

In the interaction Hamiltonian, g is a dimensionless coupling constant (of order of magnitude $\frac{1}{2}$). τ_+ and τ_- are charge creation and destruction operators, respectively. Let u_P denote the eigenfunction of a proton, u_N that of a neutron, then

$$\tau_+u_P=0, \quad \tau_-u_P=u_N, \quad \tau_+u_N=u_P, \quad \tau_-u_N=0. \quad (2.7)$$

Notice that the meson field quantity ψ in $\bar{H}_i$ has to be taken at the position $\mathfrak{y}$ of the heavy particle, giving a point interaction. The time coordinate is common for the nucleon and the meson field, i.e., $x_0=y_0$.

[12] N. Kemmer, Proc. Roy. Soc. **A166**, 143 (1938).

In order to solve (2.3) by a perturbation method we expand the Schrödinger functional Ω in powers of the coupling constant g:

$$\Omega=\Omega_0+\Omega_1+\Omega_2+\cdots. \tag{2.8}$$

Equating terms of the same power in g, we get

$$(\bar{H}_0+\bar{H}_n)\Omega_0 = id\Omega_0/dx_0, \tag{2.9}$$

$$(\bar{H}_0+\bar{H}_n)\Omega_1+\bar{H}_i\Omega_0=id\Omega_1/dx_0, \tag{2.10}$$

$$(\bar{H}_0+\bar{H}_n)\Omega_2+\bar{H}_i\Omega_1=id\Omega_2/dx_0, \tag{2.11}$$

etc.

For the zero-order functional in this perturbation problem we take

$$\Omega_0=\Psi_0\omega(0)u_P. \tag{2.12}$$

Here Ψ_0 is a function of $\mathfrak{y}$ and the spin-coordinate of the nucleon. We shall specialize to a proton initially at rest, i.e.,

$$\Psi_0=\begin{pmatrix}u_\pm\\0\end{pmatrix}\exp(-iMy_0) \tag{2.13}$$

where $u_+=\begin{pmatrix}1\\0\end{pmatrix}$ and $u_-=\begin{pmatrix}0\\1\end{pmatrix}$. Thus (2.13) is

$$\begin{pmatrix}1\\0\\0\\0\end{pmatrix}\exp(-iMy_0) \quad\text{or}\quad \begin{pmatrix}0\\1\\0\\0\end{pmatrix}\exp(-iMy_0)$$

according as to whether the spin of the nucleon is assumed to be in the positive or negative z direction.

$\omega(0)$ is the meson field functional corresponding to no mesons present. Generally we shall denote by $\omega(N_k^+, N_k^-)$ a simultaneous eigenfunction of the operators $a_k^*a_k=k_0N_k^+$ and $b_k^*b_k=k_0N_k^-$. From (2.2) and Pauli's paper[13] we see that

$$a_k^*\omega(N_k^+)=(k_0)^{\frac{1}{2}}(N_k^++1)^{\frac{1}{2}}\omega(N_k^++1),$$

$$a_k\omega(N_k^+)=(k_0)^{\frac{1}{2}}(N_k^+)^{\frac{1}{2}}\omega(N_k^+-1), \tag{2.14}$$

b_k same as a_k but for negative mesons.

We now proceed to find Ω_1 in (2.8). From (2.10) we see that we need only consider functionals for which the matrix elements of $\bar{H}_i$: $\Omega_1^*\bar{H}_i\Omega_0$ do not vanish. The only functionals satisfying this condition are of the type $\Psi_1(\mathfrak{y})\omega(1_k^+)u_N$. Physically, they denote the existence of one positive meson in a momentum eigenstate of the meson field, plus a neutron in a momentum eigenstate of the Dirac Hamiltonian. Thus

$$\Omega_1=\int d^3k\Psi_1(\mathfrak{y}, k)\omega(1_k^+)u_N. \tag{2.15}$$

Substitute in (2.10) and pre-multiply by $\omega^*(1_k^+)u_N^*$ to get

$$\bar{H}_n\Psi_1+\omega^*(1_k^+)u_N^*\bar{H}_i\omega(0)u_P=id\Psi_1/dx_0. \tag{2.16}$$

Here we have used the fact that

$$\bar{H}_0\omega(1_k^+)=id\omega(1_k^+)/dx_0;$$

i.e., $\omega(1_k^+)$, being an eigenstate of $a_k^*a_k$ and of $b_k^*b_k$, is also an eigenstate of the free meson field Hamiltonian $\bar{H}_0$; it is then taken to be a solution of the unperturbed Schrödinger equation for the meson field. This just fixes the time dependence of the meson field functional (we are using the Schrödinger representation here in which the operators are constants or else explicit functions of the time, while the wave functions have a time dependence given by Schrödinger's equation).

We put (2.16) in the form

$$(id/dx_0-\bar{H}_n)\Psi_1=(1_k^+, N|\bar{H}_i|0, P),$$

(the notation for the matrix element of $\bar{H}_i$ is obvious). Pre-multiplying by $(id/dx_0+\bar{H}_n)$ and using the commutation rules for the Dirac matrices, this becomes

$$-(d^2/dx_0^2+p^2+M^2)\Psi_1 = (id/dx_0+\bar{H}_n)\cdot(1_k^+, N|\bar{H}_i|0, P). \tag{2.17}$$

Using (2.17) and (2.13) together with (2.3), (2.6), and (2.1), we obtain

$$\Psi_1=f\frac{\exp(-i\mathbf{l}\cdot\mathfrak{y}-iMy_0)}{(k_0)^{\frac{1}{2}}(\mu^2-2Mk_0)}\begin{pmatrix}(2M-k_0)u_\pm\\-\mathbf{k}\cdot\boldsymbol{\sigma}u_\pm\end{pmatrix}. \tag{2.18}$$

Here $f=g/(2\pi)$ and $\boldsymbol{\sigma}$ is the well-known Pauli spin vector:

$$\sigma_1=\begin{pmatrix}0&1\\1&0\end{pmatrix},\quad \sigma_2=\begin{pmatrix}0&-i\\i&0\end{pmatrix},\quad \sigma_3=\begin{pmatrix}1&0\\0&-1\end{pmatrix}.$$

[13] Reference 11, page 210, Eq. (19).

The procedure just outlined involves the following approximation: (2.14) is correct only if we have an unperturbed meson field. In general we have,

$$\frac{da_k^*}{dx_0}=i[\bar{H}_i, a_k^*].$$

The approximation consists in neglecting this explicit time variation of a_k^* compared to the time variation of the term $\exp(-i\mathfrak{k}\cdot\mathfrak{y})$ in the matrix element $(1_k^+, N|\bar{H}_i|0, P)$. This means neglecting a second-order term in Ω_0 and a third-order term in Ω_1.

We finally obtain,

$$\Omega_0=\begin{pmatrix}u_\pm\\0\end{pmatrix}\exp(-iMy_0)\omega(0)u_P, \tag{2.19}$$

$$\Omega_1=f\int\frac{d^3k\exp(-i\mathfrak{k}\cdot\mathfrak{y}-iMy_0)}{(k_0)^{\frac{1}{2}}(\mu^2-2Mk_0)}\begin{pmatrix}(2M-k_0)u_\pm\\-\mathbf{k}\cdot\boldsymbol{\sigma}u_\pm\end{pmatrix}\omega(1_k^+)u_N, \tag{2.20}$$

$$\Omega_2=f^2\int\frac{d^3k\,d^3l\exp[-i(\mathfrak{k}+\mathfrak{l})\cdot\mathfrak{y}-iMy_0]\omega(1_l^+, 1_k^-)u_P}{2(k_0l_0)^{\frac{1}{2}}(\mu^2-2Ml_0)[\mu^2-M(k_0+l_0)+k_0l_0-\mathbf{k}\cdot\mathbf{l}]}$$
$$\cdot\begin{pmatrix}[(2M-k_0-l_0)(2M-l_0)+(\mathbf{k}+\mathbf{l})\cdot\mathbf{l}+i\mathbf{l}\times\mathbf{k}\cdot\boldsymbol{\sigma}]u_\pm\\[(2M-l_0)(\mathbf{k}+\mathbf{l})\cdot\boldsymbol{\sigma}-(k_0+l_0)\mathbf{l}\cdot\boldsymbol{\sigma}]u_\pm\end{pmatrix}. \tag{2.21}$$

An infinite resonance term was omitted from Ω_2. It turns out that this term may be made convergent by the λ process and can then be combined with the Hamiltonian of the heavy particle $\bar{H}_n$, giving only a slight change in its effective mass.

It may be worth while to put down the expressions for Ω_0, Ω_1, Ω_2 in the limit as $M\to\infty$. Let $u_P'=u_p\exp(-iMy_0)u_\pm$. Then these expressions are

$$\Omega'_0=\omega(0)u'_P, \tag{2.19'}$$

$$\Omega'_1=-f\int d^3k(k_0)^{-\frac{1}{2}}\exp(-i\mathfrak{k}\cdot\mathfrak{y})\omega(1_k^+)u'_N, \tag{2.20'}$$

$$\Omega'_2=f^2\int\frac{d^3k\,d^3l}{k_0^{\frac{1}{2}}l_0^{\frac{1}{2}}(k_0+l_0)}\exp(-i(\mathfrak{k}+\mathfrak{l})\cdot\mathfrak{y})\omega(1_l^+, 1_k^-)u'_P. \tag{2.21'}$$

We now proceed to calculate the diagonal element of the charge density operator ρ. To the second order in f, we have

$$\bar{\rho}=\Omega^*\rho\Omega=\Omega_0^*\rho\Omega_0+2\Omega_1^*\rho\Omega_0+2\Omega_2^*\rho\Omega_0+\Omega_1^*\rho\Omega_1, \tag{2.22}$$

where we have used the fact that the charge density operator is Hermitean. In the scalar theory it is given by

$$\rho=i\epsilon(\pi^*\psi^*-\pi\psi)=\frac{\epsilon}{2(2\pi)^3}\int\int d^3k\,d^3l\left\{\left(\frac{1}{k_0}+\frac{1}{l_0}\right)(a_k^*a_l-b_k^*b_l)\exp(-i(\mathfrak{k}-\mathfrak{l})\cdot\mathfrak{x})\right.$$
$$\left.+\left(\frac{1}{l_0}-\frac{1}{k_0}\right)(a_kb_l\exp(i(\mathfrak{k}+\mathfrak{l})\cdot\mathfrak{x})-a_l^*b_k^*\exp(-i(\mathfrak{k}+\mathfrak{l})\cdot\mathfrak{x}))\right\}. \tag{2.23}$$

It is seen that the first two terms of (2.22) vanish, and we obtain, after averaging over the two possible spin directions of the nucleon

$$\Omega_1^*\rho\Omega_1=\frac{\epsilon f^2}{2(2\pi)^3}\int\int d^3k\,d^3l\left(\frac{1}{k_0}+\frac{1}{l_0}\right)\exp[i(\mathbf{l}-\mathbf{k})\cdot(\mathbf{x}-\mathbf{y})]\frac{(2M-k_0)(2M-l_0)+\mathbf{k}\cdot\mathbf{l}}{(2Mk_0-\mu^2)(2Ml_0-\mu^2)}, \tag{2.24}$$

$$\Omega_2^*\rho\Omega_0=\frac{\epsilon f^2}{4(2\pi)^3}\int\int d^3k\,d^3l\left(\frac{1}{k_0}-\frac{1}{l_0}\right)\exp\left[-i(\mathbf{k}+\mathbf{l})\cdot(\mathbf{x}-\mathbf{y})\right]$$
$$\times\frac{(2M-k_0-l_0)(2M-l_0)+(\mathbf{k}+\mathbf{l})\cdot\mathbf{l}}{(2Ml_0-\mu^2)[M(k_0+l_0)+\mathbf{k}\cdot\mathbf{l}-k_0l_0-\mu^2]}. \quad (2.25)$$

We transform (2.25) by interchanging k and l and taking half the sum of the two integrals thus obtained. After this symmetrizing operation we drop all terms for which the final integral will contain μ/M to a power higher than the first. This is easily accomplished since M is not contained in k_0 and l_0; so it goes outside the various integrals immediately. We get, after some reduction,

$$\Omega_2^*\rho\Omega_0\doteq\frac{\epsilon f^2}{4(2\pi)^3}\int\int d^3k\,d^3l\left(\frac{1}{k_0}-\frac{1}{l_0}\right)(k_0-l_0)\exp\left[-i(\mathbf{k}+\mathbf{l})\cdot(\mathbf{x}-\mathbf{y})\right]$$
$$\cdot\frac{1-\frac{1}{2M}(k_0+l_0)-\frac{\mathbf{k}\cdot\mathbf{l}-k_0l_0-\mu^2}{M(k_0+l_0)}}{(k_0-\mu^2/2M)(l_0-\mu^2/2M)(k_0+l_0)}.$$

Using the fact that

$$\left(\frac{1}{k_0}-\frac{1}{l_0}\right)(k_0-l_0)=-\left(\frac{1}{k_0}+\frac{1}{l_0}\right)(k_0+l_0)+4$$

we can put the integral above into a form in which it can be compared with (2.24). It must be remembered that we have to take twice (2.25) and add it to (2.24). In going through the steps it will be seen that part of the integral just written down cancels (2.24) to terms of first order in μ/M. Expanding

$$(k_0-\mu^2/2M)^{-1}=\frac{1}{k_0}\left(1-\frac{\mu^2}{2Mk_0}+\cdots\right),$$

we finally obtain

$$\bar\rho=\frac{2\epsilon f^2}{(2\pi)^3}\int\int\frac{d^3k\,d^3l}{k_0l_0(k_0+l_0)}\cdot\exp\left[-i(\mathbf{k}+\mathbf{l})\cdot(\mathbf{x}-\mathbf{y})\right]$$
$$-\frac{\epsilon f^2}{(2\pi)^3}\left(\frac{1}{M}\right)\int\int\frac{d^3k\,d^3l}{k_0l_0}\left(\frac{\mu^2}{k_0l_0}+1\right)\exp\left[-i(\mathbf{k}+\mathbf{l})\cdot(\mathbf{x}-\mathbf{y})\right]$$
$$+\frac{\epsilon f^2}{2(2\pi)^3}\left(\frac{1}{M}\right)\int\int\frac{d^3k\,d^3l}{(k_0l_0)^2}\left(\frac{k_0-l_0}{k_0+l_0}\right)^2(\mathbf{k}\cdot\mathbf{l}-k_0l_0-\mu^2)\exp\left[-i(\mathbf{k}+\mathbf{l})\cdot(\mathbf{x}-\mathbf{y})\right]. \quad (2.26)$$

In the limit $M\to\infty$ this becomes

$$\bar\rho'=\frac{2\epsilon f^2}{(2\pi)^3}\int\int\frac{d^3k\,d^3l}{k_0l_0(k_0+l_0)}\exp\left[-i(\mathbf{k}+\mathbf{l})\cdot(\mathbf{x}-\mathbf{y})\right]. \quad (2.26')$$

To simplify this, we put

$$\frac{1}{k_0+l_0}=\int_0^\infty\exp\left[-(k_0+l_0)q\right]dq;\quad \mathbf{z}=\mathbf{x}-\mathbf{y};\quad r=|\mathbf{z}|,$$

and interchange orders of integration. We then obtain (cf. table of integrals at the end of the paper),

$$\bar\rho'=\frac{\epsilon g^2\mu^2}{4\pi}\int_0^\infty\frac{[H_1^{(1)}[i\mu(r^2+q^2)^{\frac{1}{2}}]]^2}{(r^2+q^2)}dq=\frac{\epsilon g^2\mu^2}{4\pi r}\int_0^{\pi/2}[H_1^{(1)}(i\mu r\sec\theta)]^2d\theta. \quad (2.27)$$

The limiting values of this expression for large and small distances from the nucleon are

$$\mu r \gg 1, \quad \bar{\rho}' \doteq \frac{\epsilon g^2 \mu^3}{4\pi^{3/2}} \frac{e^{-2\mu r}}{(\mu r)^{5/2}}, \tag{2.28}$$

$$\mu r \ll 1, \quad \bar{\rho}' \doteq \frac{\epsilon g^2 \mu^3}{4\pi^2} \frac{1}{(\mu r)^3}. \tag{2.29}$$

The total charge in the meson field $\bar{e} = \int \bar{\rho} d^3x$ thus diverges logarithmically on the standard scalar theory, in zero order in μ/M. The recoil correction terms [last two integrals in (2.26)] have not been evaluated explicitly. The second term of (2.26) gives a negatively infinite total charge, but it is easy to see that this doesn't help if one only goes back to (2.24) and (2.25). We integrate over x space and interchange orders of integration. Remembering that

$$\frac{1}{(2\pi)^3} \int \exp(i\mathbf{k}\cdot\mathbf{x}) d^3x = \delta(\mathbf{k})$$

we see that (2.25) gives zero total charge and (2.24) gives

$$\bar{e} = \epsilon f^2 \int \frac{d^3k}{k_0} \frac{(2M-k_0)^2+k^2}{(2Mk_0-\mu^2)^2}. \tag{2.30}$$

This is a positive definite form and diverges for large values of k like

$$\frac{\epsilon f^2}{2M^2} \int \frac{d^3k}{k_0}. \tag{2.31}$$

This might seem to indicate zero total charge as $M \to \infty$. In that case, however, we have to use (2.26′) and obtain a divergence of the charge in the meson field of the form

$$\epsilon f^2 \int d^3k/(k_0)^3. \tag{2.31′}$$

CHARGE DENSITY CALCULATION WITH DIRAC'S NEW METHOD OF FIELD QUANTIZATION (SCALAR THEORY)

This method, proposed by Dirac[6] in 1942, has been extensively treated by Pauli.[7] We shall use the same notation as Pauli, except for the change in Fourier decomposition corresponding to (2.1). Dirac introduces two fields ψ and ϕ. Only ψ interacts with the heavy particles, ϕ is the redundant field. The fields are decomposed into contributions of positive and negative (charge) mesons through

$$\psi = (2)^{-\frac{1}{2}}(U_p + U_n^*), \quad \phi = (2)^{-\frac{1}{2}}(U_p - U_n^*) \tag{3.1}$$

and the Fourier decompositions of U_p and U_n are

$$\begin{aligned} U_p &= (2)^{-\frac{1}{2}}(2\pi)^{-\frac{1}{2}} \int d^3k (k_0)^{-1}(a_k \exp(i\mathbf{k}\cdot\mathbf{x}) + c_k \exp(-i\mathbf{k}\cdot\mathbf{x})), \\ U_n &= (2)^{-\frac{1}{2}}(2\pi)^{-\frac{1}{2}} \int d^3k (k_0)^{-1}(b_k \exp(i\mathbf{k}\cdot\mathbf{x}) + d_k \exp(-i\mathbf{k}\cdot\mathbf{x})). \end{aligned} \tag{3.2}$$

To connect with Pauli's notation, we remark that

$$a_k = (k_0)^{\frac{1}{2}} U_{p+}(k), \quad b_k = (k_0)^{\frac{1}{2}} U_{n+}(k), \quad c_k = (k_0)^{\frac{1}{2}} U_{p-}(k), \quad d_k = (k_0)^{\frac{1}{2}} U_{n-}(k). \tag{3.3}$$

Notice that U_p and U_n contain contributions from mesons of both positive and negative energies. Dirac's proposal is to quantize the fields containing $\exp(i\mathfrak{k}\cdot\mathfrak{x})$ in the usual way, those containing $\exp(-i\mathfrak{k}\cdot\mathfrak{x})$ in the improved manner. The improved manner consists in an indefinite metric in Hilbert space, which gives rise to negative energies for those eigenstates of the meson field. The commutation relations are

$$[a_k, a_l^*]=[b_k, b_l^*]=k_0\delta(\mathbf{k}-\mathbf{l}), \quad [c_k, c_l^*]=[d_k, d_l^*]=-k_0\delta(\mathbf{k}-\mathbf{l}). \tag{3.4}$$

These rules allow us to interpret the operators

$$N_k^+=(k_0)^{-1}a_k^*a_k; \quad N_k^-=(k_0)^{-1}b_k^*b_k; \quad \tilde{N}_k^+=-(k_0)^{-1}c_k^*c_k; \quad \tilde{N}_k^-=-(k_0)^{-1}d_k^*d_k \tag{3.5}$$

as the densities in k space of numbers of mesons of (+charge, +energy), (−charge, +energy), (+charge, −energy), (−charge, −energy), respectively. The tilde over the N denotes negative energy states.

We denote by $\omega(N_k^+N_k^-\tilde{N}_k^+\tilde{N}_k^-)$ a simultaneous eigenfunctional of the operators (3.5) which is also a solution of the unperturbed Schrödinger equation

$$\bar{H}_0\omega=id\omega/dx_0 \tag{3.6}$$

where $\bar{H}_0$, the free meson field Hamiltonian, is given by

$$\bar{H}_0=\int d^3k(a_k^*a_k+b_k^*b_k+c_k^*c_k+d_k^*d_k)=\int d^3k\ k_0(N_k^++N_k^--\tilde{N}_k^+-\tilde{N}_k^-). \tag{3.7}$$

We then obtain the rules (2.14) for a_k and b_k, while

$$\begin{aligned} c_k^*\omega(\tilde{N}_k^+)&=i(k_0)^{\frac{1}{2}}(\tilde{N}_k^++1)^{\frac{1}{2}}\omega(\tilde{N}_k^++1),\\ c_k\omega(\tilde{N}_k^+)&=i(k_0)^{\frac{1}{2}}(\tilde{N}_k^+)^{\frac{1}{2}}\omega(\tilde{N}_k^+-1), \end{aligned} \tag{3.8}$$

d_k same as c_k except for negatively charged mesons.

The indefinite metric in Hilbert space shows up through the fact that c_k^* does not have a $-i$ where c_k has an i, but has a $+i$ also. Another effect of the indefinite metric manifests itself in the Hermitean conjugate of the functional $\omega(\tilde{N}_k^+)$: $\omega^*(\tilde{N}_k^+)=-[\omega(\tilde{N}_k^+)]^*$. This gives the property that an operator with only positive eigenvalues has negative expectation values in the states of negative energy.

We now proceed to calculate the charge density just as in the previous section. The Schrödinger equation which we intend to solve by the perturbation method is (2.4). The only change there is the substitution of (3.7) for (2.5). Notice that the interaction Hamiltonian (2.6) is *not* changed. Only the ψ field interacts with the nucleon, the ϕ field does not. The expansion in powers of the coupling constant g, (2.8), is kept; and we again obtain Eqs. (2.9), (2.10), (2.11). It will not be necessary this time to calculate Ω_2. The zero-order functional is given by (2.12) and (2.13), just as before. But in expanding the interaction Hamiltonian into Fourier components according to (3.1) and (3.2) it will be noticed that there are non-vanishing matrix elements not only for transitions to states with one positive charge, positive energy meson plus a neutron, but also for transitions to states with one positive charge, negative energy meson plus a neutron. We thus have to write, instead of (2.15)

$$\Omega_1=\int d^3k[\Psi_1(\mathfrak{y}, k)\omega(1_k^+)+\tilde{\Psi}_1(\mathfrak{y}, k)\omega(\tilde{1}_k^+)]u_N. \tag{3.9}$$

An entirely similar argument to the one used in the previous section leads to the result

$$\Omega_1=(2)^{-\frac{1}{2}}f\int\frac{d^3k}{(k_0)^{\frac{1}{2}}}\exp(-iMy_0)u_N\left[\frac{\exp(-i\mathfrak{k}\cdot\mathfrak{y})\omega(1_k^+)}{(\mu^2-2Mk_0)}\cdot\begin{pmatrix}(2M-k_0)u_\pm\\-\mathbf{k}\cdot\sigma u_\pm\end{pmatrix}\right.$$

$$\left.+i\frac{\exp(i\mathfrak{k}\cdot\mathfrak{y})\omega(\tilde{1}_k^+)}{(\mu^2+2Mk_0)}\cdot\begin{pmatrix}(2M+k_0)u_\pm\\\mathbf{k}\cdot\sigma u_\pm\end{pmatrix}\right]. \quad (3.10)$$

The charge density operator in the Dirac theory is given by

$$\rho=\rho^+-\rho^-,$$

$$\rho^+=\frac{\epsilon}{2(2\pi)^3}\int\int d^3k\,d^3l\left[\left(\frac{1}{k_0}+\frac{1}{l_0}\right)(a_k^*a_l\exp[-i(\mathfrak{k}-\mathfrak{l})\cdot\mathfrak{x}]-c_k^*c_l\exp[i(\mathfrak{k}-\mathfrak{l})\cdot\mathfrak{x}])\right.$$

$$\left.+\left(\frac{1}{l_0}-\frac{1}{k_0}\right)(a_k^*c_l\exp[-i(\mathfrak{k}+\mathfrak{l})\cdot\mathfrak{x}]-c_k^*a_l\exp[i(\mathfrak{k}+\mathfrak{l})\cdot\mathfrak{x}])\right] \quad (3.11),$$

ρ^- same as ρ^+ but with a and c replaced by b and d.

Notice that there are no pair creation or destruction terms in this operator. The "Zitterbewegung" terms correspond to transitions from positive to negative energies and vice versa. This simplifies the calculations considerably, since $\rho\omega(0)=0$ and therefore all terms of type $\Omega_n^*\rho\Omega_0$ vanish identically. This is the reason why we did not have to calculate Ω_2. We get

$$\bar{\rho}=\Omega_1^*\rho^+\Omega_1=\frac{\epsilon f^2}{4(2\pi)^3}\int\int d^3k\,d^3l\left(\frac{1}{k_0}+\frac{1}{l_0}\right)\frac{[(2M-k_0)(2M-l_0)+\mathbf{k}\cdot\mathbf{l}]\exp[-i(\mathbf{k}-\mathbf{l})\cdot(\mathbf{x}-\mathbf{y})]}{(\mu^2-2Mk_0)(\mu^2-2Ml_0)}$$

$$+(\mathfrak{k},\mathfrak{l}\to-\mathfrak{k},\mathfrak{l})+(\mathfrak{k},\mathfrak{l}\to\mathfrak{k},-\mathfrak{l})+(\mathfrak{k},\mathfrak{l}\to-\mathfrak{k},-\mathfrak{l}). \quad (3.12)$$

The integral splits into simple products of single integrals, which can be calculated to the first order in μ/M without any difficulty. We then get (see table of integrals)

$$\bar{\rho}=\frac{\epsilon g^2}{8\pi}\left(\frac{\mu}{M}\right)^\mu\frac{e^{-2\mu r}}{r^2}-\frac{\epsilon g^2}{2M}\frac{e^{-\mu r}}{r}\delta(r).$$

The δ-function gives a singularity at the origin. Expanding the exponential in powers of r and noting that $r^n\delta(r)=0$ for $n\geqslant 1$, we get

$$\bar{\rho}=\frac{\epsilon g^2}{8\pi}\left(\frac{\mu}{M}\right)^\mu\frac{e^{-2\mu r}}{r^2}+\frac{\epsilon g^2}{2}\frac{\mu}{M}\delta(r)-\frac{\epsilon g^2}{2M}\frac{\delta(r)}{r}. \quad (3.13)$$

The last part of this expression is not acceptable since it makes the total charge negatively infinite. It must be remembered that as yet we have not used the λ-limiting process. This will be done in the next section. So far, we can say, however, that the negative energy mesons alone do not suffice to make the theory convergent. This point is well known, of course, and (3.13) just provides an additional confirmation. Another thing worth noting is that the charge density (and therefore also the total charge) in the meson field is exactly zero in the limit as the mass M of the nucleon approaches infinity. That is, we get a change from the Coulomb law only if we consider the recoil of the nucleon upon emitting a meson.

CALCULATION OF THE TOTAL CHARGE IN THE MESON FIELD USING THE CONVERGENT (SCALAR) THEORY

In order to make the theory convergent, we still need the λ-limiting process. This is of an essentially classical nature and designed to overcome the difficulties which arise from the classical treatment of a point charge. It was first introduced by Wentzel and its application to quantum electrodynamics was simplified by Dirac.[14] Its physical basis is the following. We introduce a term into the interaction which is approximately unity at large space-time distances from the nucleon. This term becomes rapidly oscillating upon close approach to the heavy particle. In momentum space, the term becomes rapidly oscillating for large values of the wave number k. It is actually of the type $\cos(k_0\lambda_0)$ with λ_0 a real constant of the dimension of a length. To make the limiting process work, the position in space-time of the nucleon has to be approached from points within the light cone; this makes λ_0 essentially a time interval, but in our choice of units this is still a length dimensionally. λ_0 indicates in a rough manner the extent of the region around the nucleon about which we have little information.

We expect the oscillating term to cancel effectively the contribution of mesons of very high energies (small wave-lengths) to the interaction. It is from those mesons that the divergencies arise. We then go to the limit as λ_0 approaches 0. It would thus seem reasonable to expect to cancel the contribution of terms at the origin (i.e., δ-function terms) to the charge density.

The limiting process used here is regular. This means that any integral which already converges without its help is evaluated to its proper value. There is thus no point in recalculating the charge density. We do not expect a change in the first term of (3.13). Integrating over all x space gives $\frac{1}{4}\epsilon g^2\mu/M$ for the contribution of this term to the total charge in the meson field. If the λ process really cuts out the contributions of the terms at the origin to the charge density, then this is the value we would expect for the total charge in the meson field on the convergent theory.

[14] P. A. M. Dirac, Ann. de l'Inst. Poincaré 9, 13 (1939).

We now proceed to calculate this total charge directly. Since the λ process has been treated in detail by Pauli,[7] we shall only quote the necessary formulae here. The calculation of the wave functional by the perturbation method is the same as before. The only change is in the interaction Hamiltonian $\bar{H}_i$. After expanding it into Fourier components we replace a_k, a_k^*, etc. by $a_kL_k^-$, $a_k^*L_k^+$, etc., where

$$\begin{aligned} L_k^- &= \cos(\tfrac{1}{2}k_0\lambda_0)+\sin(\tfrac{1}{2}k_0\lambda_0), \\ L_k^+ &= \cos(\tfrac{1}{2}k_0\lambda_0)-\sin(\tfrac{1}{2}k_0\lambda_0). \end{aligned} \tag{4.1}$$

It must be emphasized that this change occurs only in the interaction term. The quantities which refer to the meson field alone remain unchanged. The same argument as in the previous section leads to an expression for Ω_1 which is identical with (3.10) except for a factor L_k^+ under the integral sign.

In calculating the total charge it is important to realize that Ω_1^* is not the ordinary Hermitean conjugate of Ω_1. First: $[\omega(\tilde{1}_k^+)]^*=-\omega^*(\tilde{1}_k^+)$. This comes from the indefinite metric in Hilbert space. Secondly: $(L_k^+)^*=L_k^-$. This is the generalization of the notion of Hermitean conjugate introduced by the λ process.

The total charge operator is

$$e=\epsilon\int d^3k(k_0)^{-1}(a_k^*a_k-b_k^*b_k-c_k^*c_k+d_k^*d_k). \tag{4.2}$$

Using this operator and simplifying we get for the expectation value of e

$$\bar{e}=-2\pi(M)^{-3}(2M^2-\mu^2)\epsilon f^2 \times\int_0^\infty \frac{k^4\cos(k_0\lambda_0)dk}{(k_0^2-\mu^4/(4M^2))^2}. \tag{4.3}$$

This is a well-known integral. We can split it into two parts as follows:

$$\int_0^\infty \cos(k_0\lambda_0)dk - \int_0^\infty \frac{(k_0^2-\mu^4/(4M^2))^2-k^4}{(k_0^2-\mu^4/(4M^2))^2}\cos(k_0\lambda_0)dk.$$

The first integral has been evaluated by Jauch[2] and gives zero in the limit as λ_0 approaches zero. The second integral converges even without the

limiting process, and since the process is regular we can evaluate it directly, leaving out the factor $\cos(k_0\lambda_0)$. The value of this integral is $\frac{3}{4}\pi\mu(1-(\mu/2M)^2)^{\frac{1}{2}}$. Calculating the total charge in the meson field to the first order in μ/M we get

$$\bar{e}=\tfrac{3}{4}\epsilon g^2\mu/M. \tag{4.4}$$

This is more than we expected from the first term of (3.13) only. It is easily seen that the other part comes from the second term of (3.13). Thus the limiting process did *not* cut out all the contributions from the origin, but only the divergent contribution [the third term of (3.13)].

It may be worth while to remark that it would not have been correct to keep terms of higher order in μ/M in (4.4). We used the ordinary Dirac Hamiltonian for the nucleon together with standard first quantization procedure. Thus we neglected pair creation terms in the nucleons (in the sense of Dirac's theory of holes). These terms first appear in the third order in μ/M, and that would be the order of the next term in (4.4).

DISCUSSION OF THE POSSIBILITY OF EXPERIMENTAL VERIFICATION

In the introduction we have mentioned two effects of the meson charge cloud around the proton which might provide experimental checks for the theory. One is the change in the energy levels of the s states of the hydrogen atom, with a resultant change in the fine structure of the hydrogen lines. There have been reports[15] of slight deviations from the theoretical fine structure calculated from Sommerfeld's formula; and it was mainly to see whether those deviations could be explained by the meson charge cloud around the proton that Fröhlich, Heitler, and and Kahn[3] undertook their investigation. They point out that a complete reversal of the Coulomb force at close distances from the nucleon is needed to account for the experimental data. If we take (3.13) without the last term, which is taken out by the λ process, we see that there is only a spreading out of the charge of the proton within the range of the nuclear forces $(1/\mu)$, but not a change of sign of the charge anywhere in space.

Furthermore, the effect is much too small to be observed experimentally. The influence of a potential step upon the energy levels of the s states of the H atom has been calculated by Jauch.[16] If we use the equation $\nabla^2U=-4\pi\epsilon\rho$, where U is the potential energy of a test particle of charge ϵ, we can obtain U by simple integrations from (3.13). We then get

$$U(r)=\frac{\epsilon^2}{r}-\frac{\epsilon^2g^2\mu}{2}\frac{\mu}{M}[Ei(-2\mu r)+(2\mu r)^{-1}e^{-2\mu r}] \tag{5.1}$$

where the exponential integral is defined by

$$Ei(-x)=-\int_x^\infty t^{-1}e^{-t}dt.$$

The potential energy used in Jauch's paper is of the Coulomb type in the outer region, and a constant in the inner region. Defining an equivalent inside energy U_0 by

$$\int_0^{1/\mu}U(r)4\pi r^2dr=4\pi U_0/3\mu^3$$

and comparing its value with the values necessary to give an appreciable shift in the energy levels (using the curves plotted in Jauch's paper) we see that the effect is several orders of magnitude to small for experimental determination.

In the introduction we also mentioned the possibility of anomalous scattering of charged particles of high energies on protons, caused by that meson charge cloud. But the charge cloud will not become noticeable until the incident particles have energies of the order of several hundred times the rest energy of an electron. In other words, the de Broglie wave-length of the incident particles must be comparable to the dimensions of the meson charge cloud before we can expect any anomalous scattering. But for incident particles of such tremendous energies our treatment is most certainly inapplicable. We may expect cumulative processes (showers) which we have not taken into account at all.

We thus conclude that the effect of the meson charge cloud is entirely too small to be observed experimentally.

SUMMARY

The results of Fröhlich, Heitler, and Kahn[3] are not reproduced by the convergent theory.

[15] R. C. Williams, Phys. Rev. **54**, 558 (1938); Pasternack, Phys. Rev. **54**, 1113 (1938).

[16] J. M. Jauch, Helv. Phys. Acta **13**, 451 (1940).

This fact strikingly illustrates the danger of working with divergent theories near the limits of their validity. The convergent theory leads to an effect which differs completely from the earlier result, both qualitatively and quantitatively.

The author wishes to express his thanks to Dr. J. M. Jauch for the suggestion of the problem and for many helpful discussions.

APPENDIX: TABLE OF INTEGRALS

$$\int_{-\infty}^{\infty}\frac{e^{ikr}dk}{(k_0)^{2n}}=\frac{\pi^{\frac{1}{2}}i^{n+\frac{1}{2}}r^{n-\frac{1}{2}}}{(n-1)!(2\mu)^{n-\frac{1}{2}}}H^{(1)}_{n-\frac{1}{2}}(i\mu r),$$

$k_0=(k^2+\mu^2)^{\frac{1}{2}}$, n half integer, $H_n^{(1)}(z)$ . . . Hankel function of order n and first kind.

$$\int(k_0)^{-1}\exp(i\mathbf{k}\cdot\mathbf{x})d^3k=-\frac{2\pi^2\mu}{r}H_1^{(1)}(i\mu r),$$

$$\int(k_0)^{-1}\mathbf{k}\exp(i\mathbf{k}\cdot\mathbf{x})d^3k=\frac{2\pi^2\mu^2}{r}H_2^{(1)}(i\mu r)\mathbf{e}_x,$$

$$\int(k_0)^{-2}\exp(i\mathbf{k}\cdot\mathbf{x})d^3k=\frac{2\pi^2}{r}e^{-\mu r},$$

$$\int(k_0)^{-2}\mathbf{k}\exp(i\mathbf{k}\cdot\mathbf{x})d^3k=\frac{2\pi^2}{i}\frac{d}{dr}\left(\frac{e^{-\mu r}}{r}\right)\mathbf{e}_x,$$

$$\int(k_0)^{-3}\exp(i\mathbf{k}\cdot\mathbf{x})d^3k=2\pi^2iH_0^{(1)}(i\mu r),$$

$\mathbf{e}_x$ . . . unit vector in $\mathbf{x}$ direction, $r=|\mathbf{x}|$,

$$\int\exp(-k_0q)\exp(i\mathbf{k}\cdot\mathbf{x})d^3k=2\pi^2i\mu^2q(r^2+q^2)^{-1}H_2^{(1)}[i\mu(r^2+q^2)^{\frac{1}{2}}],$$

$$\int(k_0)^{-1}\exp(-k_0q)\exp(i\mathbf{k}\cdot\mathbf{x})d^3k=2\pi^2\mu(r^2+q^2)^{-\frac{1}{2}}H_1^{(1)}[i\mu(r^2+q^2)^{\frac{1}{2}}].$$

The following integrals are correct to the first order in μ/M only:

$$\pm\int\frac{(2M\mp k_0)\exp(\pm i\mathbf{k}\cdot\mathbf{x})}{k_0(\mu^2\mp 2Mk_0)}d^3k=-\frac{2\pi^2}{r}e^{-\mu r}\mp\frac{\pi^2\mu}{M}\left[i\mu H_0^{(1)}(i\mu r)+\frac{1}{r}H_1^{(1)}(i\mu r)\right],$$

$$\int\frac{(2M\mp k_0)\exp(\pm i\mathbf{k}\cdot\mathbf{x})}{(\mu^2\mp 2Mk_0)}d^3k=\pm\frac{2\pi^2\mu}{r}H_1^{(1)}(i\mu r)+\frac{4\pi^2}{M}\delta(r)-\frac{\pi^2\mu^2}{Mr}e^{-\mu r},$$

$$\int\frac{\mathbf{k}\exp(\pm i\mathbf{k}\cdot\mathbf{x})}{k_0(\mu^2\mp 2Mk_0)}d^3k=\mp i\pi^2\frac{1+(\mu r)}{Mr^2}e^{-\mu r}\mathbf{e}_x,$$

$$\pm\int\frac{\mathbf{k}\exp(\pm i\mathbf{k}\cdot\mathbf{x})}{(\mu^2\mp 2Mk_0)}d^3k=-\frac{\pi^2\mu^2}{Mr}H_2^{(1)}(i\mu r)\mathbf{e}_x.$$

Limiting behavior of Hankel functions:

	$x\ll 1$	$x\gg 1$
$H_0^{(1)}(ix)$	$-\frac{2i}{\pi}\log\left(\frac{2}{\gamma x}\right)$	$-i\left(\frac{2}{\pi}\right)^{\frac{1}{2}}\frac{e^{-x}}{x^{\frac{1}{2}}}$
$H_1^{(1)}(ix)$	$-\frac{2}{\pi x}$	$-\left(\frac{2}{\pi}\right)^{\frac{1}{2}}\frac{e^{-x}}{x^{\frac{1}{2}}}$
$H_2^{(1)}(ix)$	$\frac{4i}{\pi x^2}$	$i\left(\frac{2}{\pi}\right)^{\frac{1}{2}}\frac{e^{-x}}{x^{\frac{1}{2}}}$.

The Cu *K* Absorption Edges of the Cuprous Halides

W. W. BEEMAN, J. FORSS, AND J. N. HUMPHREY
Department of Physics, University of Wisconsin, Madison, Wisconsin

(Received January 15, 1945)

The x-ray *K* absorption edges of copper in crystalline CuCl, CuBr, and CuI have been measured with a double crystal spectrometer. Near the edge the experimental curves have been analyzed into component absorption lines. The most intense absorption maximum is due to excitation of the *K* electron into the 4*p* level of the absorbing ion. However, the line structure is too complex to be completely explained by the unperturbed optical levels of Zn^+ or by any perturbation of these levels arising from crystalline fields. It is suggested that the excited electron is shared with neighboring ions even in the lowest states.

INTRODUCTION

THE fine structure within 30 or 40 ev of the Cu *K* edge has already been studied under high resolution in the metal,[1] certain alloys,[2] and in aqueous solutions[3] of Cu^{++}, $Cu(NH_3)_4^{++}$, and $Cu_2(CN)_4^{--}$. In most cases interpretation of the experimental results is very difficult because of the complexity of the electronic energy levels of crystals and molecules. However, for the pure metal there were available Krutter's[4] electronic band calculations and good agreement was found between theory and experiment. It was found also that the edge of hydrated Cu^{++} could be understood quite simply. It consisted of two absorption maxima which were identified as a $1s \rightarrow 4p$ transition and an unresolved mixture of $1s \rightarrow 5p$, $6p$, etc., transitions. The positions of the maxima were not altered by the water of hydration although there was considerable broadening of the absorption lines.

In extending the work to the compounds of copper it was decided to measure first the cuprous halides because the completed $3d$ shell of Cu^+ should simplify the interpretation of the absorption edge structure. The interaction between the np series electron and the unfilled $3d$ shell broadens the absorption lines of the cupric ion and makes it difficult to say just what edge structure is characteristic of the free ion and what is caused by the fields of surrounding ions or molecules. With the cuprous salts any deviation of the absorption edge from a series of sharp lines, the $1s \rightarrow np$ transitions, may be ascribed to the effects of the surroundings. The doublet separation is not large enough to be detected.

The halides have, in addition, the advantage of a known and relatively simple crystal structure. They crystallize in the zinc sulphide arrangement which is a diamond lattice with half the sites occupied by one type of ion, half by the other. The $Cu^+ - Cu^+$ separation is 3.82A in CuCl, 4.01A in CuBr, and 4.27A in CuI.

EXPERIMENTAL

The double crystal spectrometer used in this investigation was designed especially for absorption work in the 1 to 5A region and was built in the departmental machine shop. The spectrometer, x-ray tube, power supply, and counting equipment will be described at another time.

Geiger counters similar to those described by Shaw[5] were used to record x-ray intensities. The incident intensity, I_0, was constant over the frequency range concerned and also, because of the use of a tungsten filament and target, remained constant despite filament evaporation. This saved a great deal of time as it was necessary to measure I_0 but once.

The crystals were split from a specimen of calcite kindly loaned to us by Professor G. A. Lindsay. After grinding, and etching in HCl, the $(1, -1)$ half-maximum width was 11 seconds. The crystals were used with this half-width.

The absorption samples were prepared by

[1] W. W. Beeman and H. Friedman, Phys. Rev. **56**, 392 (1939).
[2] H. Friedman and W. W. Beeman, Phys. Rev. **58**, 400 (1940).
[3] W. W. Beeman and J. A. Bearden, Phys. Rev. **61**, 455 (1942).
[4] H. Krutter, Phys. Rev. **48**, 664 (1935).
[5] C. H. Shaw, Phys. Rev. **57**, 877 (1940).

mixing the finely powdered salts with a few drops of melted paraffin on a thin sheet of mica. After the paraffin had solidified, the mica was placed on a glass plate over a 15 watt lamp and the paraffin-powder mixture rolled flat. A small test tube makes an excellent rolling pin. The lamp served a double purpose. It kept the paraffin soft enough to roll easily and in addition made possible an easy control of uniformity of thickness. At the best thickness for x-ray measurements the specimens were still slightly translucent and quite small variations in thickness could be detected and eliminated. The samples were left on the mica backing which was too thin to absorb the x-rays appreciably.

The three cuprous halides were precipitated from solutions of $CuSO_4$ and the potassium halide by the addition of SO_2. As a check, alternative methods were also used. For CuCl, the cupric chloride in hydrochloric acid was reduced by boiling with copper turnings. CuBr was prepared by heating the cupric bromide to a dull red heat and CuI by adding KI to a solution of $CuSO_4$ (without addition of SO_2). The precipitates were washed with absolute alcohol and dried in vacuum. All these methods are described in Mellor's[6] treatise. In every case salts prepared by different methods gave identical absorption edges.

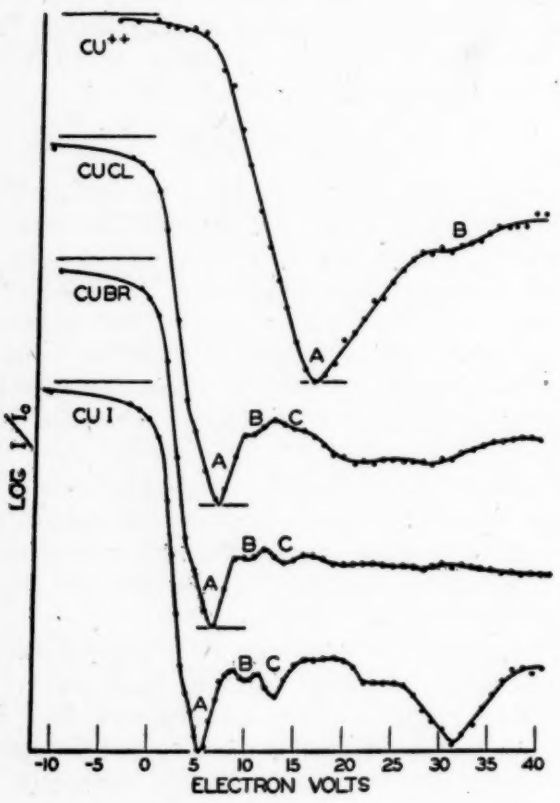

FIG. 1. Some K absorption edges of copper. Cu^{++} is redrawn from reference 3. The experimental points are averages of several runs.

TABLE I. Positions of absorption maxima (Fig. 1).

	A	B	C
Cu^{++}	16.7 ev	30.5–32.5 ev	
CuCl	7.1	11.2	14.6 ev
CuBr	6.4	10.5	14.2
CuI	5.6	10.3	13.0

The chloride and bromide hydrolyze in contact with moist air but not quickly enough to interfere with the measurements. Apparently the hydrolysis is accompanied by some oxidation as rough measurements on Merck reagent CuCl which had hydrolyzed to a pale green color (CuCl is white) showed a pronounced absorption at the position of the $1s \rightarrow 4p$ transition of Cu^{++} which is not present if the salt is freshly prepared.

In Fig. 1 are presented the three cuprous halide absorption edges and that of hydrated Cu^{++} from reference 3. The zero of the abscissa is at the energy of the first absorption line of the metal edge, i.e., the energy necessary to excite a K electron into the lowest empty level of the Fermi distribution. All the curves have been plotted to this same abscissa so that shifts of structure from one curve to the next are accurately portrayed.

The experimental points are averages over several independent runs. The statistical probable error per point is about 1 percent of the total change in $\log I/I_0$, from minimum to maximum absorption, at the K jump. This estimate is based on the total number of counts recorded at a given setting for all runs. Numerous checks have shown that at a particular spectrometer setting, with a particular absorber in place, a set of readings will vary by no more than the statistical amount. However a portion of the curve extending over several points may be in error by 3 or 4 percent of the top to bottom jump

[6] J. W. Mellor, *A Comprehensive Treatise on Inorganic and Theoretical Chemistry* (Longmans, Green and Company, London, 1928), Vol. III.

because of the movement of the beam over inhomogeneities in the absorber.

Angular settings of the crystal are reproducible to about 1 second of arc or roughly 0.1 ev at these wave-lengths. The accuracy with which the relative positions of absorption minima can be determined is limited mainly by their sharpness, about ± 0.5 ev for the $1s \rightarrow 4p$ of Cu^{++} and ± 0.2 ev for $1s \rightarrow 4p$ of Cu^{+}. None of the uncertainties is large enough to affect any of the conclusions drawn from the data.

We have listed in Table I the positions of the principal absorption maxima of the four curves.

DISCUSSION

The first absorption maximum ($1s \rightarrow 4p$) of hydrated Cu^{++} lies at 16.7 ev. It is labeled A in Fig. 1. In reference 3 the separation of the metal edge and the $1s \rightarrow 4p$ line of the cupric ion was calculated on the assumption that the ion absorbs as if in vacuum. Good agreement was obtained with the above experimental value. The calculation made use of a simple energy cycle which is easily adapted to the problem of the $Cu^{+} - Cu^{++}$ edge separation. When carried through the cycle gives 9.4 ± 0.6 ev for the energy difference of the $1s \rightarrow 4p$ transition in Cu^{+} and Cu^{++} assuming, again, that the optical levels are not influenced by neighboring ions. The uncertainty in the calculated result is due largely to the splitting of the $3d^{9}4p$ configuration of Zn^{++}. Experimentally (Table I) the separations are 9.6 ev for CuCl; 10.3 ev for CuBr and 11.1 ev for CuI if one identifies point A of each curve with the $1s \rightarrow 4p$ transition. The agreement with the calculation is close enough to give confidence in the identification.

The differences in the positions of absorption maximum A of the three cuprous halides are greater than the experimental uncertainty and must be real. Thus while the principal factor determining edge position is the valence of the absorbing ion, easily measurable shifts are produced by a change in the neighboring negative ions or in the lattice constants even when the crystal type is unaltered.

The broad maximum B of Cu^{++} was shown[3] to arise from unresolved $1s \rightarrow np$ absorption, $n = 5, 6, 7$, etc. If such transitions also contribute to the cuprous halide curves they should produce a maximum about 7.7 ev above the $1s \rightarrow 4p$ maximum. This figure was reached by taking an average of the positions of the $5p$, $6p$, and $7p$ terms of Zn^{+} giving them the relative weights 4:2:1 as determined by Parratt[7] for the absorption of argon gas. The observed separations of maxima A are C are 7.5 ev in CuCl; 7.8 ev in CuBr; and 7.4 ev in CuI, in excellent agreement with the optical terms.

However, not too much significance should be attached to this very close agreement because the unperturbed levels of Zn^{+} cannot explain at all certain other features of the experimental curves such as the absorption maximum B, the inflection point 2 or 3 ev below A in each curve, and the previously mentioned variation in the position of the $1s \rightarrow 4p$ absorption line. In addition, when the edge is analyzed into component absorption lines, it is found that apparently single absorption maxima may be composed of several lines.

Such an analysis is much more feasible for the cuprous edges than for the cupric because of the smaller number of component lines in the former. As has been previously pointed out, this simplification comes about because of the full $3d$ shell of Cu^{+}. Its effect on the experimental curves may be seen at once in the greater sharpness of the initial absorption break in the cuprous edges of Fig. 1.

The individual absorption lines are of the form[8]

$$y = A/(x^{2} + B^{2})$$

where y is proportional to the K absorption coefficient (positive y plotted down in Figs. 1 and 2), B is the half-width at half-maximum, A/B^{2} the maximum ordinate, and x the distance from the center of the line. B is inversely proportional to the lifetime of the K excited state and should be the same for all Cu K absorption lines since the most probable transitions filling the K shell involve only the inner electrons.

It is not easy to determine the correct value of B when the edge contains no single isolated absorption lines. In the work on copper metal[1] B was estimated to be about 1.0 ev (including the contribution of the calcite crystals). The

[7] L. G. Parratt, Phys. Rev. **56**, 295 (1939).
[8] F. K. Richtmyer, S. W. Barnes, and E. Ramberg, Phys. Rev. **46**, 843 (1934).

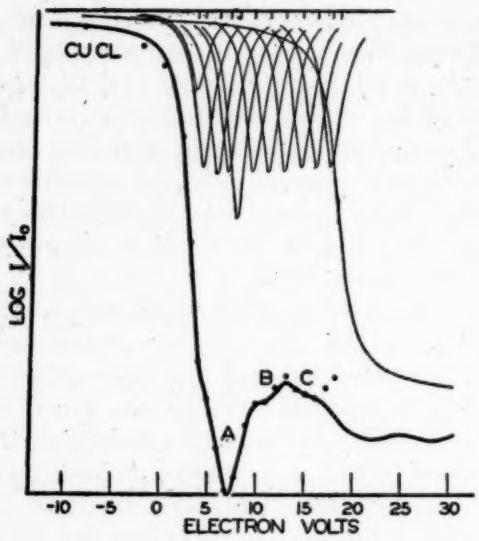

FIG. 2. The component absorption lines of the CuCl edge. The edge is redrawn from Fig. 1. The points are not the experimental points of Fig. 1, but are obtained by adding the ordinates of the component lines drawn at the top of this figure and listed in Table II.

estimate was made by matching the initial absorption of the experimental edge with a family of theoretical curves drawn for different values of B and on the assumption of a uniform distribution of absorption lines. Similar comparisons were made using the present data but assuming a single strong line to be responsible for the initial absorption. Again B was approximately 1.0 ev.

The drawing and matching of curves is laborious and always somewhat uncertain when only limited portions of the curves are compared since different combinations of horizontal and vertical scales may produce quite similar curvatures. The following semianalytic method furnishes an upper bound to B which is the more accurate the further separated are the absorption lines in the edge and which is independent of the vertical scale to which the data are plotted.

The ratio $|y'/y| = |2x/(x^2+B^2)|$ evaluated for a single absorption line has its maximum value at $x=B$, at which point $|y'/y| = 1/B$. On the initial steep part of an experimental absorption curve one can easily determine the observed maximum $|y'/y|$ and thus the maximum $B = |y/y'|$ of the component absorption lines making up the edge.

Of course at the point of maximum $|y'/y|$ on the experimental absorption curve the observed absorption coefficient will generally contain contributions from several component lines. Not all these lines will be evaluated at the abscissa for which $|y'/y|$ is a maximum. The method therefore may considerably overestimate B but cannot underestimate it. The estimate is the more accurate the smaller the overlapping of successive absorption lines.

From the cuprous halides we obtain by this method the following upper limits to B, CuCl -1.4 ev; CuBr -1.3 ev; CuI -1.1 ev. Applied to Cu^{++} this method gives $B \leq 2.4$ ev showing that at the point of maximum $|y'/y|$ several different component lines are contributing appreciably to the absorption.

In analyzing the present experimental data, absorption lines with a half width at half maximum of 1.22 ev were used. The choice was a convenient one in terms of the arbitrary abscissa on which the data were originally plotted and in terms of which the absorption lines were calculated. In view of the several experimental values around 1.0 ev, it is very doubtful that the true half width of the line can be greater than 1.22 ev. It is important not to use too narrow a line in the analysis since the mistake will not betray itself in a failure to reproduce the absorption edge, and the number of transitions making up the edge may be greatly overestimated. Any absorption edge can be analyzed into very narrow absorption lines by using a sufficient number of them. The converse, of course, is not true. No combination of broad lines can be added together to give a narrow line although one might successfully analyze an edge using too broad a component line if the edge were composed of a large number of overlapping lines. In this case $|y'/y|$ for the edge would everywhere be less than the maximum for a single absorption line.

The results of the analysis are collected in Fig. 2 and Table II. No attempt was made to analyze the edges in the region more than 12 or 15 ev beyond the initial absorption. However, the contributions made by higher energy transitions to the initial absorption were taken account of in an arctangent curve[8] with its inflection point located as indicated in Table II under "continuum." The line strength is proportional to the height of the line since the half-width is

constant. In terms of the same arbitrary unit of line strength used in Table II the maximum difference of ordinates (base line to absorption maximum A) of each edge is 31. The calculated points for just the CuCl curve are shown in Fig. 2. The other two analyses show a similar agreement with the observed curve.

Eleven lines were used for each edge and the question naturally arises whether or not as good agreement might be reached with fewer lines. Some time was spent attempting to match the CuBr edge with nine lines, but without success. When nine lines are used, the positions of maxima and minima can be reproduced, but because of the necessarily greater separation of the lines, the magnitude of the structure is exaggerated, i.e. the change in $\log I/I_0$ from maximum to minimum is too great.

The region of greatest interest is that near absorption maximum A. Careful checks on both CuCl and CuBr have shown that the observed structure cannot be reproduced with fewer than five lines (the first five lines in each edge). This is probably too low an estimate since the actual line width is almost certainly less than 1.22 ev. There is evidence to this effect in Fig. 2. The second and third calculated points (between -5 and 0 ev) fall below the experimental curve. A similar result obtained with CuBr and even more noticeably with CuI. The absorption at the beginning of the curve is not determined predominantly by any one line, but is rather made up of roughly equal contributions from the first four or five lines and the continuum. Thus no permissible reshuffling of the lines could change these two points. They could be brought onto the experimental curve only by a narrowing of all the lines and, of course, an increase in their number.

Thus the $1s \rightarrow 4p$ absorption which should be a single relatively isolated line (the $4p-5p$ separation in Zn^+ is 6.5 ev) if the ion were in vacuum is split in the crystal into at least five components with a total separation of about 4 ev. The splitting of 4 ev could easily be produced by the fields of the surrounding ions, but the number of components is not so easily understood. The surrounding ions have closed shells and will not remove the spin degeneracy. Therefore the level should be split into at most three components (ignoring the very small doublet separations), no matter how low the symmetry of the crystalline field. The additional lines observed must be an indication of sharing of the $4p$ electron with the neighboring Cu^+ ions.

Such a sharing is entirely plausible on the basis of Krutter's[4] work on the copper bands. He published a curve showing the energy of the lower limit of the $4p$ band as a function of interatomic distance. His curve was not meant to be taken quantitatively, but it indicates strongly that at the positive ion separations of about 4.0A existing in the halides, the $4p$ band should be at least 2 or 3 ev wide. The smaller size of Zn^{++} compared to Cu^+ will reduce the interaction somewhat, but there should still be an appreciable sharing of the $4p$ electron.

It will be noticed in all three edges that the ratio of the total intensity of the two lines making up the first inflection point to the three lines in the main $4p$ absorption is about 1 to 2. This suggests that the three $4p$ wave functions may have been split into a non-degenerate and a doubly degenerate level by the crystalline field and then each level further split up into a number of lines by mixing with the $4p$ functions of neighboring positive ions.

It is probably not worth while to discuss in greater detail the structure beyond the absorption maximum A. Certainly a great many more lines are present than indicated by the present analysis and probably no unique breakdown into component absorption lines is possible. This does not mean that the more distant absorption maxima may not have a simple interpretation. In all the ions and ionic compounds investigated thus far there has been an absorption maximum

TABLE II. Component lines of the cuprous halide edges.

CuCl		CuBr		CuI	
Line position	Line strength	Line position	Line strength	Line position	Line strength
3.12 ev	5	2.83 ev	5.0	2.95	5.0
3.94	10	3.65	10.0	3.76	10.0
5.37	10.5	5.07	10.0	4.99	10.0
6.59	10.3	6.13	10.0	5.80	10.0
7.61	13.3	6.91	10.0	6.82	10.0
9.24	10.3	8.28	10.3	8.56	10.0
10.77	10.3	9.97	10.0	10.09	10.0
12.36	10.3	11.36	10.0	11.62	10.0
14.14	10.0	13.03	10.0	13.15	11.0
15.56	10.0	14.37	10.0	14.57	10.0
17.13	10.0	15.89	10.0	16.00	10.0
continuum		continuum		continuum	
18.01	25.00	16.90	25.00	18.25	25.00

at the center of gravity of the $1s \rightarrow 5p$, $6p$, etc., transitions, a result which could hardly be accidental. However, these maxima are generally not very pronounced and for this reason the analysis into component absorption lines is not unique and therefore not of any great interest. One might just as well take such maxima as they are measured and attempt to correlate them with possible transitions.

The work is being extended to other crystals. If, as appears likely, the symmetry of the crystalline field, by determining the splitting of the excited levels, has an important effect on the shape of the absorption edge, then x-ray absorption measurements should find interesting applications in structural chemistry.

In conclusion, we wish to thank the Machlett Laboratories for kindly supplying the beryllium sheet used on the x-ray tube window and to express our particular appreciation of the many suggestions offered by Mr. J. P. Foerst, department mechanician, during the design of the spectrometer and of his excellent workmanship in its construction.

PHYSICAL REVIEW VOLUME 67, NUMBERS 7 AND 8 APRIL 1 AND 15, 1945

A Simple Counting System for Alpha-Ray Spectra and the Energy Distribution of Po Alpha-Particles

W. Y. CHANG AND S. ROSENBLUM
Palmer Physical Laboratory, Princeton University

(Received December 29, 1944)

An alpha-ray counting system, consisting of parallel wire electrical counters and amplifying circuits, etc., is described. The conditions of reliable operation have been carefully examined and well defined. The mechanism of the counters as to why they answer only to alpha-particles but not to even strong beta- or gamma-rays is generally discussed. The distribution form of the Po-alpha particles determined by these counters in conjunction with an alpha-ray magnetic spectrograph agrees well with that obtained from a photographic line. The resolving power for the alpha-ray lines is very high, owing to the small active region of the counters.

1. INTRODUCTION

TO count alpha-particles a parallel plate ionization chamber, a ball counter, or a tube counter is generally used. However, in the first case, the chamber is usually operating with such a small total charge that the change of potential is only of the order of a few micro-volts. Such a small change of potential is ordinarily made recordable only by means of a well-built linear amplifier of four or five stages. In the second and third cases the proportionality of counting depends on an appropriate working potential applied to the counters and the characteristics of the counters.[1] They also need an amplifier of several stages to magnify the initial electrical pulses in order to actuate a mechanical device. All of them are very liable to either mechanical or electrical disturbances.

When the counting method is employed in the case of an alpha-ray magnetic spectrograph, a great saving in time as well as other advantages can evidently be secured, if several counters are operating at the same time. These counters must be closely spaced, and each of them must be sensitive along a line of considerable length and coupled to an amplifier, preferably one which is easily built and inexpensive. These conditions are not easily fulfilled by counters of the above types. However, in the following, we shall describe a system of counters which is very simple in construction and economical in cost and has been shown to be satisfactory for determination of alpha-ray spectra. A spark counter of similar principle has been very generally described by Greinacher.[2]

2. THE COUNTER

If a thin wire is stretched in front of, and insulated from a smooth brass plate, it is found to

[1] S. A. Korff, Rev. Mod. Phys. **14**, 1 (1942).

[2] H. Greinacher, Zeits. f. tech. Physik **16**, 165 (1935).

answer very well to alpha-particles (with audible and visible sparks) but to be not affected at all by even very strong beta- or gamma-rays. The wire is at a positive potential of the order of 3000 volts with respect to the brass plate, and the counter operates in air at atmospheric pressure.

Figure 1 represents a side view of the longitudinal section of a counter which was actually used. A is a plate of hard rubber having a thickness of 2.5 cm. A rectangular trough of a length about 5 cm, a width about 2 cm and a depth about 1 cm was cut, in which a tungsten wire W of $7\frac{1}{2}$ mils diameter was stretched in front of the brass plate B and held firmly by the two springs S. The length of the wire actually exposed to the plate B was about 4 cm. The two glass tubes g of about 4 mm diameter served for adjusting the spacing between the wire and the brass plate; mica sheets could be introduced between the glass tubes and the tungsten wire. The separation of the wire from the brass plate was about 1.5 mm. It was estimated that the active region around the wire was of the order of the thickness of the tungsten wire. This small active region offers another advantage for determining an alpha-ray spectrum (cf. Section 5).

When a capacity of about 500 cm was connected across the counter, a total change of potential due to the discharge produced by an incident alpha-particle could be of the order of 50 volts. If a reasonable fraction of this change of potential is applied to the grid of a power amplifying tube, e.g., a 2A3, the power output is large enough to operate a 73511 Cenco high voltage impulse counter. However, to match the high d.c. resistance (about 3300 ohms) of the Cenco counter, it is better to use a power tube of higher plate resistance. A tube of the type 6AG7, which has a plate resistance of about 0.1 megohms and a much higher amplification, was

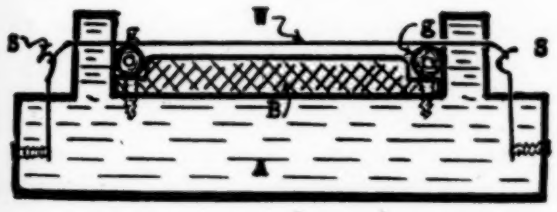

FIG. 1. Construction of the counter.

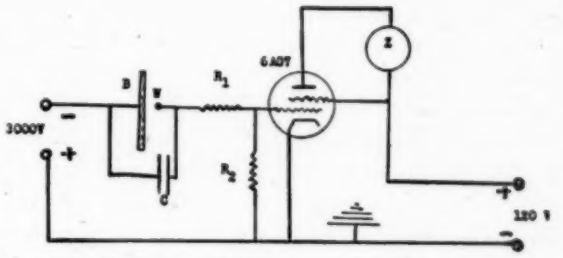

FIG. 2. Single stage amplifier: $R_1 = 10^7 - 10^8$ ohms, $R_2 = 10^6$ ohms, $C \sim 200$ cm, Z is Cenco counter.

found to be very satisfactory. In this latter case, the capacity across the counter could be reduced considerably (to about 150 cm) and hence the resolving time of the counter became smaller. It was found that in this arrangement the counting set could record the incoming alpha-particles at a rate of about 600 per minute without appreciable loss. The background was about 1 in 3 minutes if the working potential was less than 100 volts above the threshold potential, and became higher (even up to 5 per minute) as the working potential was further increased. Figure 2 shows the arrangement suitable for low rate counting.

To apply a larger fraction of the total change of potential to the amplifying tube, R_2 may be increased relatively to the extinguishing resistance R_1 (10^7 to 10^8 ohms) if a high cathode bias is used.

The condenser across the counter was made of a mica sheet with two copper foils pressed on its opposite sides, the whole being then immersed in paraffin. The electrical insulation between the two plates of the condenser is obviously very important.

3. THE HIGHER RATE COUNTER—THE MULTIVIBRATOR

In order to make the counter capable of counting alpha-particles at a higher rate, the capacity across the counter must be reduced to the minimum or even taken off. The electrical pulses produced by the discharges due to the incident alpha-particles will then be very much smaller, however, and an amplifier of higher amplification must be used. An amplifier of the multivibrator type was found to be very satisfactory.

Figure 3 shows the amplifier coupled to the

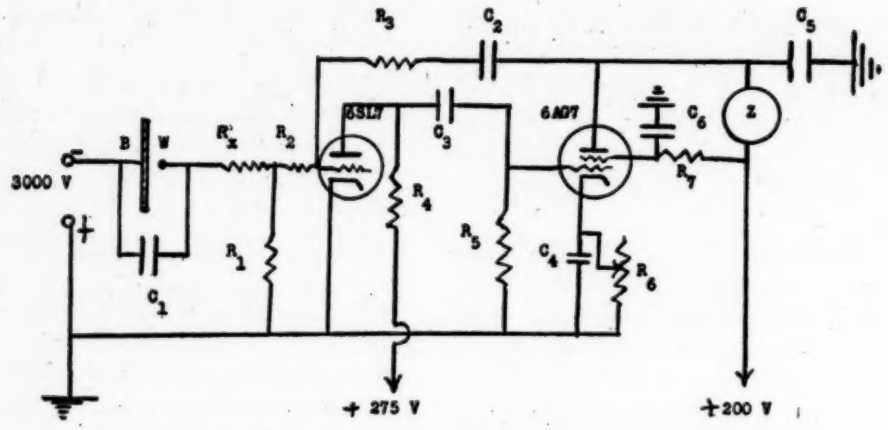

FIG. 3. The multivibrator. $R_x = 10^6 - 10^7$ ohms; $R_1, R_2, R_3, R_5 = 0.1 \times 10^6$ ohms; $R_4 = 10^4$ ohms; $R_6 = 2 \times 10^3$ ohms; $R_7 = 4 \times 10^3$ ohms. $C_1 = 0$–30 cm; $C_2 = 0.00015$ μf; C_3, $C_5 = 0.5$ μf; $C_4 = 0.1$ μf; $C_6 = 0.35$ μf. Z is Cenco counter.

electric counter with the values of the constants listed. Since the incoming pulse to the grid of the first tube was negative, the grid resistance and the anode potential of the first tube (6SL7) were so chosen that the operating point was at the top part of a longer straight portion of the I_p vs. V_g curve, while that of the second tube (6AG7) were adjusted so that the operating point was at the bottom part of a longer straight portion. In actually working condition, the plate current of the 6SL7 was about 10 ma (the two triodes being in parallel) and that of the 6AG7 about 3 ma. The residual oscillation between the two stages was eliminated by introducing the resistance R_3 in the feed-back circuit. C_6 and R_7 in the screen grid circuit of the output stage were necessary only when two or more such units were supplied with the same power pack and coupled to two or more electrical counters (cf. Section 4), while C_5 was found useful in either case in by-passing the low frequency oscillation to the earth. As before direct coupling assured more satisfactory operation than capacity coupling.

In the above arrangement the extinguishing resistance R_x could be lower than 10^7 ohms and the condenser C_1 across the counter could even be removed. The power output was still big enough to actuate the mechanical counter, and the counter was not affected again either by a strong source of beta-rays or by that of gamma-quanta. To assure reliable operation a capacity of about 30 cm was used. Under such circumstances the counting system responded to the incoming alpha-particles at a rate of about 1500 per minute or higher.

Some particular features of the above arrangement are obvious: It can lengthen the incoming pulses so as to give a better assurance of the operation of the mechanical counter. It may also help to extinguish the discharge in the counter so that a smaller value of R_x can be used and hence a smaller resolving time of the counter may be effected. The variable cathode resistance R_6 provides a convenient device for selecting the pulses of different sizes.

4. A SYSTEM OF SEVERAL COUNTERS

To determine an alpha-ray spectrum in a magnetic spectrograph, it is evidently more advantageous to use several counters at the same time than a single counter. For this purpose eight tungsten wires of the above mentioned size were stretched in front of a smooth brass plate. The arrangement of each wire with respect to the brass plate was very similar to that shown in Fig. 1. The wires were equally spaced, the distance between two adjacent wires being 5 mm. All the wires could be adjusted to work at approximately the same potential by changing their relative distances from the brass plate, mica sheets of different thicknesses being introduced into the space between the wires and the glass tubes g.

It was found that when one wire was responding to an incoming alpha-particle, the other wires near by were also answering simultaneously. This trouble was eliminated by erecting aluminium walls between any two adjacent wires. These walls were set into the brass plate. The reason for their effect was not clear. It might be either due to some mechanical vibrations in the air of the counter box, or due to some alteration of the electric field in the near-by counters. The photoelectrons (or light) emitted from the counter which was actually working might not affect the near-by counters, for as mentioned above, none of the counters responds to even strong beta- or gamma-rays.

Figure 4a represents a side view of a transverse section of the counters, which have been actually used (cf. Section 5). *A* is the box (cf. *A* in Fig. 1) made of transparent Plexiglas, *B* the brass plate and *W* the wires. The actual length of each tungsten wire was about 4 cm, and the diameter 7½ mils. When actually used, the counter box was put in the evacuated deflection chamber of an alpha-ray magnetic spectrograph with air of atmospheric pressure inside the counters and vacuum outside. Hence the box had to be air tight. A window with parallel slits, each of ½ mm width and just opposite as well as parallel to each of the wires, was made of a brass plate having a thickness of about 7 mm. The slits were the narrow gaps between the halves of brass rods about 4 mm diameter, the ends of which were fixed into the brass frame by means of screws. The round side of each rod was directed toward the incident beam of alpha-particles, and hence would prevent the particles scattered from the surface of the rod from going into the counters. Figure 4b shows a bottom view of the window. *N* is a Neoprene strip in the form of a closed square; this made the air tight joint when the window was pressed upon the counter box by six screws. A thin sheet of mica sufficiently big to cover the whole window (having a stopping power of about one cm air equivalent) was waxed on to the bottom of the window. The distance of each wire from the window was about 5 mm. The operation was found to be more satisfactory if the window was at the same negative potential as the brass plate behind the wires. The transparency of the counter box allowed one to observe each wire inside the box when the counter was working.

Two multi-vibrators were built and coupled to any two wires. They were supplied with the same power pack but well shielded from each other (cf. Section 3). When the counting rate is not high, of course an amplifier of a single stage as shown in Fig. 2 can be used for each electrical counter. As the single stage amplifier is simple and inexpensive, more sets could be built up and coupled to more wires. Figure 5 shows two or more wires coupled to two or more amplifiers, and the stabilizer for the counter voltage. In the stabilizer, the plate voltage of the 6C6 tube was between 100 and 250 volts and was indicated by a home-made electrometer; the grid voltage was a 45 volts B battery.

When the counters are used in the deflection chamber, the long leading wires, particularly the H. T. lead, between the counters and the amplifying and high voltage sets should be well insulated and shielded. C_1 and R_2 should be put as near as possible to the counters so that the

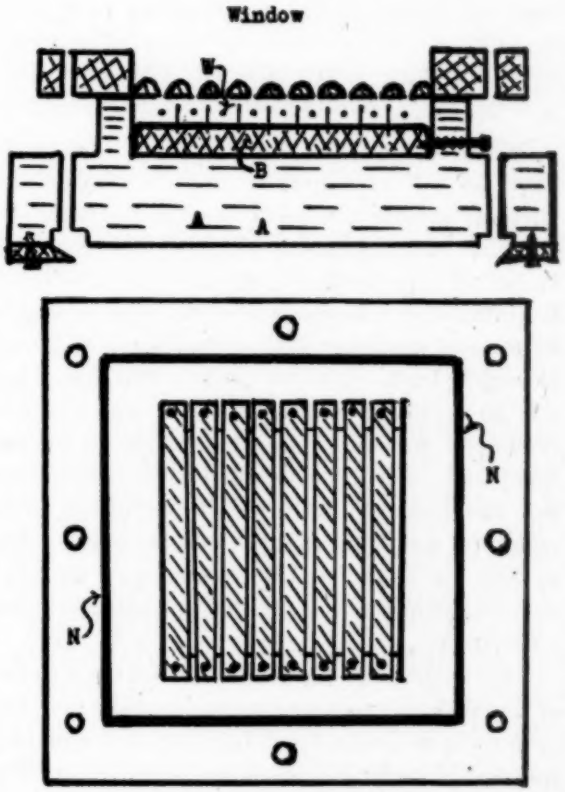

FIG. 4. (a) (above) Side view of transverse section; (b) (below) Bottom view of the window.

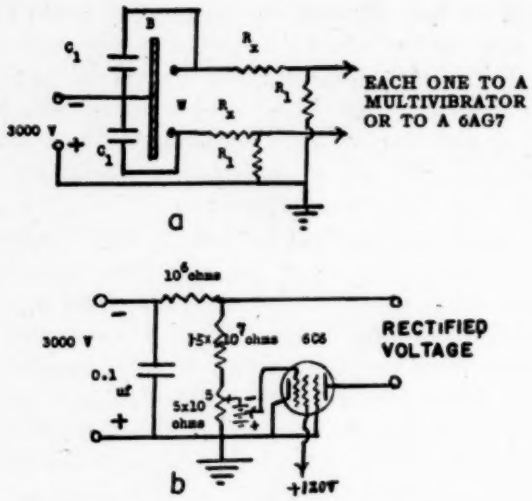

FIG. 5. (a) Coupling to multivibrator or 6AG7; (b) Stabilizer for counter voltage.

potential difference developed between the leads and the earth, when the counters are working, would be small. As mentioned above, if a high cathode bias is provided, a larger fraction of the total change of potential can be applied to the first tube by increasing R_1 relatively to R_x.

5. THE SPECTRUM OF THE PO ALPHA-PARTICLES

As mentioned above, the counter box should have air at atmospheric pressure inside and vacuum outside, when it is used in the deflection chamber of an alpha-ray magnetic spectrograph. Hence it has to be air tight. This was tested beforehand in a desiccator, which was evacuated by a small pumping system and made to permit electrical leads to come out. A Po source was put in front of the window of the counters. A shutter for the source was made of an iron sheet and could be controlled by a magnet outside the desiccator. The sensitivity of one of the counters was checked frequently over a long period, say 24 hours; the constancy of the sensitivity certainly indicated the air tightness of the counter box.

This system of counters has been used by one of us (W.Y.C.) together with an alpha-ray magnetic spectrograph to determine the alpha-ray spectra of natural radioactive substances. This spectrograph consists of the Princeton cyclotron magnet and a large Plexiglas deflection chamber and will be described elsewhere.[3] Figure 6 shows two distribution curves of the same group of Po alpha-particles, which were determined simultaneously by using two adjacent counters respectively. These two counters were coupled to the two multi-vibrators, and readings from both mechanical counters were taken at the same time after the counter box was moved to each new position. The form of the distribution curve is in agreement with that found from a photographic line, i.e., the microphotometric result, and with that from the tracks method.

The width at half intensity is less than ½ mm, which is equivalent to about 0.01 Mev, according to the energy of Po alpha-particles (5.303 Mev) and strength of the magnetic field (about 12,000 gauss).[4] This sharpness of the line must also indicate that the effect of scattering from the residual gases in the deflection chamber and from the window surfaces into the counters on the width of the line was very small. In fact it was found that the counters would not hold a voltage of about 3000 volts unless the vacuum outside the counters was better than 10^{-3} mm Hg. When the pressure outside was higher than 10^{-3} mm Hg, corona discharge occurred at the metal parts and the electrical leads of the counters. Therefore, the satisfactory operation of the counters automatically guaranteed a good vacuum in the deflection chamber and hence very small scattering of the alpha-particles from

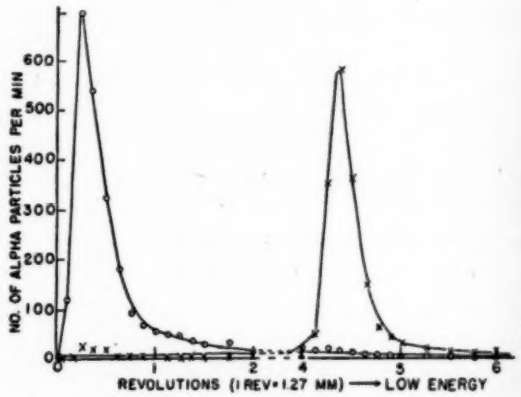

FIG. 6. Energy distribution of Po-alpha-particles. × results from Counter No. 3, ○ results from Counter No. 4.

[3] For a brief description see W. Y. Chang, Phys. Rev. 67, 58A (1945).

[4] Relation between $H\rho$ and E in Mev is given by $H\rho = 1.436 \times 10^8 E^{\frac{1}{2}}$ without relativistic correction. Hence $2d\rho = 1.436 \times 10^8 dE/(HE^{\frac{1}{2}})$, ρ being in cm.

the residual gases in the chamber, for the mean free path of an alpha-particle at this pressure or lower is very large.

As to the background, at an energy of about 5 percent lower than the main group energy the intensity is less than 0.1 percent of the main intensity. This result is quite different from that obtained by Roy Ringo.[5] His intensity at this energy is as high as 10 percent of the main intensity. However, we feel that our result is reliable, as it is reproducible when the source is properly prepared. These will be discussed elsewhere by one of us (W. Y. Chang) together with the spectrograph. It is seen that the background of one curve under the maximum of the other becomes slightly higher. This was found to be due to the pick-up by one multivibrator from the other, which was responding to the maximum number of alpha-particles. This disturbance could be cured, however, by increasing the cathode resistance R_6 of Fig. 3.

6. DISCUSSION

The exact mechanism of such counters is not completely clear. However, the reasons why they answer to alpha-particles but not to beta-particles or gamma-quanta may be easily understood from the following consideration. Since, as mentioned above, the active region of the counter is confined close to the wire, where the greater part of the counter potential drop occurs, a beta-particle or a gamma-quantum when passing through such a small region may produce too few or even no ions at all. The situation is different for an alpha-particle. Owing to its much higher ionizing power, an alpha-particle in traversing this region will produce a relatively sufficient number of primary ions, which will in turn then produce secondary ions by collision. Since the fall of potential near the wire is very steep, the secondary ionization so produced is expected to be big enough to send a spark across the counter.

The small active region of the counter has another advantage (cf. Section 2). Since the region is so narrow, the chance for several beta-particles or gamma-quanta to be incident simultaneously into this region must be very small. Hence there is no ambiguity as to whether all of the pulses are due to alpha-particles or some of them are due to simultaneous incidence of several beta-particles or gamma-quanta. In a parallel-plate ionization chamber, however, the situation is different. In this latter case, the active region is practically the whole volume between the two parallel plates. Consequently some of the pulses are inevitably originated by the simultaneous incidence of several beta-particles or gamma-quanta.

The region over which the sensitivity of the counter is more or less independent of the voltage is small, i.e., about 100 volts. Independence of sensitivity over a wider range might be expected if some other gas, e.g., air mixed with a certain organic vapor or hydrogen gas, was introduced into the counter. It might also be expected that the counter would answer to beta- or gamma-rays if the pressure was reduced from the atmospheric pressure. It is hoped that more work will be done along these lines.

We wish to express our thanks to Professor R. Ladenburg for his interest in this work and for his useful criticism and advice about the manuscript. We are also indebted to the former cyclotron group for putting some of their apparatus at our disposal and to those friends in the Electronic Division for their useful discussion about the electric circuits.

[5] Roy Ringo, Phys. Rev. 58, 942 (1940).

Study of Cosmic-Ray Air Showers With the Method of Coincident Bursts in Two Unshielded Ionization Chambers

LLOYD G. LEWIS
Ryerson Physical Laboratory, University of Chicago, Chicago, Illinois

(Received January 12, 1945)

Cosmic-ray bursts of ionization occurring in each of two unshielded, thin-walled ionization chambers were recorded simultaneously on a single piece of photographic film. This recording made it possible to study events in each chamber separately, and also to determine when a burst, occurring in one chamber, was coincident in time with a burst in the other. The graphic relation between the size of bursts and their frequency is given for a single chamber and for the coincident bursts. The relation, between burst coincidence frequency and separation of the chamber for several burst sizes, is given in a separate graph. A study of these sets of curves reveals the presence of many high density cosmic-ray air showers of heretofore unsuspectedly small lateral spread. These showers cannot originate at the top of the atmosphere but must be a secondary phenomenon.

INTRODUCTION

COSMIC-RAY Geiger-Müller counter experiments of the type performed by Auger[1] have led to the application of the cascade theory to the analysis of extensive atmospheric cosmic-ray showers. More recent Geiger-Müller counter tube measurements[2] of air showers have shown a large increase in counting rate with altitude. Computations[2] of this increase have been made by using the cascade theory of showers in combination with various assumed energy spectra for the shower producing radiation. The calculated counting rates as a function of altitude do not agree, however, with the observed curve over the whole range of observation.

Lapp[3] has shown that large bursts observed in an unshielded ionization chamber are caused by the passage through the chamber of the high density part of air showers. He used Geiger-Müller counter coincidences in conjunction with a Carnegie Model C meter. This experiment shows that the observed very large increase in burst rate with altitude[4,5] must be due to an increase in the frequency of air showers.

All computations, used for the comparison of shower experiments with the cascade theory, necessitate introducing either a mean width of the showers or a lateral density distribution function for the shower particles. This does not permit these experiments to provide a sensitive test of the theory. For the present investigation, an experimental method suggested by Euler[6] was chosen. It was expected that this method would provide a better test of the cascade theory. Euler pointed out that the observation of coincident bursts of ionization in two unshielded ionization chambers could lead to the determination of the lateral distribution of electrons in air showers. In the same paper, Euler calculated the burst coincidence frequency as a function of chamber separation. This calculation, which was carried out only for sea level, was based on an assumed energy spectrum of primary electrons and made use of several simplifying assumptions. The curves computed by Euler are for such high particle densities and, hence, for such low burst rates that they can be observed only in a prohibitive length of time.

Professor Marcel Schein has suggested that the measurement of coincident burst frequency as a function of chamber separation should be made at several altitudes. This would provide a method of determining both the energy spectrum of the shower-producing radiation and the lateral density distribution of the shower particles, provided that the showers originate close to the top of the atmosphere and that the cascade theory is

[1] P. Auger, R. Maze, and T. Grivet-Meyer, Comptes Rendus 206, 1721 (1938).
[2] N. Hilberry, Phys. Rev. 60, 1 (1941).
[3] R. E. Lapp, Phys. Rev. 64, 129 (1943).
[4] C. G. Montgomery and D. D. Montgomery, Phys. Rev. 47, 429 (1935).
[5] C. G. Montgomery and D. D. Montgomery, Rev. Mod. Phys. 11, 255 (1939).
[6] H. Euler, Zeits. f. Physik 116, 73 (1940).

correct in the domain of very high energies. This would eliminate the necessity of using an assumed primary energy spectrum in order to determine the lateral density distribution.

APPARATUS

The ionization currents produced in each of two thin-walled ionization chambers were amplified by d.c. amplifiers employing inverse feedback. Each amplifier output was connected to a string galvanometer. The deflections of both galvanometers were recorded simultaneously and continuously on the same photographic film. Coincidences between bursts of ionization in the two chambers were detected by measurement of the photographic traces with a microscope fitted with a filar-eyepiece.

The ionization chambers were steel spheres 35 cm in diameter with a wall-thickness of 0.03 cm. Each chamber had a cylindrical side-arm 7.6 cm in diameter and 20 cm long. This side-arm contained an FP-54 vacuum tube and tube shield. The collecting electrode of the ionization chamber consisted of a 7.5 cm diameter copper sphere with a 0.04 cm wall thickness and was mounted directly on the grid cap of the FP-54 tube, thus reducing the input capacity of the whole amplifier to a minimum. Each chamber with its side-arm was a single vacuum-tight volume and was filled with very pure argon to a total pressure of 100 cm Hg. A schematic cross section through the ionization chamber is given in Fig. 1.

The amplifier circuits were of a type similar to circuits described by Harnwell and Ridenour[7] and others,[8,9] but with the essential modification of the feedback connection being made to the first grid of the FP-54 vacuum tube rather than to the well-insulated second grid. This modification enabled the circuit to be sufficiently fast in its response to follow the rapid changes in the ionization current produced by a burst, and, in addition, to have inverse feedback characteristics. At the same time, the use of a large input grid resistor (10^{12} ohms) was possible. Tests for frequency response in a circuit with this feedback feature showed that the circuit had the same over-all amplification for square wave input of 3000 cycles per second that it had for direct currents. The driving signal was put across the large input grid resistor (10^{12} ohms).

The galvanometer strings were platinum wires of 0.0025 mm diameter. Each wire was 20 cm long. These strings were mounted so that each passed between carefully machined, wedge-shaped pole pieces of Alnico permanent magnets. A microscope objective focused an image of each string on a moving photographic film. A fine slit was placed directly in front of the film. This photographic registration permitted coincident bursts to be detected within a time of 0.2 second for the rate of travel of film used (75 mm/hour). This time was sufficiently short, since it was smaller than the collection time of the ions in

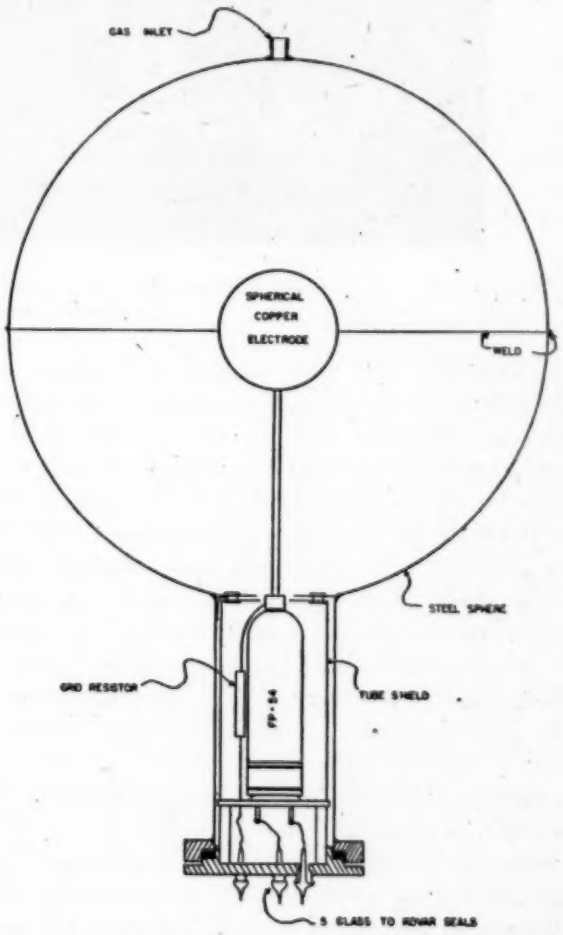

FIG. 1. Schematic cross section through an ionization chamber and its cylindrical side-arm. The line across the center of the chamber represents a weld between two hemispherical steel spinnings, and is not a partition through the chamber.

[7] G. P. Harnwell and L. Ridenour, Rev. Sci. Inst. 11, 346 (1940).
[8] Vance, Rev. Sci. Inst. 7, 489 (1936).
[9] Roberts, Rev. Sci. Inst. 10, 181 (1939).

FIG. 2. A reproduction of a portion of the photographic trace taken at a chamber separation of four meters.

the chamber. The wedge-shaped pole pieces on the galvanometer magnets produced a non-homogeneous magnetic field in the regions of the strings which increased the compression of the scale for the larger deflections. Currents as small as 0.006 of the maximum galvanometer current measurable on the film could be determined with an accuracy of about 3 percent, and, therefore, burst sizes producing amplifier output currents as small as this could be measured accurately. With the string tension used in this experiment, the galvanometers would follow 60-cycle alternating current with no noticeable change in sensitivity. However, there was approximately 20 percent decrease in current sensitivity at 200 cycles per second. These data show that the galvanometers were capable of following all changes in ionization current expected for the collecting time of the ions used in this experiment (0.4 sec.).

The apparatus was mounted in two portable houses which were equipped with sensitive thermostats (maximum variation 0.3°C). These houses were designed for Wilson cloud-chamber measurements of air showers. The constant temperature reduced the drift of the zero points of the amplifiers and galvanometers and insured constancy of the current calibration of each galvanometer.

The pressure of argon in the chambers was chosen so that the smallest burst analyzed (containing 80 cosmic-ray particles) would give a voltage signal (about 0.001 volt) which was large, compared to the noise level of the amplifier. The gain of the amplifier was then adjusted so that bursts of 80 particles would give galvanometer deflections large enough to be measured accurately. An over-all calibration of the apparatus was made frequently, during the time of the measurements, by recording the galvanometer deflections produced by known voltage signals put between the collecting electrode and the outer sphere of the ionization chambers. For a total input capacity of 15 mmf a deflection of

1 mm, as seen in the eyepiece of the microscope used for analyzing the photographic film, corresponded to a charge of $(7.83\pm0.06)\times10^{-14}$ coulomb for one chamber and $(7.95\pm0.06)\times10^{-14}$ coulomb for the other. A section of the photographic registration on a film taken at a 4-meter separation of the chambers is shown in Fig. 2.

DATA

The present paper deals only with data taken at Echo Lake, Colorado, altitude 10,650 ft. An open location of the apparatus was chosen so that the data would not be influenced by any large rock mass at the side or above the apparatus. Approximately 60,000 bursts were recorded in the two ionization chambers. These bursts were observed with the chambers placed in the two portable houses referred to above. Each house had a roof made from a piece of Douglas fir plywood, one-quarter inch thick. These roofs were constructed of material of low atomic number and with as little mass as possible, so that there would be a negligible multiplication of the shower particles passing through them.

The results of the observations are represented in Fig. 3 and Fig. 4. In Fig. 3, the number of burst coincidences per hour is plotted against the separation of the ionization chambers. These separations were measured from the center of one chamber to the center of the other chamber. The upper curve in Fig. 3, labeled ">80 particles per chamber," gives, as a function of chamber separation, the total number of burst coincidences per hour caused by more than 80 cosmic-ray particles traversing *each* chamber simultaneously. The three other curves in Fig. 3 give the number of burst coincidences per hour as a function of chamber separation for coincidences caused by more than 160, 240, and 320 cosmic-ray particles, respectively, traversing each chamber simultaneously.

In Fig. 4, the total number of burst coincidences per hour, caused by the simultaneous passage of more than a given number of particles through each chamber, is plotted against that given number of particles. The top curve gives this relation for zero separation of the chambers. The zero separation burst-coincidence frequency is numerically equal to the burst frequency in a single chamber. The four other curves give the total number of coincident bursts per hour, caused by the simultaneous passage of more than a given number of particles through each chamber, as a function of that given number of particles for chamber separations of 39 cm, one meter, four meters, and ten meters, respectively.

It will be noticed that the size of burst is given in terms of the number of particles traversing the chamber simultaneously, rather than in terms of electrical charge. This method of presentation was used in order to make the results more readily comparable with theoretical calculations. The usual computations from shower theory give number of particles per unit area, rather than ionization per unit volume. The relation between total charge developed in the chamber and the number of particles producing that charge was determined from experimental results and from calculations as follows.

Corson and Brode,[12] using delayed expansions in a cloud chamber filled with nitrogen, have measured the specific ionization of electrons. The chamber was placed in a magnetic field. These measurements provide an experimentally determined, specific ionization of electrons over a large range in particle energy. Swann[13] has determined the ratio of specific ionization in argon to that in nitrogen as 1.46. A combination of this value with the results of Corson and Brode gives the values of the specific ionization in number of ion pairs per cm path length shown in Table I.

For the separations of the chambers used at Echo Lake, Colorado, the contribution to the bursts of ionization in the ionization chambers by electrons of less than 10^6 ev, or of more than 10^{10} ev, is not large. Table I indicates that an average value of 100 ion pairs per cm path length may be used. This value is probably too low for the larger burst coincidences and is probably too high for the small bursts, especially at the larger chamber separations.

The average length $(\bar{L})$ of the path of a particle passing through the chamber is given by

$$\bar{L}=4/3\pi R^3\div\pi R^2=4/3R, \qquad (1)$$

where R = radius of chamber.

[12] Corson and Brode, Phys. Rev. **53**, 773 (1938).
[13] W. F. G. Swann, Phys. Rev. **44**, 961 (1933).

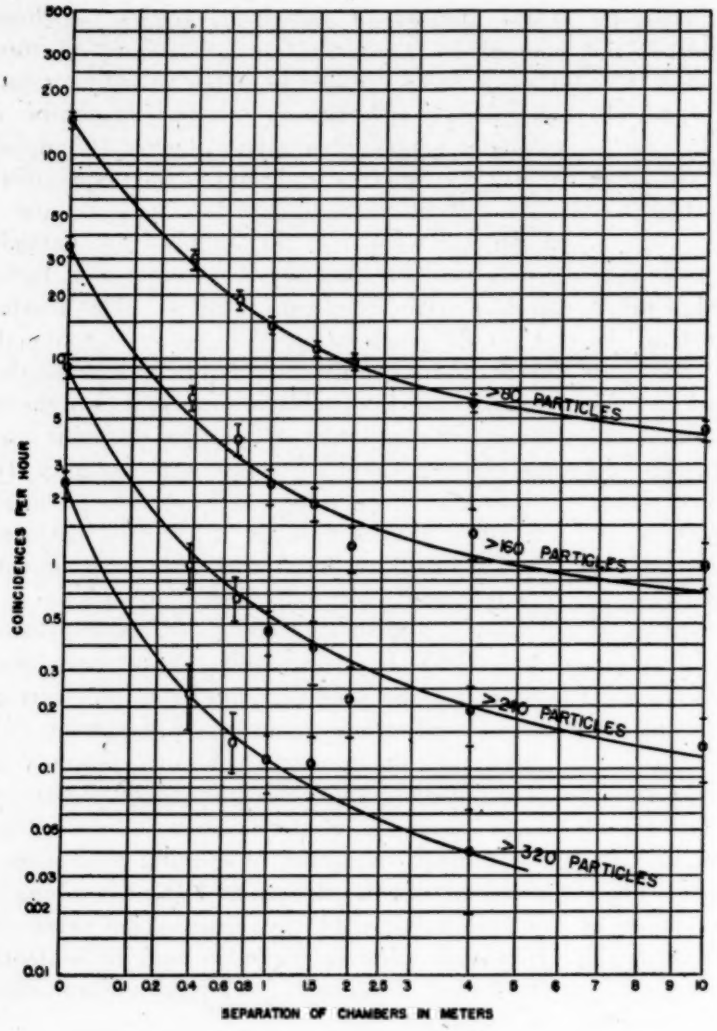

FIG. 3. The four curves of this graph give the number of burst-coincidences per hour, as a function of separation of chambers in meters, for coincidences caused by more than 80, 160, 240, and 320 cosmic-ray particles, respectively, traversing each chamber simultaneously.

For an argon pressure of 100 cm Hg and a chamber diameter of 35 cm, the charge generated by an 80 particle burst is then

$$80 \text{ part.} \times \left(\frac{4}{3} \times \frac{35 \text{ cm}}{2 \text{ part.}}\right) \times 100 \frac{\text{ion}}{\text{cm}} \times \frac{100}{76}$$

$$\times 1.59 \times 10^{-19} \frac{\text{coul}}{\text{ion}} = 3.90 \times 10^{-14} \text{ coul.} \quad (2)$$

This value was used to determine the number of particles per burst in all the results given in Fig. 3 and Fig. 4.

It is established[2] that the large increase in shower counting rate with increasing altitude is caused primarily by the increase in the frequency of showers of lower energy. This indicates that the barometric coefficient for the smaller showers is quite different from that for the larger showers. This causes difficulty in correcting the burst-coincidence rates for changes in barometer, since a given size burst may have been caused by a smaller shower striking near the apparatus, or by a larger shower striking farther away. In order to make a suitable correction, it would be necessary to know both the sizes of all showers contributing to a given point on the graphs of

TABLE I. Specific ionization in one atmosphere of argon.

Energy of electron in electron volts	Number of ion pairs per cm path length
10^{6}	70
10^{7}	82
10^{8}	102
10^{9}	124
10^{10}	146

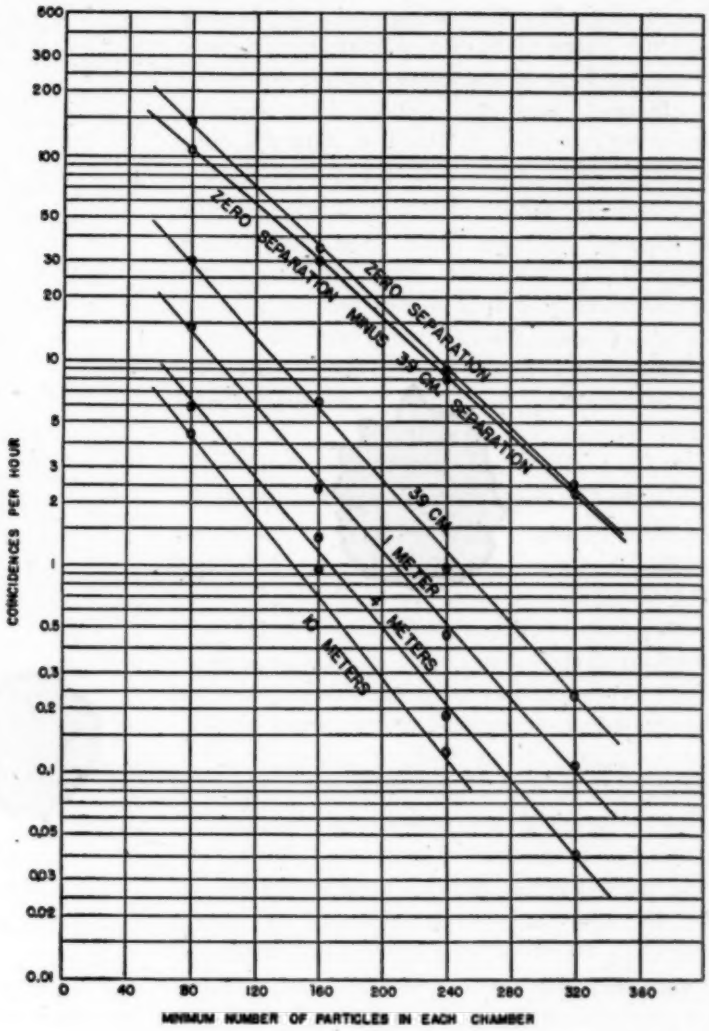

FIG. 4. This graph gives the total number of coincident bursts per hour caused by the simultaneous passage of more than a given number of particles through each chamber as a function of that given number of particles, for various separations of the two chambers.

Fig. 3 and Fig. 4, and the barometric coefficient for the showers of different size. Because of this difficulty, no attempt has been made to correct these data for barometric changes. The same difficulties are encountered in attempting a correction for changes in temperature. Therefore, the error limits associated with the experimental points in Fig. 3 are drawn to represent the sum of the probable error plus the observed mean fluctuation of the hourly rates due to atmospheric changes. The error limits on the ">80 particles per chamber" curve, Fig. 3 are almost entirely caused by atmospheric changes.

The time required for an ion to travel from the outer sphere to the inner collecting sphere of the ionization chamber was computed for one atmosphere of argon and an ion mobility of 2.4 cm/sec. per volt/cm. The time calculated was 0.65 sec. for the sweep voltage of 240 volts. The time necessary for the collection of all the ions generated in a burst was measured by determining the time required for the galvanometer string to move from its initial position to the final position produced by the burst. Careful measurements on many bursts yielded a result of 0.4 ± 0.1 sec. The resolving time of the apparatus was, therefore, taken as 0.4 second. This is justified since the electrical circuits and the galvanometers were capable of recording considerably faster changes in the ionization current, and, in addition, the trace on the photographic film could be measured within a time interval smaller than 0.4 sec. This collecting time was used in conjunction with the observed burst

rates in a single chamber to compute the chance coincidence rates of bursts. These chance coincidence rates limited the maximum separation of the ionization chambers to about 10 meters for bursts of 80 particles at 10,650 ft. altitude. The data given in Fig. 3 and Fig. 4 are corrected for the chance coincidence rates computed in the usual manner. The results of these experiments indicate that a resolving time of about a few thousandths of a second would be required for this type of apparatus to work successfully at elevations considerably higher than 10,650 ft. and at separations of chambers as large as 50 meters.

Tests for the internal consistency of the data were made. The first test was a separate study of the size-frequency distribution curves for all the bursts in each chamber. The absolute values of the size-frequency distribution curves obtained from one chamber for a particular hour closely approximated the curves from the other chamber for the same hour. Actually, the absolute values in the size-frequency distribution curves for one chamber changed from hour to hour; but since the variations in both chambers always occurred together, they could be explained only by changes in atmospheric conditions such as temperature and barometric pressure. This is demonstrated in Table II, which gives the number of bursts greater than 80 particles occurring separately in each chamber for several one-hour periods selected at random from the data taken over a period of several days.

Table II indicates also the magnitude of the fluctuations in the burst rate in a single chamber. Very few hours had a single rate as high as is indicated in Table II for the hour K. The hourly variations in the burst-coincidence rates were found to be smaller than the corresponding variations in the single chamber rates. These variations in the coincidence rates are included in the error limits in Fig. 3, as previously explained.

A measurement of the total ionization current produced in one chamber by all ionizing rays was made by measuring the voltage drop across the large grid resistor of the FP-54 tube. Since the exact value of this resistor was not known, the value of the total ionization current determined this way cannot be considered as very exact. The manufacturer measured the value of this resistor as 1.0×10^{12} ohms. With this value, the total ionization current was found to be 2×10^{-13} ampere.

TABLE II. Bursts of greater than 80 particles in one-hour periods selected at random.

Hour	Number of bursts in one chamber Chamber I	Chamber II
A	131	127
B	130	131
C	113	117
D	127	116
E	140	135
F	145	148
G	160	155
H	151	136
I	158	166
J	148	149
K	181	175

The fraction of the total ionization current generated by those atmospheric showers which produced bursts greater than 80 particles in one chamber was determined by computation from the size-frequency distribution curve for one chamber given in Fig. 4. These data from Fig. 4 were first replotted to give the differential size-frequency distribution curve. This curve was then divided into K equal intervals taken along the abscissa, and the following sum was formed:

$$Q=\sum_{n=1}^{K} S_n N_n q_t, \tag{3}$$

where S_n = average number of particles per burst for the size interval n, N_n = average number of bursts per hour for interval n, q_t = charge per track as previously computed. These K intervals covered the range from 80 to 960 particles per burst. Q, then, is the total charge generated in one chamber per hour by showers producing bursts of more than 80 particles. The average ionization current caused by these showers is found by dividing this charge by the number of seconds in an hour. The current found in this manner was 2.88×10^{-15} ampere. It follows, then, that the fraction of the total ionization current caused by showers producing bursts of more than 80 particles was 1.4 percent. The inclusion of bursts of less than 80 particles in these computations may not increase the fraction of the total ion current due to showers to more than a few percent.

A further check of the reliable and consistent

operation of the apparatus was made by determining the smallest burst distinctly observable on the trace. A burst containing approximately 30 particles could be detected at many places along the photographic trace. This fact illustrates that very few, if any, of the 80 particle bursts could have been overlooked in this investigation.

Measurements of bursts in unshielded ionization chambers are complicated by the fact that the very large number of cosmic-ray particles, not associated with showers, are subject to the usual statistical fluctuations. The number of these particles traversing the chamber during a given time interval may differ sufficiently from the average number to produce a relatively sudden deflection of the galvanometer string.[14] It is, then, necessary to construct the apparatus so that these statistical fluctuations can be easily distinguished from real bursts due to air showers. This differentiation was accomplished by making the collection time of the ions in the chamber as small as possible. This establishes a minimum value of the grid resistor R since the time constant (RC value) of the collecting system for the chamber must be long as compared with the collecting time of the ions. If this were not the case, the voltage signal, due to a burst, would be a function of the point in the chamber where the ions are formed.

Schiff and Evans[15] have given a formula for computing the standard deviation of a counting rate meter. This meter consists of a circuit for placing some charge q_1 per count on a condenser C which has a resistor R connected across it. The voltage built up across the resistor R will be a measure of the counting rate. The capacity of each ionization chamber in conjunction with the grid resistor of the FP-54 tube acted essentially as a counting rate meter, within the approximation that the charge generated in the chamber by each cosmic-ray particle is a constant. The formula given by Schiff and Evans for the standard deviation is applicable for the conditions which obtained in the chambers. This is:

$$\sigma = \frac{1}{(2RCn)^{\frac{1}{2}}}, \tag{4}$$

where σ = standard deviation in the voltage across grid resistor R, n = number of rays traversing the chamber per second, C = total input capacity of chamber and amplifier. Evaluation of this formula gives, for the chambers used here, $\sigma = 0.0089$, which corresponds to a deviation in the galvanometer deflection equivalent to that produced by a 60 particle burst. These variations had a long period and produced a continuous trace of an irregular character on the photographic film. These long period irregularities caused by this phenomenon were very seldom larger than the deflections due to 150 particle bursts. In contrast, the bursts were observed as very sharp discontinuities in this irregular trace. However, statistical fluctuations occurring within a time interval equal to the collecting time of the ions (0.4 sec.) could also produce rapid galvanometer deflections which might be mistaken for bursts due to showers.[14] The average number of cosmic-ray particles traversing the chamber in 0.4 sec. was approximately 170. The fluctuation equivalent to the standard deviation would then be 13 particles. The apparatus was not capable of recording a burst as small as this, but a fluctuation occurring within the collection time of the ions generated by a particular shower could reduce or increase the true size of a burst by the amount of this fluctuation. This means that a statistical fluctuation of ten particles would make an 80 particle burst appear as 90 particles, or 70 particles, depending on the direction of the fluctuation. The net result of these fluctuations is to change the slope and the absolute value of the size-frequency distribution curve for a single chamber, making the observed burst rate higher than the true rate. The equation describing this phenomenon, together with methods of determining the correction to be made, will be discussed at length in a paper now in preparation. The correction amounts to about 15 percent at the 80 particle size and decreases to less than 7 percent at the 320 particle size for the chambers used in this experiment. Undoubtedly, the number of observed coincidences will also be too high.

[14] Evaluation of the formula given in Bennett, Brown, and Meyer, Phys. Rev. 47, 437 (1935) for the burst rate caused by statistical fluctuations gives less than one 80-particle burst per year for the conditions of observation at Echo Lake.

[15] L. I. Schiff and R. D. Evans, Rev. Sci. Inst. 7, 456 (1936).

The equation describing the relation between observed and true coincidence rates is yet to be solved. This phenomenon, which is important for small burst sizes, has been neglected in previous size-frequency distribution measurements. Both the chance burst-coincidence rates and the statistical fluctuations can be very much reduced by reducing the collection time of the ions in the chamber. For this reason the author feels that the data given in this paper for the smaller size bursts and at the larger separations of the chambers should be compared with data taken with an instrument of higher resolving power.

A possible source of error, giving rise to too many small burst coincidences at the smaller separations of the chambers, is the presence of slow, heavily ionizing particles. These particles are found in cloud chambers at high altitudes. It is doubtful if this could have an appreciable effect on the number of coincidences observed for several reasons. First, there was very little heavy material in the neighborhood of the chambers in which slow protons could be produced. Second, such heavily ionizing particles do not have sufficient range to traverse a path of 70 cm in argon and penetrate three ionization chamber walls. Third, the decrease in coincidence rate with increasing separation of the chambers is more rapid for the very largest sized bursts than for the smallest. The slow particles would rarely have an ionization density as large as 320 times the average for a single particle, or 500 times the minimum density of a single particle, and, hence, could not affect the larger size bursts.

DISCUSSION

If one assumes the lateral structure predicted by diffusion equations of the cascade theory, the data presented here constitute a direct experimental demonstration of the existence of extensive cosmic-ray air showers containing regions of high particle density which cover at least 100 square meters area. Some of the largest showers observed had a minimum density of 6000 particles per square meter over this 100 square meter area and, hence, contained at least 600,000 particles. In other cases, showers were found which had a minimum density of 9000 particles per square meter over an area of at least 15 square meters. Estimates, from the cascade theory, of the total energy of these showers, based on the assumption that they originate from primary particles at the top of the atmosphere, give a value of nearly 10^{17} ev which represents the highest energy so far reported.

All of the size-frequency distribution curves, Fig. 4, for bursts in a single chamber and for coincident bursts, are better represented by an exponential function than by a power law. The cascade theory, applied to showers originating at the top of the atmosphere from primary electrons having a power law spectrum, gives a size-frequency distribution function of a power law type for bursts in the single chamber. The statistical fluctuations which cause an error in the size of the small bursts cannot explain this discrepancy, since this error changes the slope and absolute values of the size-frequency distribution curve, but does not appreciably change the shape of the curve except for burst sizes smaller than 80 particles. Failure to record all the smaller bursts would result in a deviation of the experimentally determined size-frequency distribution curve away from the power law distribution and toward the exponential distribution. No appreciable number of the smaller bursts could have been overlooked; therefore, the frequencies of the small bursts cannot be expected to be too low. In fact, a considerable difficulty arises because the observed burst frequencies in a single chamber are very much higher than those computed on the basis of a cascade multiplication of electrons entering the earth's atmosphere and having an energy spectrum assumed by Euler[6] and Hilberry.[2]

The frequencies of coincident bursts as a function of separation of the chambers show, for all curves, a rapid decrease in frequency with increasing separation. This decrease is much larger than can be accounted for by the lateral density distribution of cascade showers started from the top of the atmosphere. The strikingly small extension of the high density region of the majority of the showers is shown by the curve in Fig. 4 labeled "zero separation minus 39 cm separation." This curve gives the size-frequency distribution of bursts in one chamber not accompanied by bursts of 80 particles or more in the other chamber, when the chambers are separated

by a distance of 39 cm. This curve reveals that the majority of bursts in one chamber are not in coincidence with a burst in the other chamber. In most cases, even for bursts of several hundred particles in one chamber, no measurable coincident burst was found in the other. An extreme case of such an event was a burst of 960 particles traversing one chamber unaccompanied by as many as 30 particles traversing the other chamber. In this particular case, only 4 cm separated the outer walls of the two chambers (39 cm separation).

The results of this experiment strongly indicate the presence of showers with a very small extension of their high density region. Such showers most probably originate far below the top of the atmosphere, which means that they must be started by high energy electrons or photons of secondary origin. A possible process which could produce electrons at great depths below the top of the atmosphere is the disintegration of a mesotron of very short mean life. The existence of such mesotrons was proposed in the theory of nuclear forces.[16] Hamilton, Heitler and Peng[17] have used this type of mesotron to explain the lower energy soft component close to the top of the atmosphere.

Electrons of high energy could be produced far down in the atmosphere by such a process and might account for the narrow showers of high particle density observed at 10,650 ft. altitude. These showers, then, could produce a high density of particles in one chamber without having as high an energy as would be needed if the showers were started from the top of the atmosphere. This could also explain the high burst rate observed in a single chamber and the lack of a high coincidence rate at small separations of the two chambers.

The author is indebted to Dean A. H. Compton for his generous cooperation which made this work possible; to Professor Marcel Schein for much advice and for suggesting the problem; to E. W. Lewis for her continued help during the recording and analyzing of the data; and to Mr. I. Kalberg for his valuable help in constructing the galvanometers. He wishes to thank General Lawson and Captain Innes-Taylor for their generous assistance throughout the stay of the expedition at Camp Echo; and Mr. Cramner of the Denver Mountain Parks and Dr. Hyslop of the University of Denver for arranging the stay of the expedition in Colorado.

[16] Møller and Rosenfeld, Kgl. Danske Vid. Sels. Math.-Fys. Medd **17** (1940).
[17] Hamilton, Heitler, and Peng, Phys. Rev. **64**, 78 (1943).

PHYSICAL REVIEW VOLUME 67, NUMBERS 7 AND 8 APRIL 1 AND 15, 1945

Theoretical Calculations on Extensive Atmospheric Cosmic-Ray Showers

LINCOLN WOLFENSTEIN
Ryerson Physical Laboratory, University of Chicago, Chicago, Illinois
(Received January 12, 1945)

Large cosmic-ray showers in air, investigated with ionization chambers and coincidence counters, have been explained hitherto as originating from primary electrons of very high energy. In recent experiments at an altitude of 3100 meters Lewis measured the frequency of coincident bursts in two unshielded ionization chambers. The theoretical cumulative frequency $H(P, D)$ of such coincidences is calculated as a function of the electron density P and the separation D of the chambers for this altitude and for sea level. The cumulative size-frequency distribution $H(P)$ for bursts in a single chamber is also computed. All calculations are based on the cascade theory of showers and the theory of the multiple scattering of electrons. The theoretical frequencies compared with those of experiments show (1) a much smaller absolute value, (2) a much slower drop as the chambers are separated, (3) a different form for the cumulative size-frequency distributions, and (4) a smaller increase with altitude. It is pointed out that the large number of narrow showers of high energy observed must originate much nearer to the chamber than the top of the atmosphere if they are to be explained by the cascade theory. It is concluded that the assumption of primary electrons is of little help in explaining the experimental results.

INTRODUCTION

LARGE cosmic-ray showers in air have been explained hitherto as originating from primary electrons of very high energy. The quantitative development of this theory has seemed to be in general agreement with experiments in the two cases it has been carried out. Euler[1] has computed the frequency of sea level bursts in a single unshielded ionization chamber as a function of the size of the burst, and his results are in rough agreement with the experiments of Carmichael[2] and the more recent ones of Lapp.[3] Hilberry[4] has indicated that the results of his experiments on counter coincidences at various altitudes are in agreement with the theory at least for the higher altitudes (2000–4000 meters). None of these experiments, however, gives a complete picture of the shower since experiments with a single chamber do not reveal the extent of the shower and those with counters do not reveal the density in the shower. In recent experiments at Echo Lake, Colorado, Lewis[5] used two unshielded ionization chambers and measured the frequency of coincident bursts as a function of the size of the bursts and the separation of the chambers. These data of Lewis' provide a more critical test for the theory.

To compute theoretically the results of these experiments, a form of the primary electron spectrum at the top of the atmosphere is assumed and the cascade theory of the multiplication in a shower is applied together with the theory of the multiple scattering of electrons. The frequency $H(P)$ of bursts of electron density greater than P in a single unshielded chamber and the frequency $H(P, D)$ of coincident bursts of electron density greater than P in each of two chambers separated by a distance D are calculated for showers detected at Echo Lake (altitude above sea level: 3100 m.; pressure: 52 cm Hg; depth from the top of the atmosphere: 709 g/cm^2 or 16.5 radiation units.) Electron densities from 500/m^2 to 2000/m^2 and chamber separations up to 10 meters are considered. The calculated results, are compared with the experimental results of Lewis.[6] The functions $H(P)$ and $H(P, D)$ are also calculated for showers detected at sea level, and the altitude effect is

[1] H. Euler, Zeits. f. Physik **116**, 73 (1940).
[2] H. Carmichael and D. Chang-Ning Chou, Nature **144**, 325 (1939).
[3] R. Lapp, Phys. Rev. **64**, 129 (1943).
[4] N. Hilberry, Phys. Rev. **60**, 1 (1941).
[5] L. G. Lewis and E. W. Lewis, Phys. Rev. **65**, 63A (1944). The complete work of Lewis is published elsewhere in this issue. The writer wishes to thank Mr. Lewis for giving him the experimental data cited in this paper in advance of publication.
[6] In comparing theory and experiment, it is assumed that the observed bursts are solely due to electrons.

discussed. The function $H(P, D)$ has not as yet been determined experimentally for sea level.

CALCULATIONS FOR SHOWERS DETECTED AT ECHO LAKE

1. Basic Assumptions

The theoretical computation follows the general method used by Euler,[1] but different forms of the functions representing the spatial distribution and energy distribution of the shower electrons are employed. In addition, the zenith angle effect neglected by Euler is considered. Since the calculations are made for large electron densities and small separations of the chambers, the results depend chiefly on the high density region of the showers and on shower electrons above the critical energy in air (about 10^8 ev). This means that the approximations necessary in treating low energy ($<10^8$ ev) shower electrons do not have a great effect on the results.

From the cascade theory the average number of electrons of energy between E and $E+dE$ at a depth of t radiation units from the top of the atmosphere in a shower initiated by a primary electron of energy E_0 can be given by

$$\pi(E_0, E, t)dE = k(t)K(E_0/E, t)\mu(E)E_0/E^2dE. \quad (1)$$

For $t=16.5$, the value[7] of $k(t)$ is 0.034. The function $K(E_0/E, t)$ is equal to unity for that depth t at which $\pi(E_0, E, t)$ is a maximum, but is considerably less for significant departures from the maximum. For $t=16.5$, the function $K(E_0/E)$ was calculated for $E>10^8$ ev and is plotted against $\log_{10}(E_0/E)$ in Fig. 1. For $E<10^8$ ev the cascade theory has not been worked out sufficiently to give $K(E_0/E)$; as an approximation, therefore, $K(E_0/E)$ has been replaced by a factor $K'(E_0)$ depending only on the primary energy E_0. This factor has been determined so that

$$\int_0^{10^8 \text{ ev}} \pi(E_0, E, t)dE$$

is equal to the total number of electrons with energy $E<10^8$ ev in a shower due to a primary electron of energy E_0 as given by the cascade theory. The factor $K'(E_0)$ actually turns out to be very nearly the same as the value of $K(E_0/E)$ in Fig. 1 corresponding to $E=10^8$ ev. The function $\mu(E)$ accounts for the ionization loss of the shower electrons and approaches unity for $E \gg 10^8$ ev. Rossi and Greisen[7] give the form of μ for $E>10^8$ ev, while Richards[8] gives μ down to $E=4\times10^6$ ev.[9]

In treating the spatial distribution of the shower electrons it is assumed that the only significant cause of the lateral spread of the shower is the multiple scattering of electrons in the shower. It is also assumed that the distribution of shower electrons of one particular energy E along an axis perpendicular to the axis of the shower is given by a Gaussian function.[10] Then

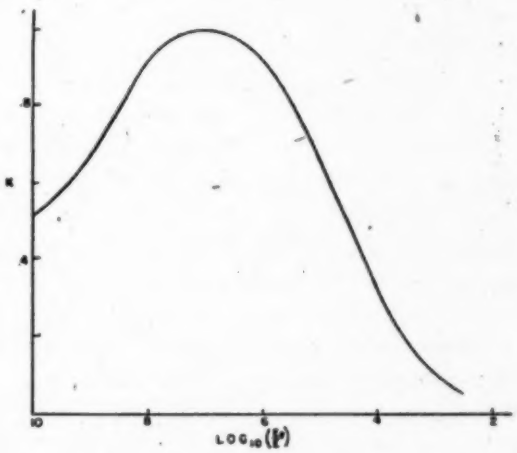

FIG. 1. The function $K(E_0/E)$ for $t=16.5$ and $E>10^8$ ev plotted against $\log_{10} E_0/E$.

[1] Calculations were made from the cascade theory as presented by Rossi and Greisen, Rev. Mod. Phys. 13, 240 (1941).

[8] J. A. Richards and L. W. Nordheim, Phys. Rev. 61, 735 (1942). The complete thesis of Richards, as well as that of Roberg (Note 12), was kindly sent to Dr. Schein at the University of Chicago by Dr. Nordheim in advance of publication. The writer wishes to thank Dr. Nordheim for his permission to use the results obtained in these calculations.

[9] μ is also a function of E_0/E; however, for energies $E>10^8$ ev this dependence can be neglected. For $E<10^8$ ev this dependence is not known.

[10] In a simple problem of the multiple scattering of a beam of particles (for example, mesotrons) of a single energy it is easily shown that the resultant spatial distribution is given by a Gaussian function. In the case of the shower electrons, however, the multiple scattering equation must be combined with the diffusion equations. The combined equations [given by Landau, J. Phys. USSR 2, 237 (1940)] have never been solved. It has been assumed previously (e.g., by Euler) and is also assumed here that the spatial distribution for shower electrons of one particular energy E is not affected critically by the diffusion part of the combined equations and may be given to a good approximation by a Gaussian function.

the probability that an electron of energy E is at a distance between R' and $R'+dR'$ from the axis of the shower in a plane perpendicular to the axis can be given by

$$\varphi(R', E)2\pi R'dR' = (1/2\pi)\, E^2/(0.8\alpha E_s)^2 \times \exp\left(-\frac{R'^2E^2}{2(0.8\alpha E_s)^2}\right)2\pi R'dR', \quad (2)$$

where the distance R' is given in radiation units. The value of the exponent in the Gaussian function is chosen so that the root mean square radial spread for electrons of energy E is equal to $0.8\alpha(E_s/E)\sqrt{2}$ radiation units.[11] The value of $0.8\alpha(E_s/E)\sqrt{2}$ is given by Roberg,[12] and is strictly valid only for energies E corresponding to the maximum of $\pi(E_0, E, t)$ as a function of t (for which $K(E_0/E)=1$). Roberg finds that α is a function of the electron energy E, approaching unity for $E \gg 10^8$ ev. E_s represents a characteristic energy for the scattering of electrons, which has been used in previous calculations of multiple scattering and has a value of 1.5×10^7 ev, independent of material. The dependence of the scattering on E_0/E, which is only important when $\pi(E_0, E, t)$ is far from its maximum, is not known and therefore must be neglected in the calculations. In the present case, however, in which $t=16.5$ and densities between $500/m^2$ and $2000/m^2$ are being considered, the values of $\pi(E_0, E, t)$ used are chiefly those near the maximum. The function $\varphi(R', E)$ is normalized so that

$$\int_0^\infty \varphi(R', E)2\pi R'dR' = 1.$$

It is convenient to introduce as the unit of energy the critical energy in air, about 10^8 ev, and as the unit of length the root mean square lateral spread of shower electrons of the critical energy. This unit of length is equal to 60.6 meters at Echo Lake and is introduced by the equation[13]

$$R' = 0.8E_s r = 0.139r. \quad (3)$$

Introducing this unit into Eq. (2) one obtains

$$\varphi(r, E)2\pi r dr = (1/2\pi)\, E^2/\alpha^2 \exp\left(-\frac{r^2E^2}{2\alpha^2}\right)2\pi r dr. \quad (2')$$

The primary spectrum assumed here for the high energy electrons entering the earth's atmosphere is the same as that which is used for primaries of lower energies. The number of primary electrons of energy greater than E_0 (in critical energy units) incident at the top of the atmosphere per unit time and per unit area is given by

$$N(E_0) = H_1E_0^{-\gamma}, \quad \gamma = 1.8, \quad H_1 = 6\times10^9/\text{hr. m}^2; \quad (4)$$

$$n(E_0) = h_1E_0^{-\gamma}, \quad \gamma = 1.8, \quad h_1 = 2.2\times10^{13}/\text{hr. (60.6 m)}^2. \quad (4')$$

This spectrum is the same as that used by Euler[1] and is very similar to that arrived at by Hilberry.[4]

2. Electron Density Function

The average electron density $\rho(r, E_0)$ recorded by an ionization chamber the center of which is at a distance r from the axis of a shower due to a primary electron of energy E_0 can be given by[14]

$$\rho(r, E_0) = \int_\beta^\infty \varphi(r, E)\pi(E_0, E)dE = \frac{kE_0}{2\pi}\int_\beta^\infty K(E_0/E)\mu(E)/\alpha^2(E) \times \exp\left(-\frac{r^2E^2}{2\alpha^2}\right)dE. \quad (5)$$

The density per square meter is given by

$$P(R, E_0) = \frac{\rho(r, E_0)}{(60.6)^2} = 10^{-3.57}\rho(r, E_0), \quad (5')$$

[11] The value used for the actual length of the radiation unit is that of a radiation unit at the place of observation (436 m at Echo Lake). Because of the fact that the actual length becomes greater with elevation in the atmosphere above the place of observation, one should use a larger value in all the calculations. Since, however, the correct value has not been calculated so far, the value of the radiation length at the place of observation has been used.

[12] Roberg, Phys. Rev. **61**, 735 (1942); **62**, 304 (1942). (See note 7).

[13] Quantities expressed in terms of this unit of length are given in small letters, those expressed in radiation units are given in primed capital letters, and those expressed in meters are given in unprimed capital letters.

[14] The depth t will no longer be given as a variable since the calculations of this part all refer to Echo Lake ($t=16.5$).

TABLE I. $\log_{10} P(R, E_0)$. Electron density as a function of primary energy E_0 and distance R from the axis of the shower.

Log E_0 (in ev)	R (in meters) 0	0.3	0.6	1.2	1.8	2.4	3	4.2	6	12	30	60	85	106
14.5	3.09	2.73	2.51	2.29	2.15	2.04	1.96							
15.2	4.03	3.60	3.35	3.10	2.94	2.83	2.73	2.60	2.45	2.14	1.70	1.28	.98	
15.7		4.18	3.92	3.65	3.48	3.37	3.27	3.13	2.97	2.64	2.20	1.77	1.47	1.22
16.2			4.45	4.17	4.00	3.88		3.62	3.45	3.12	2.67	2.24	1.94	1.69
16.7										3.57	3.10	2.67	2.37	2.12

where $R=60.6r$. It is assumed that no multiplication takes place in the walls of the chamber, but that there is a lower limit β to the energy E of electrons which can penetrate the walls. The value used for the energy β is 4 Mev; however, using $\beta=0$ does not change the values of the density function significantly except for $r>1$ ($R>60$ m).

Equation (5) is based on the assumption that the density recorded by the chamber is equal to the density at the center of the chamber. This assumption is approximately true except in the relatively rare instances that the axis of the shower is within the chamber (r less than the radius of the chamber). For such values of r and for values of $E(>2\times10^{10}$ ev) for which the root mean square radial spread is of the same order of magnitude as the radius of the chamber, the integrand in the integral of Eq. (5) must be replaced by the density of these high energy shower electrons averaged over the chamber. This consideration enters the calculations only in the case $r=0$ and turns out to have very little effect on the final calculated burst frequencies. For the calculation of $\rho(0, E_0)$ the radius was taken to be about 17.5 cm so that the results would correspond to the experiments of Lewis.[5]

The explicit form of the electron density $\rho(r, E_0)$ as a function of r may be seen readily for primary energies E_0 of about 10^{16} ev and for values of r between 0.02 and 0.10 (1.2 to 6 m) since in this case the energies E contributing mainly to the integral of Eq. (5) have values between 10^8 and 10^{10} ev for which the functions $K(E_0/E)$, $\mu(E)$, and $\alpha(E)$ are all close to unity. Using the approximation $K=\mu=\alpha=1$ in Eq. (5), we have

$$\rho(r, E_0)\simeq 1.25kE_0/2\pi r. \qquad (6)$$

For very small values of r, higher values of E and correspondingly lower values of the function $K(E_0/E)$ contribute significantly to the integral, causing the electron density $\rho(r, E_0)$ to rise less rapidly than the function $(1/r)$. For large values of r, electrons of energy E less than 10^8 ev become relatively more important; this causes the electron density $\rho(r, E_0)$ to fall more rapidly than $(1/r)$.

The values of the electron density $\rho(r, E_0)$ for various distances r from the axis of the shower and various primary electron energies E_0 have been found by numerical integration of Eq. (5). The values of the $\log_{10} P(R, E_0)$ are given in Table I for values of R between 0 and 106 m and values of E_0 between $10^{14.5}$ and $10^{16.7}$ ev. For two values of the primary energy E_0 representative of those important in this problem, $10^{15.2}$ and $10^{16.2}$ ev, the density $P(R, E_0)$ is plotted as a function of R on a double logarithmic graph in Fig. 2. The broken curve in the figure represents the lower curve placed a cycle higher so that the form of the function may be compared for the two values of the primary energy. It can be seen that the electron density as a function of R is almost independent of the primary energy E_0, although for the larger value of E_0 the density is relatively greater near the axis of the shower and less far from the axis than for the smaller value.

To a first approximation, therefore, the density $\rho(r, E_0)$ may be represented for primary energies E_0 between 10^{15} and $10^{16.5}$ ev and for all values of r by

$$\rho(r, E_0)=E_0q(r)/r. \qquad (6')$$

The electron density function of Eq. (6') with $q(r)$ set equal to an exponential function of the form e^{-r} is practically the same as that of Euler.[1] Euler's unit of length, however, is much smaller, since his calculation of the root mean square ra-

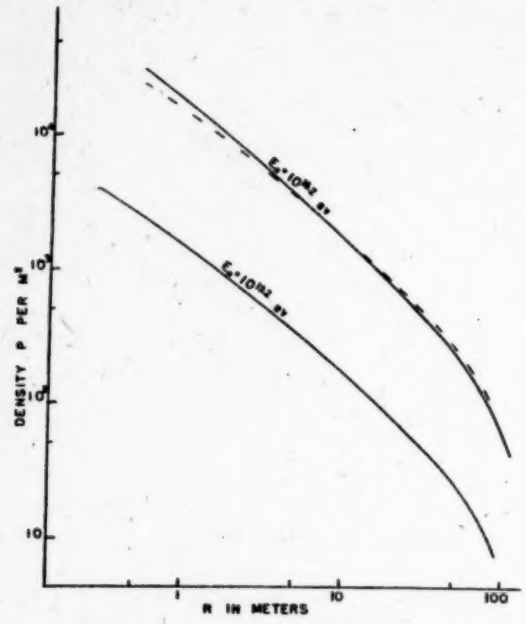

FIG. 2. Electron density $P(R, E_0)$ at Echo Lake plotted as a function of the distance R from the axis of the shower for primary energies E_0 of $10^{15.2}$ and $10^{16.2}$ ev. The broken curve shows the lower curve placed a cycle higher.

dial spread of shower electrons gives a value only one-third of that calculated by Roberg.[12] A less important difference is that the function $q(r)$ in the present calculation falls off somewhat less rapidly than an exponential for $r<1.5$ ($R<90$ m). This difference is most likely due to Euler's failure to consider the factor $\alpha(E)$.

The approximate percentage contributions of shower electrons of different energy ranges E to the value of $P(R, E_0)$ are shown in Table II for different distances R. For $R<12$ meters this is given for a shower of primary energy E_0 equal to $10^{15.7}$ ev, while for $R\geq 12$ meters it is given for the particular case in which the function $K(E_0/E)$ is always 1. It was found that to a good approximation the values in Table II can be considered as correct for all values of E_0 between $10^{14.5}$ and $10^{16.5}$ ev.

3. Frequency of Single and Coincident Bursts

From the values of $\rho(r, E_0)$ which have been calculated the theoretical frequency of bursts in a single chamber and of coincident bursts in two chambers can be obtained. Inverting $\rho(r, E_0)$ we find $E_0(\rho, r)$, which is the minimum energy of a primary electron in order that on the average the shower it produces has an electron density greater than ρ at a distance r from the axis. Then, introducing the primary spectrum (Eq. (4)), the number of showers per unit time and per unit area having a density greater than ρ at a distance r from their axes is given by

$$n(E_0)=h_1E_0^{-\gamma}(\rho, r). \tag{7}$$

Considering all values of r, the frequency of all bursts of density greater than ρ in the chamber is given by

$$H'(\rho)=2\pi h_1\int_0^\infty E_0^{-\gamma}(\rho, r)rdr. \tag{8}$$

Similarly from a simple geometrical construction[1] the frequency of simultaneous bursts of densities greater than ρ in each of two chambers separated by a distance d is given by

$$H'(\rho, d)=2\pi h_1\int_{d/2}^\infty E_0^{-\gamma}(\rho, r)\frac{\arccos(d/2r)}{\pi/2}rdr. \tag{9}$$

Notice that $H'(\rho, 0)=H'(\rho)$. It is also of interest to consider the median values $\bar{r}(\rho, d)$ and $\bar{E}_0(\rho, d)$ defined by:

$$\tfrac{1}{2}H'(\rho, d)=2\pi h_1\int_{d/2}^{\bar{r}} E_0^{-\gamma}(\rho, r)\frac{\arccos(d/2r)}{\pi/2}rdr \tag{10}$$

$$\bar{E}_0(\rho, d)=E_0(\rho, \bar{r}). \tag{10'}$$

Equations (8) and (9) would give the actual frequencies only if all the primary electrons were directed close to the vertical. However, it seems probable that the directions of these extremely high energy electrons are distributed uniformly over a solid angle of 2π. The electrons entering at a large angle θ to the vertical must traverse a much greater thickness t of the atmosphere and

TABLE II. Approximate percentage contribution of electrons of energy ranges E to $P(R, E_0)$ for various values of R.

	R (in meters)											
E (in ev)	0.6	1.2	1.8	2.4	3.0	4.2	6	12	18	30	60	85	106
$<10^8$	1	2	3	4	5	7	10	23	35	54	84	95	99
10^8–10^9	9	17	25	30	37	49	70	74	65	46	16	5	1
10^9–10^{10}	62	78	72	66	58	44	20	3					
$>10^{10}$	28	3	0.2										

therefore will produce a lower electron density $\rho(r, E_0)$ and a lower coincidence frequency $H'(\rho, d)$ than those coming from the vertical. The exact calculation of such a zenith angle effect, which would require the computation of $H'(\rho, d, \theta)$ for primary electrons entering at various angles θ, has not been carried out here in view of the fact that it would not affect the nature of the results. As a first approximation to take the zenith angle effect into account, however, the function $H'(\rho, d)$ has been multiplied by a factor $z(\rho, d)$ depending only on the median energy $\bar{E}_0(\rho, d)$.

To find this factor the energy $E_0'(\theta, E_0)$ defined as the minimum primary energy of an electron entering at an angle θ necessary to produce the same total number of electrons at the level of observation as a primary of energy E_0 entering vertically, is calculated from the cascade theory. If we define $z(E_0)$ by

$$z(E_0)=\int_0^{\pi/2}\frac{n(E_0')}{n(E_0)}\sin\theta d\theta, \qquad (11)$$

then the factor $z(\rho, d)$ can be given by

$$z(\rho, d)=z(\bar{E}_0). \qquad (11')$$

The value of z varies from 0.28 for $\bar{E}_0=10^{15.5}$ ev to 0.42 for $\bar{E}_0=10^{16.5}$ ev. If we introduce this factor, the frequency of coincident bursts can be given by

$$H(\rho, d)=2\pi h_1 z(\rho, d)\int_{d/2}^{\infty}E_0^{-\gamma}(\rho, r)\times\frac{\arccos(d/2r)}{\pi/2}rdr. \qquad (9')$$

The frequency of bursts in a single chamber follows directly:

$$H(\rho)=H(\rho, 0)=2\pi h_1 z(\rho, 0)\int_0^{\infty}E_0^{-\gamma}(\rho, r)rdr. \qquad (8')$$

TABLE III. Calculated frequency per hour $H(P, D)$ of coincident bursts at Echo Lake.

Separation D (in meters)	Density P 500/m²	1000/m²	2000/m²
0	0.064	0.0198	0.0060
0.6	0.0605	0.0183	0.00545
1.2	0.058	0.0172	0.0051
2.4	0.053	0.0156	0.0046
4.8	0.0455	0.0131	0.00385
9.6	0.036	0.0101	0.00285

The exact calculation of $z(\rho, d)$ might change the absolute values of the calculated frequencies by 20 percent, but this would not be a significant change in the results. The most important change that might be effected by the exact calculation is in the form of $H(\rho, d)$ as a function of d, but it is more likely that the effect would be to decrease rather than to increase the slope of this curve.

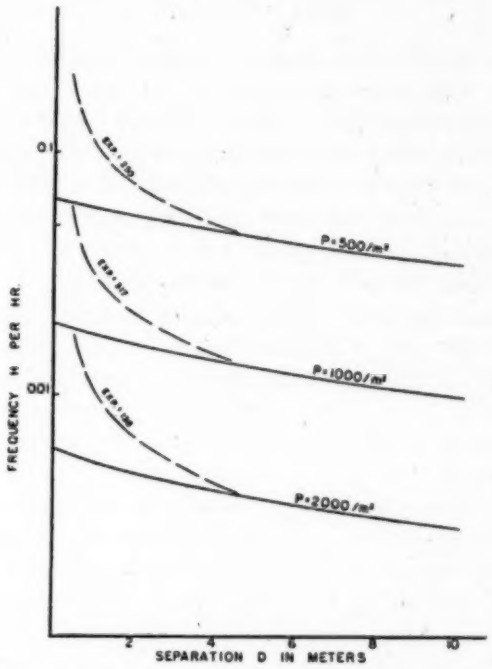

FIG. 3. Calculated coincidence frequency per hr $H(P, D)$ for Echo Lake as a function of D for densities P greater than 500/m², 1000/m², and 2000/m². The broken curves show the corresponding experimental frequencies divided by factors of 250, 317, and 136, respectively, for values of D between 0.6 m and 4.5 m.

To get an approximate picture of $H(\rho)$ as a function of ρ one can use the approximation for $\rho(r, E_0)$ given in Eq. (6'). Solving for E_0 one obtains

$$E_0(\rho, r)=\frac{\rho r}{q(r)} \qquad (12)$$

and, substituting this value of $E_0(\rho, r)$ into Eq. (8'),

$$H(\rho)=2\pi h_1 z(\rho, 0)\rho^{-\gamma}\int_0^{\infty}[q(r)]^{\gamma}r^{-\gamma+1}dr. \qquad (13)$$

For values of ρ corresponding to densities from 500/m² to 2000/m², 70 percent of the integral of

Eq. (13) is contributed by values of $E_0(\rho, r)$ between 10^{15} and $10^{16.5}$ ev, for which the approximations used in obtaining Eq. (6′) are reasonably good. Neglecting the variation of $z(\rho, 0)$ with ρ for this range of densities, we find

$$H(\rho) = \text{const } \rho^{-\gamma}. \qquad (14)$$

This means that $H(\rho)$ is a power function of ρ with the same exponent γ as figures in the primary spectrum $N(E_0)$. If the variation of $z(\rho, 0)$ with ρ is introduced, the approximate form of $H(\rho)$ can still be given by Eq. (14), but the absolute value of the exponent must be decreased slightly (from 1.8 to about 1.7).

Table III and the corresponding Figs. 3 and 4 show the result of the exact evaluation of Eqs. (8′) and (9′).[15] Figure 3 shows the frequency $H(P, D)$ of coincidences between two ionization chambers as a function of the distance D between them up to 10 meters for densities P greater than 500/m², 1000/m², and 2000/m². In Fig. 4 the frequency $H(P, D)$ of coincidences is plotted on a double-logarithmic graph as a function of the density P for separations D of 1.2, 4.8, and 9.6 meters; the cumulative size-frequency curve $H(P)$ for bursts in a single chamber ($D=0$) is also shown. It is seen that each of the theoretical curves of Fig. 4 approximately satisfies Eq. (14) and thus reflects the primary energy spectrum $N(E_0)$. Table III gives all the calculated values of $H(P, D)$.

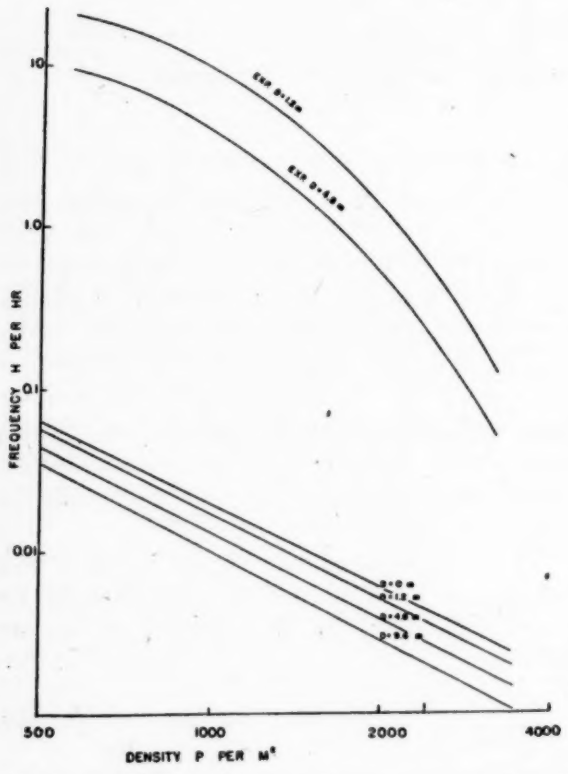

FIG. 4. Calculated coincidence frequency per hr $H(P, D)$ for Echo Lake as a function of P for separations D of 1.2, 4.8, and 9.6 m. The curve labeled $D=0$ is the cumulative size-frequency curve $H(P)$ for bursts in a single chamber. The two top curves are the corresponding experimental functions for $D=1.2$ m and $D=4.8$ m.

Table IV shows the percentage contribution of different ranges of r and of the corresponding ranges of the minimum energy $E_0(\rho, r)$ to the function $H'(\rho)$ (Eq. 8) for densities ρ corresponding to 500/m² and 2000/m². The corresponding values of $\bar{R}$ and $\bar{E}_0$ are also given. Because $H'(\rho)$ does not take into account the zenith angle effect, Table IV gives only an approximation to the contributions to the total burst frequency $H(P)$ of different primary energies E_0 and of different distances R of the chamber from the axis of the shower. Table IVa shows the approximate percentage contributions to the function $H'(\rho)$ from different energy ranges E for the same densities. It therefore gives an approximation to the average energy distribution of electrons in bursts of densities greater than 500/m² and 2000/m², respectively.

From Table IV it is seen that the frequencies depend very little on values of $R>60$ m ($r>1$), which has the consequence that the lower limit β to admitted energies E has little effect on the results. Similarly values of $R<20$ cm contribute very little, so that the results are almost independent of the size of the chamber for those chambers generally used. Table IVa indicates a 20 percent contribution to the results from values of $E<10^8$ ev, for which the calculations are only approximate. It should be noted that the contribution of these low energies is greater for the lower densities and also for the greater separations of the chambers, so that these results have to be considered less accurate. Table IV also indicates that for the 2000/m² density there is at least a 7 percent contribution to the calculated results from primary energies greater than 10^{17} ev. Experiments in which

[15] The functions $H(P, D)$ and $H(P)$ are obtained from $H(\rho, d)$ and $H(\rho)$, respectively, by the relations: $P=\rho/3700$ and $D=60.6d$.

TABLE IV. Percentage contribution of ranges of R and of the corresponding minimum energies $E_0(P, R)$ to the integral $H'(P)$ (Eq. (8)).

Density P	E_0	$10^{14.2}$–10^{15}	10^{15}–$10^{15.5}$	$10^{15.5}$–10^{16}	10^{16}–$10^{16.5}$	$10^{16.5}$–10^{17}	$>10^{17}$ ev	
500/m²	R	0–1.8	1.8–7.0	7.0–20	20–43	43–73	>73 m	$\bar{R}=7.5$ m
	%	18	29	26	18	7.5	1.5	$\bar{E}_0=10^{15.88}$ ev
2000/m²	R	0–0.4	0.4–1.7	1.7–5.4	5.4–15	15–36	>36 m	$\bar{R}=5.4$ m
	%	7	17	25	27	17	7	$\bar{E}_0=10^{16}$ ev

larger densities are measured and larger separations of the chambers are used than in those experiments carried out hitherto would be required to determine whether any showers of such enormous energies exist.

If the unit of length, that is, the root mean square radial spread of shower electrons is divided by a factor σ, it can be shown that the approximate effect is to multiply the burst frequency $H(P)$ by a factor of $\sigma^{2(\gamma-1)}$. Thus, the effect of using Euler's value for the radial spread would be to multiply $H(P)$ by a factor of $3^{1.6}$, or 6.

4. Comparison with Experiment

The experimental observations of Lewis[5] at Echo Lake, which are also shown in Figs. 3 and 4,[16] differ from the results of the present calculations in three striking ways. (*a*) The experiments show a much sharper decrease in the frequency of coincident bursts as the separation of the two chambers is increased up to 3 m. This is seen from the broken curves of Fig. 3, which represent the experimental frequencies reduced in magnitude so that the forms of the experimental and theoretical curves may be compared. The experimental curves are not shown for values of D between 5 and 10 m because the difference between the forms of the experimental and the theoretical curves for these values cannot be considered significant. (*b*) The experimental cumulative size-frequency distributions for different separations D of the chambers are represented by similar curves of an exponential type in contrast to the theoretical power-law curves. Figure 4 shows two such curves for $D=1.2$ m and $D=4.8$ m plotted on a double-logarithmic graph. (*c*) The absolute values of the observed single and coincident burst frequencies are much greater than the corresponding theoretical values. For example, for densities greater than 1000/m² the observed values are greater by a factor of about 550 in the case of the two chambers separated by a distance of 1 m and by a factor of about 300 in the case of 5 m separation. As the density increases above 1000/m², however, the corresponding theoretical and observed cumulative frequencies approach each other in value (Fig. 4).

TABLE IVa. Approximate contribution of ranges of values of electron energy E to $H'(P)$.

E (in ev)	$<10^8$	10^8–10^9	$>10^9$
Density P			
500/m²	23	43	34
2000/m²	15	35	50

[16] The experimental curves shown in Figs. 3 and 4 do not pass through actual experimental points, but were obtained by graphical interpolation of the experimental data. The experimental results shown for densities P less than 800/m² were obtained by extrapolation.

CALCULATIONS FOR SHOWERS DETECTED AT SEA LEVEL

A similar calculation of the frequencies $H(P)$ and $H(P, D)$ has been carried out for sea level ($t=24$) for electron densities P of 500/m² and 2000/m² and separations D up to 14 meters. This calculation is less accurate than that for Echo Lake because of the fact that for these densities at sea level there is a much larger contribution from shower electrons of energies E less than 10^8 ev. It was pointed out before that in this case special approximations have to be made. This also means that the results are more dependent on the lower limit β to admitted energies. In addition to this, for the primary energies which contribute most to the results for the above-mentioned densities (E_0 about 10^{16} ev), $\pi(E_0, E, t)$ (Eq. (1)) must be used farther from its maximum as a function of t, so that Eq. (2) for the spatial distribution of the shower electrons is less valid. From Eq. (3), for $t=24$, the unit of length is 42 meters.

Table V gives the calculated values of $H(P)$ and $H(P, D)$. The results, particularly for the lower density, must be considered as first approximations. The general form of the cumulative size-frequency distribution $H(P)$ can be obtained by the method used before (Eqs. (12–14)). It is found that for primary energies around 10^{16} ev the approximation

$$\rho(r) = (E_0)^{1.2} q'(r)/r, \qquad (15)$$

should be used in place of Eq. (6′). This gives

$$H(\rho) = \text{const } \rho^{-\gamma/1.2} = \text{const } \rho^{-1.5}. \qquad (16)$$

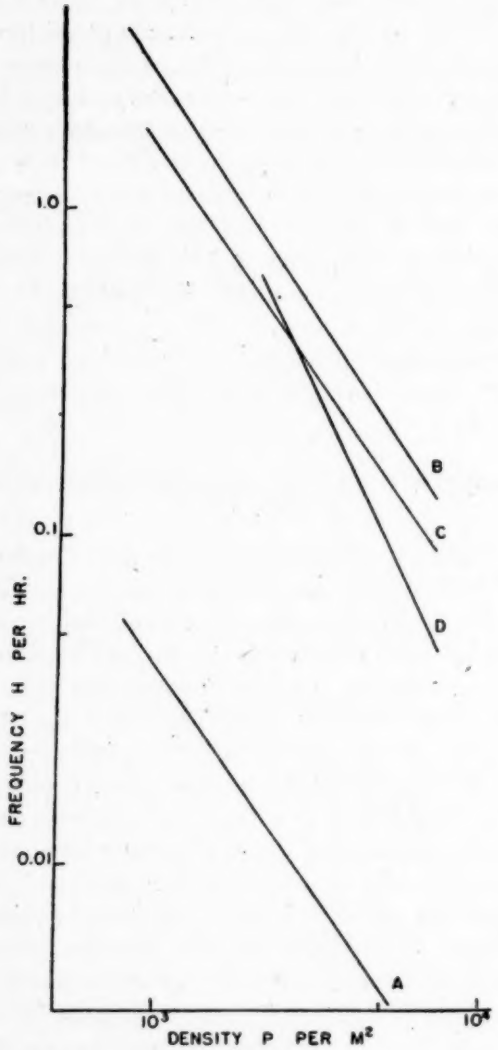

FIG. 5. Cumulative size-frequency function $H(P)$ for bursts in a single chamber at sea level. Curve A shows the results of the present calculations, curve B represents the corresponding theoretical results of Euler, while curves C and D show the experimental results of Carmichael and Lapp, respectively.

Introducing $z(\rho, 0)$ to account for the zenith angle effect results in a change of the exponent of Eq. (16) from 1.5 to 1.4. Curve A in Fig. 5 shows the calculated form of the function $H(P)$, curve B represents the corresponding theoretical results of Euler,[1] and curves C and D show the experimental results of Carmichael[2] and Lapp,[3] respectively. All the curves are approximated as straight lines, and only a representative portion of each is shown. The main reasons for the large discrepancy between the theoretical results obtained here and those obtained by Euler are the small value used by Euler for the mean square radial spread and the fact that he neglected completely the zenith angle effect. It is seen from Fig. 5 that even at sea level the experimental burst frequencies are about forty times greater than the theoretical ones. Furthermore the exponent in Lapp's experimental cumulative frequency function is greater than 2 in contrast to the theoretical Eq. (16).

Of particular interest is the remarkable difference which exists between the calculated and experimental altitude effects for bursts in an unshielded ionization chamber. The observed increase in frequency from sea level to Echo Lake (3100 meters) appears to be as much as 400[17] for densities greater than 2000/m², which is much larger than that observed in counter experiments on extensive atmospheric showers. According to the theory, the bursts discussed here are on the average due to higher primary energies than the energies responsible for the counter observations and therefore should show an even smaller altitude effect. The calculations give an increase of frequency with altitude of 5.7 for densities greater than 1000/m² and 4 for densities greater than 2000/m².

CONCLUSION

The relatively large discrepancies which have been noted between the theoretical results and those of experiment do not seem to be explainable in any simple manner. Changing the form of the lateral distribution of shower electrons from the

[17] This may be calculated approximately by using the experimental results of Lapp and Carmichael at sea level and those of Lewis at Echo Lake. Unpublished sea-level data obtained at the University of Chicago with the same ionization chamber as that used by Lewis also give this result.

assumed Gaussian function or changing the form of the assumed primary electron spectrum (Eq. (4)) could, at best, it seems, resolve only part of these discrepancies. The sharp drop in frequency of coincidences observed by Lewis as the two chambers were separated indicates the presence at an altitude of 3100 meters of relatively narrow showers of high particle density which must originate fairly close to (a few radiation units above) the chambers if they are to be explained by the cascade theory. Since, for a given electron density in the chamber the total energy contained in such showers can be much less than that contained in showers close to their maximum development, it is reasonable that the narrow showers are observed more frequently even though the probability of any one shower's hitting the chambers is much less. The presence of these narrow showers, therefore, might explain in part the much larger absolute values of the experimental frequencies in comparison to the theoretical ones. The method by which the high energy ($>5\times10^{11}$ ev) electron or photon necessary to originate such a shower can be brought to the level at which such showers start is not known. Any explanation must also account for the large altitude effect for the bursts. It would be of great interest to know whether this altitude effect for bursts in an unshielded ionization chamber continues to be so large as the altitude increases above 3100 meters.

One might think now that the results could be explained by considering two types of showers, the narrow showers of an unexplained origin and the showers from primary electrons of very high energy. The introduction of such narrow showers, however, fails to explain the discrepancy that still seems to exist between the theoretical frequencies calculated above and the frequencies observed by Lewis for coincident bursts between two chambers separated by distances of 5 to 10 meters. This discrepancy exists both in the absolute values and in the form of the cumulative size vs. frequency distribution. These coincident bursts might be explained by showers originating higher than the narrow showers but well below the top of the atmosphere. The total energy in such a shower for a given density need not be so great as in a shower due to primaries, and consequently the frequency of these showers might be greater. It should be noted that in any case for such coincident bursts the energy of the electron initiating the shower must be greater than 10^{14} ev, if the shower is of the cascade variety. Only for the largest densities and separations of the chambers in the experimental results does it appear that a significant fraction of the observations can be explained by showers due to primary electrons; these, however, could be just as well explained by showers initiated by secondary electrons produced near the top of the atmosphere.

TABLE V. Calculated coincidence frequency per hour $H(P, D)$ at sea level.

Separation D (in meters)	Density P 500/m²	2000/m²
0	0.0105	0.00148
.85	0.0100	0.00141
3.4	0.0090	0.00126
6.8	0.0079	0.00108
13.6	0.0063	0.00087

It may therefore be concluded that the assumption of primary electrons is of little help in explaining the observations on extensive atmospheric showers detected at an altitude of 3100 meters. The experiments carried out at sea level are too incomplete to allow conclusions to be drawn from them.

I wish to thank Dr. L. W. Nordheim for providing unpublished theoretical results used in this paper and to express my sincere appreciation to Professor Marcel Schein, who suggested this problem and who devoted many hours to advice and discussion on it.

The Electron Optics of Mass Spectrographs and Velocity Focusing Devices

R. G. E. HUTTER*
Division of Electron Optics, Stanford University, California
(Received January 29, 1945)

The well-known results of the theory of mass spectrometers and velocity focusing devices are derived again by a different method which is simpler than the ones previously used and which brings out more clearly the electron optical nature of the deflecting and focusing properties of the fields employed in these types of instruments.

THE deflecting and focusing properties of electrostatic and magnetic fields used in mass spectrometers and velocity focusing devices have been treated theoretically by R. Herzog[1] and W. Henneberg.[2] These authors derived expressions for the optical quantities of such systems. The methods employed are, however, not adequate to the electron optical nature of the problem. Because Newton's force equations were used as the basic equations, the time had to be eliminated by special manipulations so that path equations could be obtained. These derivations are therefore rather involved. It might be useful to give a derivation of the results in a manner which has become the typical method for the treatment of electron optical phenomena. This method has been used by O. Scherzer[3] for electron lenses of rotational symmetry about an axis, by J. Picht, J. Himpan,[4] and G. Wendt[5] for the deflecting fields in television tubes and cathode ray tubes. A paper by G. Wendt[6] deals with the dioptrics of electron optical devices with arbitrarily curved axes. The general expressions obtained there could be applied to yield the formulae derived in the present work as far as the first-order properties are concerned. Since we are going to investigate also second-order aberrations and chromatic aberration, it seems advisable to give a complete theory of the problems involved.

(1) THE GENERAL PATH EQUATION

The index of refraction of an electromagnetic field in cartesian coordinates x,y,z is given by:

$$n=[(2e/m)\varphi(xyz)]^{\frac{1}{2}}-(e/m)(\mathbf{A}\cdot\mathbf{s}), \quad (1)$$

where $\varphi(xyz)$ is the electrostatic potential, $\mathbf{A}$ is the magnetic vector potential, $\mathbf{s}$ is a unit vector in the direction of the path, e and m are charge and mass of the particle respectively, and $(\mathbf{A}\cdot\mathbf{s})$ is the scalar product of the two vectors $\mathbf{A}$ and $\mathbf{s}$.

Fermat's principle can then be written in the form

$$\delta\int_{P_1}^{P_2}[[(2e/m)\varphi(xyz)]^{\frac{1}{2}}-(e/m)(\mathbf{A}\cdot\mathbf{s})]ds=0. \quad (2)$$

Transforming this expression to cylindrical coordinates r, θ, z, we get:

$$\delta\int_{P_1}^{P_2}[[(2e/m)\varphi(r,\theta,z)]^{\frac{1}{2}}[r^2+(r')^2+(z')^2]^{\frac{1}{2}} -(e/m)(A_r r'+A_\theta r+A_z z')]d\theta=0, \quad (3)$$

since

$$ds=[r^2+(r')^2+(z')^2]^{\frac{1}{2}}d\theta. \quad (4)$$

The prime signifies derivation with respect to θ.

The necessary conditions for Eq. (3) to be true are the following differential equations, called the Euler-Lagrange equations:

* The author is now a research physicist with Sylvania Electric Products, Inc., New York. The paper was completed while he was Research Associate in the Division of Electron Optics at Stanford University, California.

[1] R. Herzog, Zeits. f. Physik **89**, 447 (1934).

[2] W. Henneberg, Ann. d. Physik **19**, 335 (1934); Ann. d. Physik **20**, 1 (1934); Ann. d. Physik **21**, 390 (1934)

[3] O. Scherzer, Zeits. f. Physik **101**, 593 (1936).

[4] J. Picht and J. Himpan, Ann. d. Physik **39**, 409 (1941); Ann. d. Physik **39**, 436 (1941); Ann. d. Physik **39**, 478 (1941).

[5] G. Wendt, Die Telefunkenroehre **15**, 100 (1939).

[6] G. Wendt, Zeits. f. Physik **120**, 720 (1943).

$$\left[\frac{2\varphi(r\theta z)}{r^2+(r')^2+(z')^2}\right]^{\frac{1}{2}}\frac{d}{d\theta}\left\{r'\left[\frac{2\varphi(r\theta z)}{r^2+(r')^2+(z')^2}\right]^{\frac{1}{2}}\right\}$$

$$=\frac{\partial\varphi(r\theta z)}{\partial r}+\frac{2\varphi(r\theta z)}{r^2+(r')^2+(z')^2}r$$

$$-\left(\frac{e}{m}\right)^{\frac{1}{2}}[rH_z-z'H_\theta]\cdot\left[\frac{2\varphi(r\theta z)}{r^2+(r')^2+(z')^2}\right]^{\frac{1}{2}},$$

$$\left[\frac{2\varphi(r\theta z)}{r^2+(r')^2+(z')^2}\right]^{\frac{1}{2}}\frac{d}{d\theta}\left\{z'\left[\frac{2\varphi(r\theta z)}{r^2+(r')^2+(z')^2}\right]^{\frac{1}{2}}\right\}$$

$$=\frac{\partial\varphi(r\theta z)}{\partial z}-\left(\frac{e}{m}\right)^{\frac{1}{2}}[r'H_\theta-rH_r]$$

$$\cdot\left[\frac{2\varphi(r\theta z)}{r^2+(r')^2+(z')^2}\right]^{\frac{1}{2}}. \tag{5}$$

Use has been made of the definition of **A** as:

$$\mathbf{H}=\text{curl }\mathbf{A},$$

or in components

$$H_r=-\frac{\partial A_\theta}{\partial z}+\frac{1}{r}\frac{\partial A_z}{\partial\theta},\quad H_\theta=-\frac{\partial A_z}{\partial r}+\frac{\partial A_r}{\partial z},$$

$$H_z=\frac{1}{r}\left(\frac{\partial}{\partial r}(rA_\theta)-\frac{\partial A_r}{\partial\theta}\right). \tag{6}$$

We now consider the following field combination given by:

$$H_\theta=H_r=0,\quad H_z=H\neq 0,\quad \varphi=\varphi(r). \tag{7}$$

Equations (5) become

$$\left[\frac{2\varphi(r)}{r^2+(r')^2+(z')^2}\right]^{\frac{1}{2}}\frac{d}{d\theta}\left\{r'\cdot\left[\frac{2\varphi(r)}{r^2+(r')^2+(z')^2}\right]^{\frac{1}{2}}\right\}$$

$$=\frac{2\varphi(r)}{r^2+(r')^2+(z')^2}-\left(\frac{e}{m}\right)^{\frac{1}{2}}\left[\frac{2\varphi(r)}{r^2+(r')^2+(z')^2}\right]^{\frac{1}{2}}r$$

$$\cdot H+\frac{\partial\varphi(r)}{\partial r}, \tag{8a}$$

$$\left[\frac{2\varphi(r)}{r^2+(r')^2+(z')^2}\right]^{\frac{1}{2}}\frac{d}{d\theta}\left\{z'\cdot\left[\frac{2\varphi(r)}{r^2+(r')^2+(z')^2}\right]^{\frac{1}{2}}\right\}=0. \tag{8b}$$

From Eq. (8b) we can see that z' is identically equal to zero if it was equal to zero for $\theta=0$, i.e., electron paths remain in the plane $z=$const. if their initial slope z' was zero. If we therefore exclude all rays whose initial slope z' is different from zero, we need consider only Eq. (8a) which can be reduced to:

$$\frac{d}{d\theta}\left\{r'\cdot\left[\frac{2\varphi(r)}{r^2+(r')^2}\right]^{\frac{1}{2}}\right\}=\left[\frac{2\varphi(r)}{r^2+(r')^2}\right]^{\frac{1}{2}}r$$

$$-\left(\frac{e}{m}\right)^{\frac{1}{2}}r\cdot H+\left[\frac{r^2+(r')^2}{2\varphi(r)}\right]^{\frac{1}{2}}\frac{d\varphi(r)}{dr}. \tag{9}$$

The electrostatic field $\varphi(r)$ shall now be that of a cylinder condenser which we can write in the form

$$\varphi(r)=\phi_0+[(V_2-V_1)/(\ln R_2/R_1)]\ln(r/r_0) \tag{10}$$

where V_2-V_1 is the potential difference between the two coaxial cylinders of radii R_1 and R_2. ϕ_0 is the superimposed constant potential. We therefore have:

$$\varphi(r_0)=\phi_0.$$

The condition for a path to be circular is:

$$r'\equiv 0.$$

Hence the radius of the circular path is given by:

$$r_0=\frac{(V_2-V_1)/(\ln R_2/R_1)+2\phi_0}{(2e\phi_0/m)^{\frac{1}{2}}}\cdot\frac{1}{H}, \tag{11}$$

with

$v_0=(2e\phi_0/m)^{\frac{1}{2}}$, initial velocity of the particle,

and

$\omega_0=v_0/r_0$, angular velocity of the particle,

we get:

$$ev_0\cdot H=e\frac{V_2-V_1}{\ln R_2/R_1}\cdot\frac{1}{r_0}+m\frac{v_0^2}{r_0}=e\cdot\frac{d\varphi}{dr}+m\frac{v_0^2}{r_0}.$$

This is Newton's force equation for a particle moving on a circular path through the combined electrostatic and magnetic field.

It has been shown by W. Henneberg that the final formulae are simple if expressed in terms of a quantity y defined by:

$$y=-(V_2-V_1)/(2\phi_0\ln R_2/R_1), \tag{12}$$

or

$$y=-[e(V_2-V_1)(1/r_0)/(\ln R_2/R_1)]/m(v_0^2/r_0).$$

y is therefore that fraction of the centrifugal force on the circular path which is compensated

by the electrostatic force. We have $y=0$ for a purely magnetic field and $y=1$ for a purely electrostatic field.

Equation (9) can only be solved by methods of approximation. In order to achieve this, we need a number of expansions of expressions occurring in Eq. (9). With

$$r=r_0+x, \quad \text{or} \quad r/r_0=1+x/r_0=1+z, \tag{13}$$

and Eqs. (11) and (12) we get:

$$\begin{aligned}
(2\varphi)^{\frac{1}{2}}&=(2\phi_0)^{\frac{1}{2}}(1-yz+\tfrac{1}{2}y(1-y)z^2\\
&\quad -\tfrac{1}{6}y(2-3y+3y^2)z^3+\cdots),\\
2\varphi^{-\frac{1}{2}}&=(2\phi_0)^{-\frac{1}{2}}(1+yz-\tfrac{1}{2}y(1-3y)z^2\\
&\quad +\tfrac{1}{6}y(2-9y+15y^2)z^3+\cdots),\\
(r^2+(r')^2)^{\frac{1}{2}}&=r_0(1+z+\tfrac{1}{2}(z')^2-\tfrac{1}{2}z(z')^2+\cdots),\\
(r^2+(r')^2)^{-\frac{1}{2}}&=(1/r_0)(1-z+z^2-\tfrac{1}{2}(z')^2\\
&\quad +\tfrac{3}{2}z(z')^2-z^3+\cdots),\\
d\varphi/dr&=-(1/r_0)2\phi_0 y(1-z+z^2-z^3)+\cdots,\\
H\cdot r_0&=(2\phi_0 m/e)^{\frac{1}{2}}\cdot(1-y).
\end{aligned} \tag{14}$$

If we exclude all third and higher order terms in z and z' Eq. (9) becomes:

$$\begin{aligned}
[d/d\theta][z'-(1-y)zz']&=-[z+y^2z\\
&\quad +\tfrac{1}{2}y(1-3y^2)z^2+\tfrac{1}{2}(1-y)(z')^2].
\end{aligned} \tag{15}$$

The method which is typical to electron optical investigations proceeds now as follows. The first step towards a solution of Eq. (15) will lead to a path function fundamental to the Gaussian dioptrics of the system by taking into account only first order terms in Eq. (15). After this has been achieved, the effect of second-order terms will be investigated.

(2) THE GAUSSIAN DIOPTICS

We assume that:

$$z\ll 1, \quad z'\ll 1, \tag{16}$$

so that z^2, zz', $(z')^2$ can be neglected compared with z and z'. We then get the following so-called paraxial equation:

$$[d/d\theta][z_g']=-[1+y^2]z_g. \tag{17}$$

The index g shall indicate that the solution is correct only if the conditions (16) are satisfied, i.e., within the limits of the Gaussian dioptrics.

The solution of Eq. (17) is well known; it is

$$z_g=a\sin(1+y^2)^{\frac{1}{2}}\theta+b\cos(1+y^2)^{\frac{1}{2}}\theta, \tag{18}$$

where a and b are two constants of integration. If $r=r_0$ for $\theta=0$, we have with (13):

$$r=r_0+ar_0\sin(1+y^2)^{\frac{1}{2}}\theta. \tag{19}$$

We therefore see that all (paraxial) electron paths leaving the point $\theta=0$, $r=r_0$ pass again through the (circular) axis ($r=r_0$) at:

$$\theta=\pi/(1+y^2)^{\frac{1}{2}}. \tag{20}$$

For a purely magnetic field we have $y=0$ and hence

$$\theta=\pi=180°.$$

For a purely electrostatic field we have $y=1$ and hence

$$\theta=\pi/\sqrt{2}=127°\ 17'.$$

In order to derive the expressions for the optical quantities of the system, we make use of the general results of the theory developed by W. Glaser.[7]

If the field has a finite extent along the optical axis and if the paraxial ray equation is a linear differential equation of the second order, the optical quantities can be expressed in terms of two linearly independent solutions of the ray equation. The shape of the field is shown in Fig. 1. Let z_{g1} and z_{g2} be two linearly independent solutions of Eq. (17) which satisfy the following conditions:

$$\begin{aligned}
z_{g1}(\theta_a)&=1, \quad z'_{g1}(\theta_a)=0,\\
z_{g2}(\theta_a)&=0, \quad z'_{g2}(\theta_a)=1.
\end{aligned} \tag{21}$$

Such a pair of solutions is:

$$\begin{aligned}
z_{g1}&=\cos(1+y^2)^{\frac{1}{2}}(\theta-\theta_a),\\
z_{g2}&=(1+y^2)^{-\frac{1}{2}}\sin(1+y^2)^{\frac{1}{2}}(\theta-\theta_a).
\end{aligned} \tag{22}$$

We then obtain the expressions for the optical quantities by substituting the functions (22) into Glaser's formulae.

[7] W. Glaser, Zeits. f. Physik **80**, 451 (1933); Zeits. f. Physik **81**, 649 (1933); Zeits. f. Physik **83**, 104 (1933); Zeits. f. Physik **97**, 177 (1935).

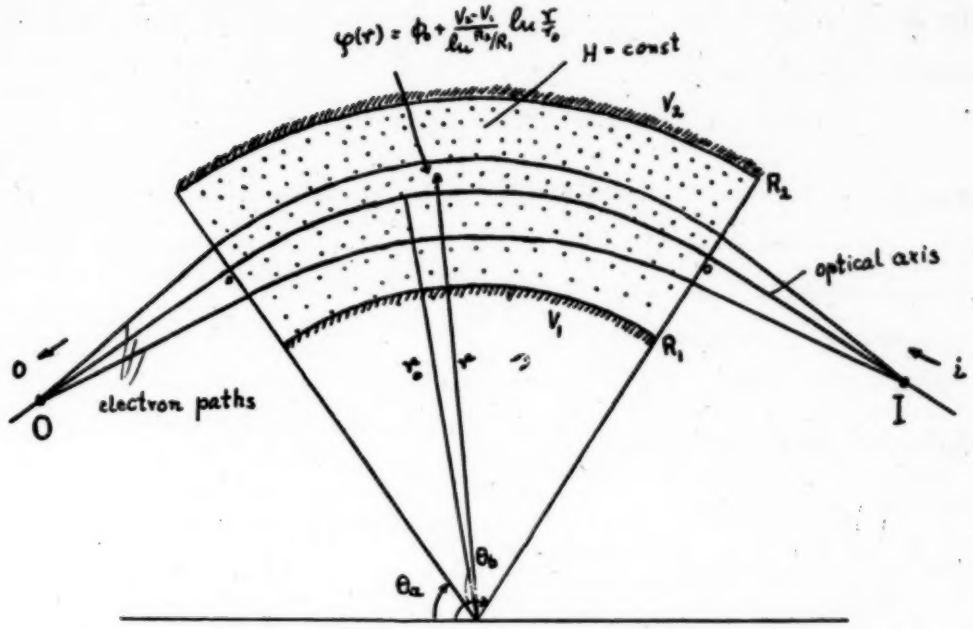

FIG. 1. The geometry of the fields.

Focal lengths:

$$f_0=\frac{z'_{g1}(\theta_b)z_{g2}(\theta_b)-z_{g1}(\theta_b)z'_{g2}(\theta_b)}{z'_{g1}(\theta_b)}r_0$$

$$=\frac{r_0}{(1+y^2)^{\frac{1}{2}}}\frac{1}{\sin(1+y^2)^{\frac{1}{2}}(\theta_b-\theta_a)}, \tag{23}$$

$$f_i=-\frac{1}{z'_{g1}(\theta_b)}r_0$$

$$=\frac{r_0}{(1+y^2)^{\frac{1}{2}}}\frac{1}{\sin(1+y^2)^{\frac{1}{2}}(\theta_b-\theta_a)}.$$

Focal points:

$$F_0=-\frac{z'_{g2}(\theta_b)}{z'_{g1}(\theta_b)}r_0=\frac{r_0}{(1+y^2)^{\frac{1}{2}}}\cot(1+y^2)^{\frac{1}{2}}(\theta_b-\theta_a), \tag{24}$$

$$F_i=-\frac{z_{g1}(\theta_b)}{z'_{g1}(\theta_b)}r_0=\frac{r_0}{(1+y^2)^{\frac{1}{2}}}\cot(1+y^2)^{\frac{1}{2}}(\theta_b-\theta_a).$$

Principal points:

$$H_0=-f_0+F_0=-\frac{r_0}{(1+y^2)^{\frac{1}{2}}}\tan\tfrac{1}{2}(1+y^2)^{\frac{1}{2}}(\theta_b-\theta_a), \tag{25}$$

$$H_i=-f_i+F_i=-\frac{r_0}{(1+y^2)^{\frac{1}{2}}}\tan\tfrac{1}{2}(1+y^2)^{\frac{1}{2}}(\theta_b-\theta_a).$$

Object-image relation:

$$(i-H)\cdot(0-H)=f^2. \tag{26}$$

The system of coordinates is chosen so that the origins are the boundaries of the field θ_a and θ_b. In both regions the direction from the left to the right is defined as the positive direction.

(3) SECOND-ORDER ABERRATION

Taking now into account the second-order terms in Eq. (15), we can determine the line width which is the actual image of a mathematical line of the object space. To obtain this line width, we proceed in a manner typical to electron optics. We replace in Eq. (15) z and z' in the second-order terms by z_g and z'_g since these terms will differ very little from the actual ones. We therefore have:

$$[d/d\theta][z']+[1+y^2]z$$
$$=(1-y)(d/d\theta)(z_g z'_g)-\tfrac{1}{2}y(1-3y^2)z_g^2$$
$$+\tfrac{1}{2}(1-y)(z'_g)^2. \tag{27}$$

The general solution of this equation is the sum of the general solution of Eq. (17) and a particular solution of Eq. (27). With the expression (22) Eq. (27) becomes:

$$z''+A\cdot z=C_1+C_2\cos m\theta+C_3\sin m\theta. \tag{28}$$

A particular solution is given by:

$$z_p=(C_1/A)+[C_2/(A-m^2)]\cos m\theta + [C_3/(A-m^2)]\sin m\theta, \quad (29)$$

where

$$\begin{aligned} A&=1+y^2,\\ C_1&=-\tfrac{1}{4}(a^2+b^2)(1+y^2-4y^3),\\ C_2&=\tfrac{1}{4}(a^2-b^2)(3-2y+3y^2-6y^3),\\ C_3&=\tfrac{1}{2}ab(3-2y+3y^2-6y^3),\\ m&=2(1+y^2)^{\frac{1}{2}}. \end{aligned} \quad (30)$$

The general solution of Eq. (27) is therefore:

$$\begin{aligned} z=a\sin(1+y^2)^{\frac{1}{2}}\theta+b\cos(1+y^2)^{\frac{1}{2}}\theta \\ -\tfrac{1}{4}(a^2+b^2)\frac{1+y^2-4y^3}{(1+y^2)} \\ -\tfrac{1}{12}(a^2-b^2)\frac{3-2y+3y^2-6y^3}{(1+y^2)}\cos 2(1+y^2)^{\frac{1}{2}}\theta \\ -\tfrac{1}{6}ab\frac{3-2y+3y^2-6y^3}{(1+y^2)}\sin 2(1+y^2)^{\frac{1}{2}}\theta. \end{aligned} \quad (31)$$

The initial conditions for z shall now be:

$$\begin{aligned} z(0)&=b-\tfrac{1}{4}(a^2+b^2)\frac{1+y^2-4y^3}{1+y^2} \\ &\quad -\tfrac{1}{12}(a^2-b^2)\frac{3-2y+3y^2-6y^3}{1+y^2}=0. \end{aligned} \quad (32)$$

$$z'(0)=a\left(1-\tfrac{1}{2}b\frac{3-2y+3y^2-6y^3}{1+y^2}\right)(1+y^2)^{\frac{1}{2}}=\alpha.$$

At $\theta=\pi/(1+y^2)^{\frac{1}{2}}$ we then have:

$$\begin{aligned} z\left[\frac{\pi}{(1+y^2)^{\frac{1}{2}}}\right]&=-b-\tfrac{1}{4}(a^2+b^2)\frac{1+y^2-4y^3}{1+y^2} \\ &\quad -\tfrac{1}{12}(a^2+b^2)\frac{3-2y+3y^2-6y^3}{1+y^2}, \end{aligned} \quad (33)$$

or with Eq. (32)

$$z[\pi/(1+y^2)^{\frac{1}{2}}]=-2b. \quad (34)$$

Since b will be proportional with α^2 we have:

$$b=C\alpha^2. \quad (35)$$

If we neglect now all terms higher than α^2 in (31) we get:

$$C=1+\tfrac{1}{3}y+y^2+3y^3/(1+y^2)^2, \quad (36)$$

hence

$$z\left[\frac{\pi}{(1+y^2)^{\frac{1}{2}}}\right]=-\alpha^2\frac{1+\frac{1}{3}y+y^2+3y^2}{(1+y^2)^2}, \quad (37)$$

the line width will then be

$$L=-\alpha^2\frac{1+\frac{1}{3}y+y^2+3y^3}{(1+y^2)^2}r_0. \quad (38)$$

In case of a purely magnetic field ($y=0$)

$$L_m=-\alpha^2 r_0.$$

For an electrostatic field ($y=1$)

$$L_e=-(4/3)\alpha^2 r_0.$$

(4) CHROMATIC ABERRATION

If the wedge of electrons entering the field is not homogeneous with respect to the velocity, the image line will again be of a finite width. In order to obtain an expression for this width we let:

$$\varphi(r)=\phi_0+\Delta\phi_0+[(V_2-V_1)/(\ln R_2/R_1)]/\ln r/r_0, \quad (39)$$

where

$$|\Delta\phi_0/\phi_0|\ll 1. \quad (40)$$

The solution of Eq. (9) will be assumed to be of the form:

$$r=r_0+x+\delta$$

or

$$\frac{r}{r_0}=1+\frac{x+\delta}{r_0}=1+z+\sigma=1+z_1. \quad (41)$$

We expand again the expressions in Eq. (9) in power series of z_1 and z_1' similarly to those of Eq. (14). The differential equation for z_1 then becomes:

$$\begin{aligned} \frac{d}{d\theta}\left[z'_1\left(1+\frac{1}{2}\frac{\Delta\phi_0}{\phi_0}\right)\right]&=\frac{1}{2}\frac{\Delta\phi_0}{\phi_0}(1+y) \\ &\quad -z_1(1+y^2)-\frac{1}{2}\frac{\Delta\phi_0}{\phi_0}yz_1(1+3y). \end{aligned} \quad (42)$$

If the particle travels initially perpendicularly to the field lines and would describe the circular path of radius r_0 ($\Delta\phi_0=0$) we have $z=0$. If

$\Delta\phi_0 \neq 0$ the deviation from the circular path is therefore given by the following differential equation:

$$\sigma''+\sigma(1+y^2)=\tfrac{1}{2}(1+y)\Delta\phi_0/\phi_0. \quad (43)$$

The general solution of this equation is given by:

$$\sigma=a\sin(1+y^2)^{\frac{1}{2}}\theta+b\cos(1+y^2)^{\frac{1}{2}}\theta+\tfrac{1}{2}(1+y)\Delta\phi_0/\phi_0. \quad (44)$$

With the initial conditions:

$$\sigma=\sigma'=0 \text{ for } \theta=0, \quad (45)$$

we get:

$$a=0, \quad b=-\frac{1}{2}\frac{(1+y)}{(1+y^2)}\frac{\Delta\phi_0}{\phi_0}. \quad (46)$$

At $\theta=\pi/(1+y^2)^{\frac{1}{2}}$ we therefore have:

$$\sigma\left[\frac{\pi}{(1+y^2)^{\frac{1}{2}}}\right]=\frac{1+y}{1+y^2}\frac{\Delta\phi_0}{\phi_0}. \quad (47)$$

Since $(2e\phi_0/m)^{\frac{1}{2}}=v_0$ we have:

$$\frac{d\phi_0}{\phi_0}=2\frac{dv_0}{v_0}, \quad (48)$$

and since $\delta=\sigma\cdot r_0$, we get for the line width D:

$$D=2\frac{1+y}{(1+y^2)}r_0\frac{dv_0}{v_0}. \quad (49)$$

Since the velocity resolution is only noticeable if it causes the line width to be greater than that due to second-order aberrations, a quantity τ has been introduced called the reduced resolution. It is defined by:

$$\tau=|D/L|\alpha^2. \quad (50)$$

We get for τ:

$$\tau=2\left|\frac{1+y+y^2+y^3}{1+\frac{1}{3}y+y^2+3y^3}\right|. \quad (51)$$

PHYSICAL REVIEW VOLUME 67, NUMBERS 7 AND 8 APRIL 1 AND 15, 1945

On Permanent Charges in Solid Dielectrics

I. Dielectric Absorption and Temperature Effects in Carnauba Wax

B. Gross and L. Ferreira Denard
National Institute of Technology, Rio de Janeiro, Brazil

(Received February 6, 1945)

The influence of the temperature upon dielectric absorption is studied for carnauba wax. Isothermic and non-isothermic current-time curves are measured. It is shown that a considerable part of the absorbed charge can be "frozen in," if the temperature is reduced to a value sufficiently inferior to that prevailing during the charging period before the system is short-circuited. The "frozen" charge dissipates extremely slowly, if the temperature is kept low, but it is liberated rapidly if the temperature is raised again. The effect is explained by the increase of the charging and discharging rates with increasing temperature. It is closely related to the permanent moment of the electret.

I. INTRODUCTION

An electret is a dielectric body that retains an electric moment after the externally applied electric field has been reduced to 0. It was shown by Eguchi[1] that permanent electrets are obtained when certain waxes and resinous materials, mainly carnauba wax, previously melted, are allowed to solidify while exposed to strong electric fields. Eguchi's results were considered very startling ones because for a long time it was the general opinion that any self-maintained electric field in solid bodies would soon be neutralized in consequence of the movement of the free electric charges existing in all substances. But these results have been confirmed and completed by various authors.[2] While the behavior of the electret is now fairly well known, no generally accepted explanation of its

[1] M. Eguchi, Phil. Mag. 49, 178 (1925).

[2] A. Gemant, Phil. Mag. 20, 929 (1935); W. M. Good and J. D. Stranathan, Phys. Rev. 56, 810 (1939).

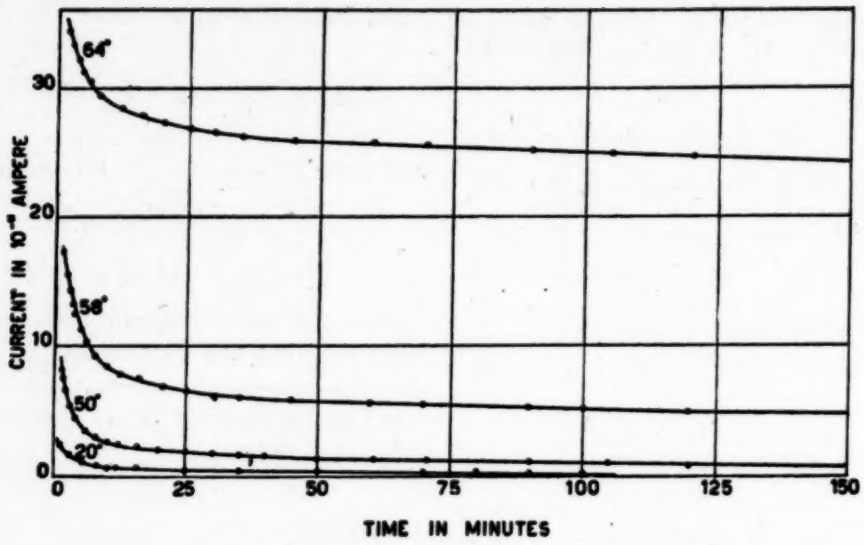

FIG. 1. Charging currents for different temperatures.

physical mechanism has been established so far. Formally, the existence of a permanent electric moment of a dielectric body must be considered as representing one more form of the "anomalous" behavior of solid dielectric. The fundamental form of anomalous behavior is dielectric absorption, which for solid dielectrics is characterized by the appearance of the reversible *absorption* or *anomalous charging* current. The condition of reversibility granted, other forms of anomalous behavior—variance of capacitance with time, dielectric loss, and residual charge—can be calculated quantitatively from the data for the absorption current.[3] This suggests the existence of a physical relationship between dielectric absorption and the permanent moment of the electret. And it can be expected that further information about the properties of electrets would derivate from the systematic study of the influence of temperature upon dielectric absorption for dielectrics which are submitted to a heat treatment similar to that of Eguchi's electret.

The influence of the temperature upon dielectric absorption has been treated in a general way by K. W. Wagner.[4] He showed that for heterogeneous dielectrics the total amount of absorption is nearly independent of the temperature, while the rate of absorption increases strongly with increasing temperature. Wagner was able to establish a simple relationship between the form of the absorption currents for different temperatures, which he exemplified by the results of many measurements performed with technical insulators. Many other measurements are due to J. B. Whitehead.[5] Non-isothermic current-time curves for quartz are reported by Altheim.[6] Groetzinger[7] observed considerable discharge currents when capacitors containing beeswax previously solidified under the influence of an electric field were reheated beyond the melting point of the wax.[7] Other authors who have studied the conductance of crystalline dielectrics occasionally also refer to non-isothermic effects.[8]

In this paper we relate a series of measurements of temperature effects for carnauba wax.

II. TECHNIQUE OF MEASUREMENT

Samples of carnauba wax, 1 mm in thickness and having an area of about 15 cm², were chemically silvered on both faces and put between

[3] E. v. Schweidler, "Die Anomalien der dielektrischen Erscheinungen," in L. Graetz, ed. *Handbuch d. Elektrizitaet u. d. Magnetismus* (Johann Ambrosius Barth, Leipzig, 1918), Vol. I, p. 232.

[4] K. W. Wagner, in H. Schering ed., *Die Isolierstoffe der Elektrotechnik* (Verlagsbuchhandlung Julius Springer, Berlin, 1924), p. 24.

[5] J. B. Whitehead, Physics **2**, 82 (1932).

[6] O. G. v. Altheim, Ann. d. Physik **35**, 417 (1939).

[7] H. Frei and G. Groetzinger, Physik. Zeits. **37**, 720 (1936).

[8] A. F. Joffé, *The Physics of Crystals* (McGraw-Hill Book Company, Inc., New York, 1928), p. 109; F. Quittner, Zeits. f. Physik **56**, 597 (1929).

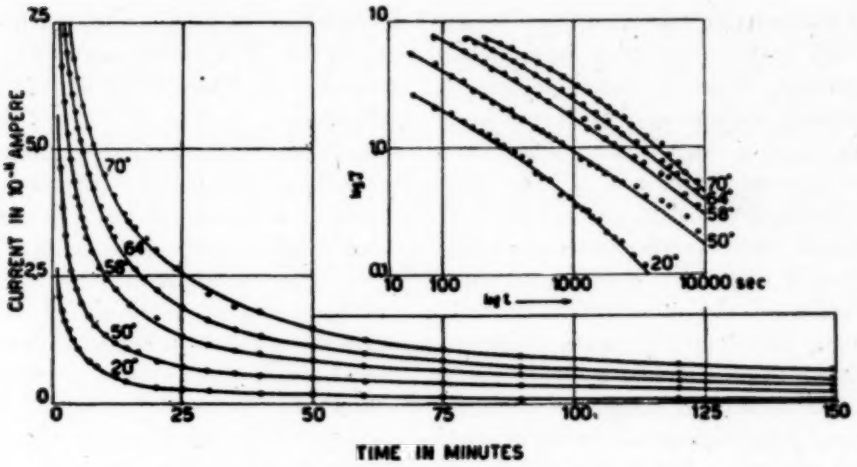

FIG. 2. Discharge currents for different temperatures.

plates in a small oven suitable for measurements up to 100°C. Readings of the temperature were taken with the aid of a mercury thermometer put closely at the side of the sample. The current was measured in most cases by the potential difference it produced across the terminals of a high-ohm resistor (10^{10}–10^{12} ohm) connected in series with the sample. But sometimes the current was measured by taking the charging time curve of an air capacitor (50 to 2.000 $\mu\mu$f) connected in place of the resistor. The potential difference in both cases was measured with a one-string fiber electrometer. The tension applied to the system was furnished by dry cells. In most measurements it was equal to 118 v.

III. ISOTHERMIC CURRENT-TIME CURVES

Figure 1 gives the charging currents for different temperatures between 20°C and 70°C. The currents at the higher temperatures are considerably stronger than those at the lower temperatures, but the main increase is obviously due to a rise of the steady state current. The influence of the temperature upon this latter

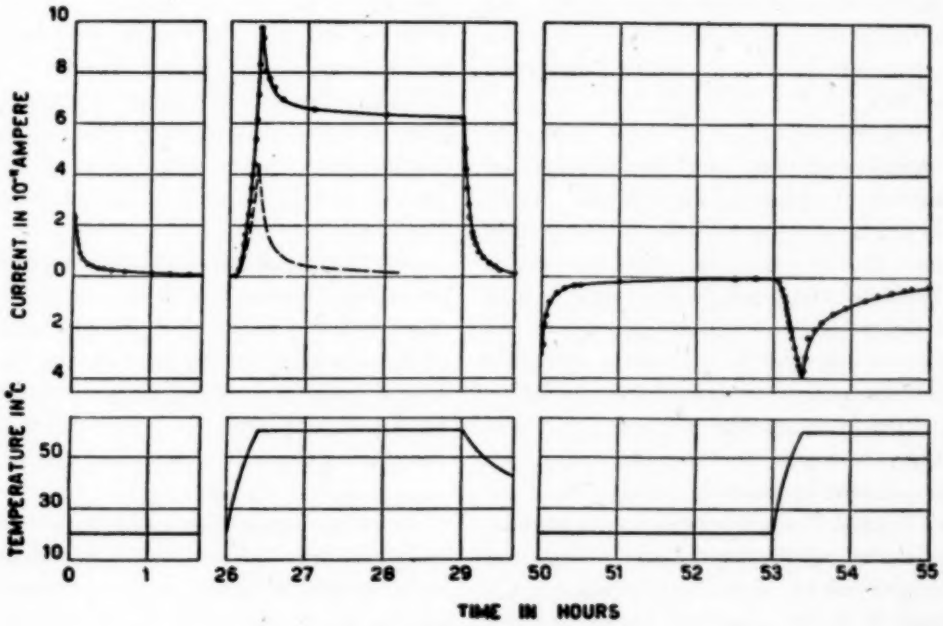

FIG. 3. Non-isothermic effect.

component of the current is known; here we are interested mainly in the behavior of the transient current component. This is shown in Fig. 2, where the discharge currents are indicated in an ordinary scale and a logarithmic scale. The charging time, in every case, was 20 hours; the temperature during the charge was the same as that indicated for the corresponding discharge. These currents rise with increasing temperature. Within the limits of the experiment, the discharged quantity of electricity and, therefore, the dielectric absorption, increase with increasing temperature. No saturation value and no intersection of curves belonging to different temperatures were observed. Yet an intersection of curves for different temperatures may still occur at times greater than those for which measurements could be taken.

IV. NON-ISOTHERMIC EFFECTS

And now we investigated the influence of temperature changes upon capacitors, which either were energized by a constant voltage source or were kept in short-circuit after having been subjected to a constant tension. The general aspect of the currents so produced is seen from Fig. 3. There are 5 phases of the experiment.

(1) *A constant potential difference is applied to the capacitor* at low temperature (20°C). The usual absorption current is observed. After one day, this current has decreased to a very low value. No measurable steady state current is observed at 20°C.

(2) *The temperature of the energized capacitor is rapidly heightened*, then maintained constant again. A sudden increase of the current is observed; it is due in part to the rise of the steady state current. But a transient also appears; it manifests itself by the peak in the current-time curve, the occurrence of which coincides with the moment when the temperature becomes constant. This transient is found to depend on the temperature and on the slope of the temperature-time curve; if the temperature rises rapidly, the current increase is stronger and the peak higher than if the temperature rises slowly.

The appearance of the transient can be predicted from the study of the isothermic curves of Figs. 1 and 2. If the capacitor is charged, for the same time, once at a low temperature and a second time at a high temperature, then according to the data of the isothermic curves, in the second case more electricity is stored up in the system than in the first one. Therefore, if the temperature of the same capacitor, while energized by a constant voltage source, is raised from a low to a high level, the system passes from a state of low absorption to a state of high absorption. This must have the same effect as a voltage jump. Accordingly, the increase in temperature is followed by a transient current. The current subsequent to a slow increase of the temperature is lower than the current subsequent to a rapid increase, just as it happens for variations of the applied potential difference.

The temperature is maintained high for a time sufficiently long to let the transient decay far below the level of the steady state current.

(3) *The temperature of the energized capacitor is reduced* to the initial low value. The current falls off very rapidly, but it depends now on the instantaneous values of the temperature only, not on the slope of the temperature-time curve. No transient is observed. We conclude that the current-temperature function obtained during the cooling period gives the relation between steady state current and temperature. The knowledge of this function enables us to evaluate what fraction of the current during the heating period is due to the steady state current and what is due to the transient. To obtain the latter, from every point of the current-time curve obtained during the heating period one must subtract the current value observed for the corresponding temperature during the cooling period. In this way, the dashed curve of Fig. 3 was obtained.

(4) *The capacitor is short-circuited* at low temperature (20°C). The usual discharge current is observed. Its magnitude at any instant is that of the corresponding value of the charging current belonging to the same temperature. This behavior shows that in spite of the additional absorption caused by the heating, the principle of superposition remains valid.

More generally, it could be established that the discharge current does not depend on the temperature at which the capacitor is charged, provided this temperature is not inferior to the temperature during the discharge. This condition

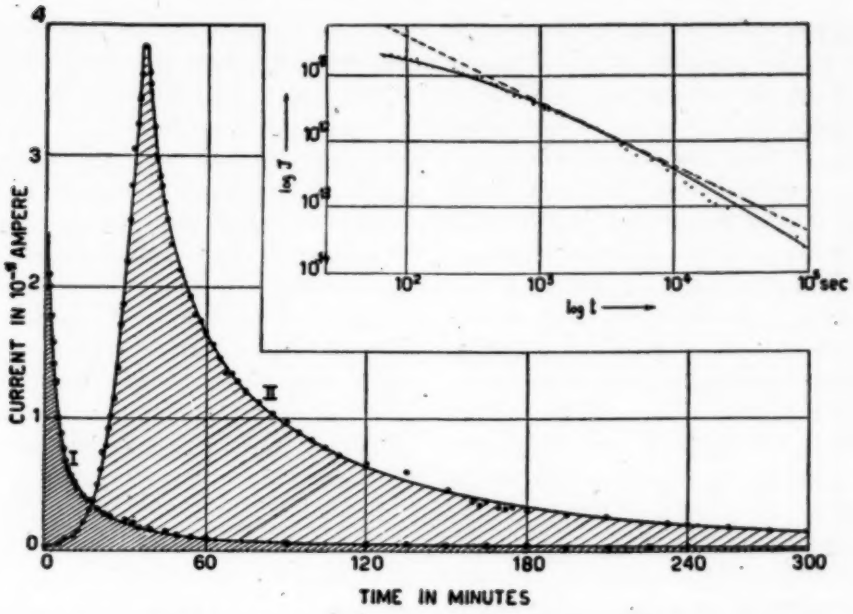

FIG. 4. I—Discharge current at 26°C. II—Discharge current raised in consequence of reheating of the dielectric to 70°C, 24 hours after short-circuiting. Inset—Absorption current at 26°C.

granted, the discharge current at any temperature has the same values which would be observed under the conditions of the isothermic experiment to which Figs. 1 and 2 refer.

(5) *The temperature of the shorted capacitor is raised* in the same way as before, then maintained constant. Again a transient is observed, similar to that subsequent to the first heating, but now in the direction of a discharge current. This behavior confirms our earlier conclusion that the first transient is a reversible absorption current, by which electric charge is stored up in the capacitor. During the cooling of the energized capacitor, no discharge takes place—this is testified by the absence of any transient during this stage of the experiment. After the short-circuit at low temperature, the charge stored up in the system is removed at the same slow rate as it was absorbed during the first stage of the experiment. The quantity of electricity absorbed during the heating period remains apparently "frozen" in the dielectric. It is liberated by the reheating of the capacitor.

The amount of liberated charge is independent of the rate of the previous cooling. It increases with increasing temperature and duration of the charging period; it decreases slowly when the interval of time between short-circuiting and reheating is lengthened. In one case, for example, an increase of this interval from 165 min. to 15 days resulted in a reduction of less than 20 percent of the liberated charge. This slowness of dissipation was confirmed by other measurements covering the period of 2 years.

With regard to the influence of the voltage, a linear relationship was found for values up to 10.000 v/cm.

V. THE PHENOMENON OF THE "FROZEN" CHARGE

There are two characteristic features of the effect: (1) No transient appears during the cooling of the energized capacitor. (2) The discharge current depends only on the temperature of the capacitor during the discharge. We conclude therefrom that the effect does not involve any variation with temperature of the total absorption capacitance (defined by the integral over the relaxation function), but that it must be explained by the variance of the charging and discharging rates. It follows that the absorption capacitance must be much higher than could have been inferred so far from measurements far below the melting point. At such temperatures, the rate of absorption is so low that it is practically impossible to charge the capacitor to any

considerable degree. The charge, which is absorbed during weeks or even years, would be only a fraction of the saturation value. With increasing temperature, the rate of absorption increases; then, during the same time, more charge can be absorbed than before although saturation may still be far ahead. Conversely, if a charged capacitor is cooled and is shorted at a temperature far below that at which it was charged, the rate of discharge at the low temperature is so low that the quantity of electricity discharged during a long time represents only a small part of the quantity of electricity previously absorbed. The same reason which does not allow the capacitor to be completely charged at the low temperature, now prevents it from being completely discharged. And so, if one has succeeded in getting the capacitor strongly charged by charging it at a high temperature, one may trap the bulk of the absorbed charge by the cooling experiment.

Some numerical data may be obtained from Fig. 4. The capacitor, to which this figure refers, was charged with 118 v at 70°C during 24 hours. Then it was cooled to room temperature (26°C) and shorted; 24 hours after the sudden short-circuit it was heated again to 70°C and remained at this temperature for one day. Curve II gives the discharge current flowing during the reheating; the area under this curve gives the liberated charge. During the first 5 hours of discharge 1.3×10^{-7} coulomb are liberated. The absorption current at 26°C is given by Curve I in a simple and in a logarithmic scale (inset). An upper limit to the observed values of the current is represented by the dashed curve (inset), given by $J=4\times10^{-9}/t$ (J in amperes, t in seconds). An extrapolation of this function to greater values of t permits an evaluation of the rate of dissipation of the frozen charge; according to this equation, 100,000 years after the sudden short-circuit there would still be left in the capacitor almost half the charge, which at 70°C is absorbed within a few hours. A lower limit for the total amount of the absorbed charge of the capacitor can be calculated from the areas under Curves I and II; one obtains 1.6×10^{-7} coulomb. If one takes into account the value of the applied potential difference and the dimensions of the sample, there results for the static dielectric constant a lower limit of 135. In consequence of the extrapolations involved, these calculations have only a purely qualitative value. But they show at least that in the low temperature range one has to count with relaxation times of the order of thousands of years. This order of magnitude is at first sight surprising. But it may be remembered that similar values occur for the elastic after-effect, the relation of which to the electric effect has been observed repeatedly.[9] The discharge current curves for different temperatures must overlap themselves mutually. But at low temperatures, the points of intersection are so far from origin that they are inaccessible to direct observation. They must approach the origin for higher temperatures and finally a state of saturation should be arrived at. But the corresponding temperatures are probably so near the melting point that observation again is made difficult.

The very nature of the phenomena here described as well as the references in the literature[6,7] and my own observations made with other substances make it clear that this is an effect of a very general kind, not restricted to carnauba wax alone; this being so, the static dielectric constant of many solid dielectrics may be of an order of magnitude which hitherto has been considered as exceptional and the dielectric relaxation function must approach 0 still more slowly than is believed generally. The same opinion has been recently emphasized by Cole,[10] whose conclusions are entirely confirmed by the result of the measurements here reported.

VI. DIELECTRIC ABSORPTION AND THE FIELD OF THE ELECTRET

The phenomenon of the "frozen" charge shows that the charges associated with dielectric absorption can be preserved over very large periods of time. In this respect it meets the basical requirement to be fulfilled by any mechanism, which may be held responsible for the permanent charges of the electret. But, with regard to opinions occasionally expressed,[11] it may be

[9] R. Simha, J. App. Phys. **13**, 201 (1942); N. W. Taylor, J. Phys. Chem. **47**, 235 (1943).
[10] K. S. Cole and R. H. Cole, J. Chem. Phys. **10**, 98 (1942).
[11] G. Nadjakoff, Physik. Zeits. **39**, 226 (1938).

mentioned that a dielectric containing a "frozen" charge is not necessarily an electret, i.e. it may or may not be found to produce an electric field when the plates are detached. It must also be pointed out that in Eguchi's heat treatment the melting point of the substance is exceeded, while in our measurements we have confined ourselves to the range of temperatures between room temperature and melting point. But the difference between the two cases is apparently a purely qualitative one. According to our measurements covering so far a period of nearly 2 years, disks of carnauba wax polarized below the melting point produce electric fields which are very enduring although somewhat smaller than those reported by Eguchi.

Reversible dielectric absorption in homogeneous substances, according to present theories, may be caused by an anomaly either of displacement or of conduction. In the first case, referring to polar substances, the dielectric polarization lags behind the externally applied electric field in consequence of hindered dipole rotation. In the second case, ions free to move within the dielectric but unable to discharge freely at the electrodes, built up slowly appearing and slowly disappearing space charges. Both effects lead to the formation of an electric moment of the dielectric body, which persists for a certain time after the externally applied field has been reduced to zero. The side of the dielectric, which is adjacent to the positive polarizing electrode, takes a negative charge; the side, which is adjacent to the negative polarizing electrode, takes a positive charge. The field of the charges residing in the dielectric induces charges on the plates of the shorted capacitor. The value of the charge of either electrode, at any moment t after the sudden short-circuit, is given by $q=\int_t^\infty J(\tau)d\tau$, where $J(t)$ is the anomalous discharge current associated with dielectric absorption. The formula is exact for the dipolar effect and approximately valid for the ionic effect, in the presence of which the true value of q may be somewhat greater than the value given by the integral, because after the short-circuit, some of the ions which constitute the space charge eventually do not return to within the dielectric, but are lost by discharge at the electrodes. The value of the induced charge of the electrodes is taken as a measure of what has been called the "free surface charge" of the electret. A heat treatment perpetuates the existence of the charges associated with dielectric absorption. The electret behavior of strongly absorptive dielectrics cannot therefore be a surprise. For example, with the data of Fig. 4, a surface charge of the order of 10^{-8} coul/cm^2 and field strength of the order of 10^5 v/cm are calculated. Still higher values would result if a higher voltage had been applied to the dielectric. Nevertheless, dielectric absorption alone is insufficient to account for the electret effect. Experiments with electrets indicate not only surface charges and fields many times lower than those here obtained, but a polarity of the charges, which is contrary to that expected, when the polar moment of the electret is produced exclusively by one of the mechanisms just discussed. And indeed, there exists another mechanism—leakage of charge from the plates to the surface of the dielectric—which yields the accumulation, on the dielectric, of "compensation" charges of the contrary polarity, the field of which neutralizes and partially overcomes the field of the "frozen" charge. The most direct evidence for the working of this third mechanism is given by Franklin's experiment of the dissectible Leyden jar, which proves that at high tensions the charge of the electrodes is transferred to the dielectric itself.[12] A tentative theory of the electret on this basis was given in a preliminary note.[13] A more complete discussion shall be given in the second part of this paper.

We express our gratitude to the Director of the National Institute of Technology, Professor E. L. da Fonseca Costa, who made this study possible.

[12] B. Gross, Am. J. Phys., in press.
[13] B. Gross, Phys. Rev. **66**, 26 (1944).

PHYSICAL REVIEW VOLUME 67, NUMBERS 7 AND 8 APRIL 1 AND 15, 1945

A Theorem of Larmor and Its Importance for Electrons in Magnetic Fields

LEON BRILLOUIN*
Columbia University, New York, New York
(Received January 15, 1945)

The importance of a well-known theorem, originally due to Larmor, is emphasized. It enables a definition of "momentum" and "moment of momentum" for electrons in a magnetic field, hence the possibility of writing the conservation of these quantities when the geometry of the structure is convenient. As typical examples of the method, two special cases are discussed: a plane electron beam and a cylindrical electron beam with longitudinal magnetic field. In both cases it is found that the space-charge density of the beam is entirely controlled by the magnetic field and that the maximum current is obtained for a suitable optimum magnetic field.

I. A GENERAL THEOREM ABOUT ELECTRONIC MOTIONS

THERE is a very important result about the mechanics of electrons, so important it may be granted the name of "theorem" and should be called after Larmor. The famous English physicist always attempted to reduce problems of electrons to the standard pattern of classical mechanics, with its famous canonical equations: principle of least action, Lagrange and Hamilton formulas. The difficulty was the "Lorentz force" of a magnetic field on a moving electron, a formula which does not seem to offer any similarity with any mechanical problem. Larmor first discovered the similarity with problems of rotating bodies and stressed the significance of the angular velocity

$$\omega_H = -\mu_0 \frac{e}{2m} H, \tag{1}$$

where μ_0 is the permeability, e is the charge of the electron, m is the mass, and H is the magnetic field. He also felt that this was not a special case, but only one instance of a more general law.[1] This took shape progressively, through contributions of H. A. Lorentz, and Schwarzschild, and is now found in every textbook on electromagnetism or quantum-theory. This theorem is also essential in the derivation of Dirac's equation for the spinning electron.

Let us sum up the results, and refer to textbooks for more details:[2] we shall use m.k.s. unit and the standard notations of J. A. Stratton.[3]

Let $\phi A_1 A_2 A_3$ be the components of the scalar and vector potentials in a system of rectangular coordinates $x_1 x_2 x_3$. The E and H components of the electric and magnetic field are (Stratton, p. 24)

$$E_k = -\partial\phi/\partial x_k - \partial A_k/\partial t, \quad k = 1 \cdot 2 \cdot 3 \tag{2}$$
$$\mu_0 H = \text{rot } A, \quad \mu_0 H_3 = \partial A_2/\partial x_1 - \partial A_1/\partial x_2.$$

We want to study the motion of an electron according to the well-known formula

$$m\ddot{x}_k = eE_k + e\mu_0[v \times H], \tag{3}$$

where the second term is the Lorentz force.

These laws of motion can be reduced to the standard Lagrange scheme if one uses as *Lagrange function*

$$L(\dot{x}_1\dot{x}_2\dot{x}_3, x_1x_2x_3, t) = \tfrac{1}{2}\, mv^2 - e\phi + e(v \cdot A), \tag{4}$$
$$(v \cdot A) = \dot{x}_1 A_1 + \dot{x}_2 A_2 + \dot{x}_3 A_3.$$

The proof is straight forward. First, we define the momentum of the electron by the standard Lagrange relation:

$$p_k = \partial L/\partial \dot{x}_k = m\dot{x}_k + eA_k, \tag{5}$$

and we emphasize the importance of this definition with its additional term containing the vector potential. Next, we write Lagrange's

* Publication assisted by the Ernest Kempton Adams Fund for Physical Research of Columbia University.

[1] J. Larmor, *Aether and Matter* (Cambridge University Press, Cambridge, England, 1900), Ch. VI.

[2] J. H. Van Vleck, *Theory of Electric and Magnetic Susceptibilities* (Clarendon Press, England, 1932), p. 19; L. Brillouin, *Atome de Bohr* (Presses Universitaires, Paris, 1931), pp. 98–100 and 107–112.

[3] J. A. Stratton, *Electromagnetic Theory* (McGraw-Hill Book Company, Inc., New York, 1941).

equation of motion:

$$\frac{dp_k}{dt}=\dot{p}_k=\frac{\partial L}{\partial x_k}=-e\frac{\partial \phi}{\partial x_k}+e\left(\dot{x}_1\frac{\partial A_1}{\partial x_k}+\dot{x}_2\frac{\partial A_2}{\partial x_k}+\dot{x}_3\frac{\partial A_3}{\partial x_k}\right). \quad (6)$$

The important point is that d/dt means a derivative taken along the trajectory of the electron

$$\frac{d}{dt}=\frac{\partial}{\partial t}+\dot{x}_1\frac{\partial}{\partial x_1}+\dot{x}_2\frac{\partial}{\partial x_2}+\dot{x}_3\frac{\partial}{\partial x_3}. \quad (7)$$

Hence, the translation of Eq. (6)

$$m\ddot{x}_k+e\frac{\partial A_k}{\partial t}+e\left(\dot{x}_1\frac{\partial A_k}{\partial x_1}+\dot{x}_2\frac{\partial A_k}{\partial x_2}+\dot{x}_3\frac{\partial A_k}{\partial x_3}\right)=-e\frac{\partial \phi}{\partial x_k}+e\left(\dot{x}_1\frac{\partial A_1}{\partial x_k}+\dot{x}_2\frac{\partial A_2}{\partial x_k}+\dot{x}_3\frac{\partial A_3}{\partial x_k}\right). \quad (8)$$

Taking $k=1$, we note that the first terms in each bracket cancel each other, and we are left with

$$m\ddot{x}_1=-e\frac{\partial A_1}{\partial t_1}-e\frac{\partial \phi}{\partial x_1}+e\dot{x}_2\left[\frac{\partial A_2}{\partial x_1}-\frac{\partial A_1}{\partial x_2}\right]+e\dot{x}_3\left[\frac{\partial A_3}{\partial x_1}-\frac{\partial A_1}{\partial x_3}\right],$$

or, according to Eq. (2)

$$m\ddot{x}_1=eE_1+\mu_0 e\dot{x}_2H_3-\mu_0 e\dot{x}_3H_2, \quad (9)$$

which is exactly Eq. (3).

The Lagrange function appears in the principle of least action

$$\int \delta L dt=0 \quad (10)$$

as usual and can be used to build up the Hamilton function

$$\mathfrak{H}(p_1p_2p_3x_1x_2x_3t)=\Sigma_k p_k\dot{x}_k-L, \quad (11)$$

or, according to Eqs. (4) and (5),

$$\mathfrak{H}=\Sigma_k(m\dot{x}_k^2+e\dot{x}_kA_k)-\tfrac{1}{2}m\Sigma_k\dot{x}_k^2+e\phi-e\Sigma_k\dot{x}_kA_k,$$
$$\mathfrak{H}=\tfrac{1}{2}\,\mathrm{mv}^2+e\Phi. \quad (12)$$

The terms in A cancel out, and in case of conservative systems (electric potential Φ independent of time), the Hamilton function represents the total energy as usual. The fact that it does not contain the vector potential any more corresponds to the result that Lorentz forces do not do any work. If Hamilton's function $\mathfrak{H}$ is to be used in Hamilton's equations, it must be expressed as a function of the momenta p.

$$\mathfrak{H}=\frac{1}{2m}\Sigma_k(p_k-eA_k)^2+e\varphi. \quad (13)$$

Hence the equation of motion

$$\dot{x}_k=\frac{\partial \mathfrak{H}}{\partial p_k}=\frac{1}{m}(p_k-eA_k), \quad (14a)$$

$$\dot{p}_k=-\partial\mathfrak{H}/\partial x_k. \quad (14b)$$

Equation (14a) is just the reverse of Eq. (5), and Eq. (14b) is identical with Eq. (6).

The same general scheme can be extended to relativistic mechanics for very fast electrons (L. B., *Atome de Bohr*, p. 107). It represents the safest way to attack problems of electron trajectories.

II. SOME EXAMPLES OF VECTOR POTENTIALS

In order to show how to use these general relations, we shall build the expressions for the vector potential corresponding to some examples of special importance.

A. Plane Problem

Assuming all fields independent of the coordinate x_1, we can use the following expression

$$A_1=-F(x_3)x_2, \quad A_2=0, \quad A_3=0, \quad (15)$$

which results in

$$\mu_0H_1=0, \quad \mu_0H_2=-\frac{dF}{dx_3}\cdot x_2, \quad \mu_0H_3=F(x_3). \quad (16)$$

The H_3 component of the magnetic field is constant in the x_1x_2 planes, but may depend upon x_3. These definitions satisfy the fundamental relation:

$$\mathrm{div}\,A+\mu_0\epsilon_0(\partial\phi/\partial t)=0 \text{ Lorentz}, \quad (17)$$

$\mathrm{div}\,H=0$ (see Stratton, Eq. (12), p. 24).

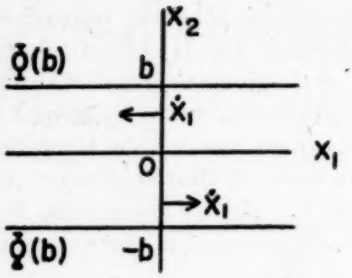

FIG. 1. Electrons are emitted from a filament along X_1. X_2 and H_3 are perpendicular to the X_1X_2 plane.

The Lorentz relation is obviously fulfilled when the scalar potential ϕ does not contain the time.

B. Cylindrical Symmetry

We want a field H depending only upon the distance r to the x_3 axis. Furthermore, the magnetic field lies along the axis (as is the case for the field of a coil centered on the x_3 axis, for instance).

Here we choose

$$A_1=-\tfrac{1}{2}F(x_3)x_2, \quad A_2=\tfrac{1}{2}F(x_3)x_1, \quad A_3=0, \quad (18)$$

hence

$$\mu_0H_1=-\frac{1}{2}\frac{dF}{dx_3}x_1, \quad \mu_0H_2=-\frac{1}{2}\frac{dF}{dx_3}x_2, \quad \mu_0H_3=F(x_3). \quad (19)$$

If the H_3 field is not constant, there is a radial component of the field,

$$\mu_0H_r=-\frac{1}{2}\frac{dF}{dx_3}r. \quad (20)$$

The relations (17) are again automatically fulfilled.

III. CONSERVATION PRINCIPLES IN ELECTRON MECHANICS

The general theorem discussed in Section I leads directly to some important conservation principles:

Conservation of Energy

$$\tfrac{1}{2}\,mv^2+e\varphi=\text{Const}\ (=0), \quad (21)$$

when Φ does not depend upon time. The sum of kinetic and potential energy remains constant. In case of electrons emitted without velocity by a cathode at potential zero, the constant is zero. This first result is well known.

Conservation of Momentum

In addition to this, we may have conservation of some components of momentum or of the moment of momentum. This will depend upon the symmetry of the structure. These additional conditions are very important to keep in mind and were too often overlooked by many authors, who proposed solutions which obviously did not satisfy these relations.

A. Plane Problem

Electrons are emitted by a filament located along the x_1 axis ($x_2=x_3=0$) and the magnetic field on this cathode is H_{3_0} (Fig. 1). Electrons move between two plane electrodes, located at

$$x_2=\pm b.$$

In Fig. 1, the cathode is supposed to be behind the plane of the drawing, and we are looking at a cross section of the electron beam between the $\pm b$ electrode at potential $\varphi(b)$. These electrodes are supposed to extend both ways to infinity.

In such a structure, there is no electric force acting on the electron in the x_1 direction, hence

$$p_1=\text{const.}, \quad (22)$$

a condition which means conservation of the No. 1 component of the momentum, as, defined in Eq. (5). Now, on the cathode

$$p_{1_0}=m\dot{x}_{1_0}+eA_{1_0}=0-e\mu_0H_{3_0}x_2=0, \quad (23)$$

since the initial velocity is zero, and the vector potential is given by Eq. (15). After the electrons travelled a distance x_3, we must still find $p_1=0$, but it now means

$$p_1=m\dot{x}_1-e\mu_0H_3x_2=0,$$

hence

$$\dot{x}_1=(e/m)\mu_0H_3(x_3)x_2=-2\omega_Hx_2, \quad (24)$$

where ω_H is defined by Eqs. (1) as Larmor's angular velocity corresponding to $H_3(x_3)$.

We obtained the relation Eq. (24) from our general theorem, but it can also be proved directly. The equation of motion in the x_1

direction according to Eq. (9) and Eq. (16) is

$$m\ddot{x}_1=e\mu_0(\dot{x}_2H_3-\dot{x}_3H_2)$$
$$=e\mu_0\left[\dot{x}_2H_3+x_2\frac{dH_3}{dx_3}\dot{x}_3\right], \quad (25)$$

but

$$\dot{x}_3dH_3/dx_3=dH_3/dt,$$

where the d/dt derivative is taken along the electron's trajectory. Hence

$$\ddot{x}_1=(e/m)\mu_0(d/dt)(x_2H_3), \quad (26)$$

which results in Eq. (24).

The same results are obtained for a cathode of any arbitrary shape located in a region where the magnetic field H_{30} vanishes, since these conditions make again p_{10} zero in Eq. (23).

B. Cylindrical Problem

Electrons are emitted by a point cathode at $x_1=x_2=x_3=0$ where the magnetic field is H_{30}. If the magnetic field H_{30} is constant (zero for instance) in the region of the cathode, the cathode may be a filament of finite length extending along the x_3 axis. These electrons move afterwards inside a cylindrical anode of radius b, centered on the x_3 axis (Fig. 2).

Here the symmetry calls for the conservation of the moment of momentum about the x_3 axis, and the constant value of the moment of momentum is zero, according to the conditions of emission by the cathode:

$$p_2x_1-p_1x_2=0, \quad (27)$$

hence

$$m(\dot{x}_2x_1-\dot{x}_1x_2)+e(A_2x_1-A_1x_2)=0,$$

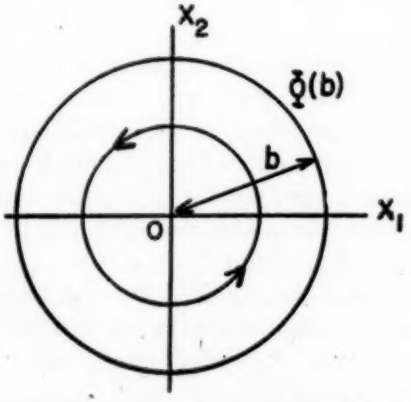

FIG. 2. Arrangement of a cathode along the X_3 axis. X_3 and H_3 are perpendicular to the X_1X_2 plane.

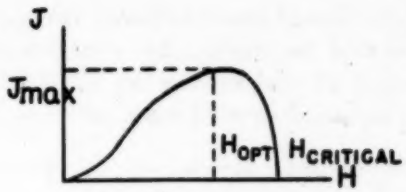

FIG. 3. Current *versus* magnetic field.

where the vector potential is given by Eq. (18):

$$\dot{x}_2x_1-\dot{x}_1x_2=-\tfrac{1}{2}(e/m)\mu_0H_3(x_3)(x_1^2+x_2^2), \quad (28)$$

or in cylindrical coordinates r, θ, x_3

$$r^2\dot{\theta}=\omega_Hr^2, \quad \dot{\theta}=\omega_H. \quad (29)$$

We can generalize this result if we assume the *cathode* to be a circular ring of *radius a* (or a circular cylinder of radius a extending about x_3 axis in a region of constant magnetic field H_{30}).

In this case, the constant moment of momentum is not zero but

$$p_2x_1-p_1x_2=m(\dot{x}_{20}x_{10}-\dot{x}_{10}x_{20})$$
$$+e(A_{20}x_{10}-A_{10}x_{20})=0+\frac{e}{2m}\mu_0H_{30}(x_{10}^2+x_{20}^2)$$
$$=\frac{e}{2m}\mu_0H_{30}a^2=-\omega_{H0}a^2, \quad (30)$$

since our electrons are emitted on a radius a without velocity. The relation (29) is now replaced by

$$\dot{\theta}=\omega_H-\omega_{H0}(a^2/r^2). \quad (31)$$

In a *cylindrical magnetron*, the cathode is in the same constant magnetic field as the anode, and we obtain

$$\dot{\theta}=\omega_H[1-(a^2/r^2)], \quad (32)$$

a relation which can be proved directly[4] as in the preceding case. These last formulas (31) and (32) yield infinite angular evlocity on the axis, which means that conditions near the axis should be discussed carefully if the structure does not prevent electrons from reaching that region.

IV. PLANE ELECTRON BEAM IN STEADY MOTION

Let us consider the problem A of the preceding section and look for the conditions corresponding

[4] L. Brillouin, Phys. Rev. **60**, 385 (1941), Eq. (1), (2), (3), (15).

to a steady motion of the beam along the x_3 axis. We assume that no current flows to the plane electrodes $x_2=\pm b$ and we use Eq. (24). The $\dot{x}_3$ component may still depend upon x_2:

$$\dot{x}_1=-2\omega_H x_2, \quad \dot{x}_2=0, \quad \dot{x}_3=f(x_2), \tag{33}$$

hence, by Eq. (21)

$$-\frac{2e}{m}\phi=\dot{x}_1^2+\dot{x}_2^2+\dot{x}_3^2=4\omega_H^2x_2^2+f^2. \tag{34}$$

In order to keep $\dot{x}_2$ zero, we must insure a compensation between electric and Lorentz forces in the x_2 direction.

$$0=-e\frac{\partial\phi}{\partial x_2}+e\mu_0[v\times H]_2=4m\omega_H^2x_2 + mf\frac{df}{dx_2}-e\mu_0\dot{x}_1H_3=mf\frac{df}{dx_2}.$$

The field H is given by Eq. (16), ω_H was defined in Eq. (1), and $\dot{x}_1$ results from Eq. (33). The term compensation proves that

$$\dot{x}_3=f(x_2)=v_3, \text{ a } \textit{constant}. \tag{35}$$

Hence the *whole beam is moving with a constant* velocity v_3 along the x_3 axis, and the potential distribution (34) is simply

$$\phi=-\frac{m}{e}(2\omega_H^2x_2^2+\tfrac{1}{2}v_3^2). \tag{36}$$

This yields a *constant space charge density*

$$\partial^2\phi/\partial x_2^2=-\rho/\epsilon_0, \quad \rho=4\epsilon_0\omega_H^2(m/e), \tag{37}$$

and the current I per unit length in the x_1 direction is

$$I=2b\rho\dot{x}_3=8b(m/e)\epsilon_0\omega_H^2\dot{x}_3. \tag{38}$$

What is physically measured is this current I and the voltage $\phi(b)$ of the plates. Let us rewrite it this way:

$$U=-(2e/m)\phi(b)=\alpha\omega_H^2+\dot{x}_3^2, \ \alpha=4b^2, \qquad J=(2e/m\epsilon_0)I=(1/\beta)\omega_H^2\dot{x}_3, \ \beta=1/16b. \tag{39}$$

We introduce the α, β coefficients in order to enable us to use the following discussion in other examples, (cylindrical structures) where similar relations will be found.

The problem to be discussed is about the maximum possible current in the beam when the voltage ϕ is given. Eliminating $\dot{x}_3$, we have

$$U=\alpha\omega_H^2+(\beta^2/\omega_H^4)J^2, \quad \beta^2J^2=U\omega_H^4-\alpha\omega_H^6, \tag{40}$$

where ω_H measures the magnetic field intensity and $\alpha\beta$ are geometrical factors. If we vary the magnetic field, we obtain

$$\text{Zero current } J=0 \text{ for } \begin{cases}\omega_H=0, & \rho=0\\ \omega_H=\omega_c, & \dot{x}_3=0,\end{cases} \tag{41}$$

where the *critical magnetic field* H_c corresponds to

$$U=\alpha\omega_c^2. \tag{42}$$

The maximum current is found for a certain optimum magnetic field (see Fig. 3).

$$\partial J/\partial\omega_H=0, \quad H_{\text{opt}}=(\tfrac{2}{3})^{\frac{1}{2}}H_{\text{critical}}, \quad \omega_{\text{opt}}=(\tfrac{2}{3})^{\frac{1}{2}}\omega_c \tag{43}$$

$$\alpha\omega_{\text{opt}}^2=\tfrac{2}{3}U, \quad J_{\max}=\frac{1}{\alpha\beta\sqrt{2}}(\tfrac{2}{3}U)^{\frac{1}{2}},$$

or

$$I_{\max}=-\frac{\epsilon_0}{\alpha\beta}\left(\frac{-e}{m}\right)^{\frac{1}{2}}(\tfrac{2}{3}\phi)^{\frac{1}{2}}.$$

The point is that this maximum current can be obtained only for a certain definite value of the magnetic field. It is proportional to the power 3/2 of the voltage, as in Langmuir's formula.

V. STEADY CYLINDRICAL BEAMS

We will find similar results for the cylindrical structure discussed in section III-B, where we found [Eq. (21), (29)]

$$U=-\frac{2e}{m}\varphi=\dot{r}^2+r^2\dot{\theta}^2+v_3^2=r^2\omega_H^2+v_3^2, \tag{44}$$

since Eq. (29) gave $\dot{\theta}=\omega_H$ and $\dot{r}$ must be zero in a steady beam with no radial motion. The longitudinal velocity v_3 might depend upon r and be different on successive cylindrical layers. A reasoning, very similar to the one used in the plane problem Eq. (33) and (35), will prove that v_3 must be a constant.

The radial electric field E_r and the Lorentz force must compensate the centrifugal force in order to give no radial acceleration and to maintain $\dot{r}$ zero. This means

$$eE_r+\mu_0eHr\dot{\theta}+mr\dot{\theta}^2=0, \tag{45}$$

$$\dot{\theta}=\omega_H=-\tfrac{1}{2}\mu_0(e/m)H,$$

and

$$E_r=\partial U/\partial r=(m/2e)(\partial U/\partial r)$$
$$=m/e[r\omega_H^2+v_3(\partial v_3/\partial r)]. \quad (46)$$

Term compensation proves that $\partial v_3/\partial r$ must be zero which makes v_3 a constant.

We may now use Poisson's relation

$$(1/r)(\partial/\partial r)(rE_r)=\rho/\epsilon_0=2(m/e)\omega_H^2 \quad (47)$$

and we obtain a constant space-charge density ρ equal to one-half the space-charge density in the plane problem. Let us call $\phi(b)$ the voltage of the anode;

$$U=-(2e/m)\varphi(b)=\alpha\omega_H^2+v_3^2, \quad \alpha=b^2. \quad (48)$$

The total current I is

$$I=\pi b^2\rho v_3=2\pi\epsilon_0 b^2(m/e)\omega_H^2 v_3,$$
$$J=(2e/m\epsilon_0)I=(1/\beta)\omega_H^2 v_3, \quad \beta=1/4\pi b^2. \quad (49)$$

Hence, the problem is reduced to the same scheme as in the preceding section [Eq. (39)] only with different values for the geometrical coefficients α, β. The results are again given by Eq. (43) and Fig. 3.

This applies for a beam filling completely the pipe of radius b.

We may also discuss the case of a beam of radius b surrounded by a larger pipe of radius $R>b$.

The equations inside the beam are the same as before, and outside the beam a logarithmic potential is obtained. This term must insure potential and field continuity on the beam's surface $r=b$; hence

$$U=-(2e/m)\varphi=\omega_H^2 b^2[1+2\log(r/b)]+v_3^2. \quad (50)$$

Equation (49) for the current J is unchanged, and the coefficient α in Eq. (48) becomes

$$\alpha=b^2[1+2\log(R/b)]. \quad (51)$$

This is the only modification in the result.

VI. ELECTRON BEAM WITH INITIAL ROTATION

The electron beam may enter the magnetic field with an initial rotation, or it may be generated inside the magnetic field from a cylindrical cathode of radius a, as assumed in Eq. (31) of Section III, B. In such cases, the angular velocity will be given by

$$\dot{\theta}=\omega_H[1+(A/r^2)], \quad (52)$$

Eq. (31) corresponding to the case

$$A=-a^2(\omega_{H_0}/\omega_H),$$

but A may eventually take positive values. Rewriting Eq. (44) to Eq. (46) of preceding section, we obtain

$$U=r^2\dot{\theta}^2+v_3^2=\omega_H^2\left(r^2+2A+\frac{A^2}{r^2}\right)+v_3^2,$$
$$E_r=\frac{m}{2e}\frac{\partial U}{\partial r}=\frac{m}{e}\omega_H^2\left(r-\frac{A^2}{r^3}\right)+\frac{m}{e}v_3\frac{\partial v_3}{\partial r}, \quad (53)$$

but E_r must satisfy a condition similar to Eq. (45)

$$E_r=2\omega_H\frac{m}{e}r\dot{\theta}-\frac{m}{e}r\dot{\theta}^2=\frac{m}{e}\omega_H^2 r\left(1-\frac{A^2}{r^4}\right), \quad (54)$$

which again results in the condition that v_3 must be a constant and yields

$$\rho=2\epsilon_0(m/e)\omega_H^2[1+(A^2/r^4)], \quad (55)$$

instead of Eq. (47).

$$U=-(2e/m)\phi=\omega_H^2[r+(A/r)]^2+v_3^2. \quad (56)$$

The formulas become infinite at $r=0$, hence the experimental device should prevent electrons from reaching the axis. This means that we shall deal with a hollow cylindrical beam extending from $r=a$ to $r=b$, instead of a solid cylindrical beam ($0\leqslant r\leqslant b$), as in the preceding sections. This beam can be obtained experimentally in a coaxial cable with electrodes of radii $R_1\leqslant a$ and $R_2\geqslant b$. Eventually we may do without the central electrode if the potential be constant and the electric field zero inside the beam ($r<a$).

In order to simplify the formulas, we shall assume that the radii of the electrodes are

$$R_1=a, \quad R_2=b. \quad (57)$$

Otherwise, we would obtain the same field and space-charge distributions inside the beam ($a\leqslant r\leqslant b$) to be completed by convenient logarithmic potentials in $D_1\log r+D_2$ in the charge free

regions $R_1 \leqslant r \leqslant a$ or $b \leqslant r \leqslant R_2$. The solution could be worked out for such problems if needed.

Using formula (56) we obtain the potentials on radius a and radius b

$$U(a)=\omega_H^2[a+(A/a)]^2+v_3^2,$$
$$U(b)=\omega_H^2[b+(A/b)]^2+v_3^2, \tag{58}$$

and the current

$$I=v_3\int_a^b \rho 2\pi r dr = 4\pi\frac{m\epsilon_0}{e}\omega_H^2 v_3\int_a^b\left(1+\frac{A^2}{r^4}\right)r dr$$
$$=(2\pi m\epsilon_0/e)\omega_H^2 v_3|r^2-(A^2/r^2)|_a^b, \tag{59}$$

hence

$$J=(2e/m\epsilon_0)I$$
$$=4\pi\omega_H^2 v_3[b^2-(A^2/b^2)-a^2+(A^2/a^2)]. \tag{60}$$

The field on the inner cylinder is

$$(m/2e)(\partial U/\partial r)_{r=a}=(m/e)\omega_H^2[a-(A^2/a^3)]. \tag{61}$$

Let us first assume a hollow electron beam with no central electrode. This is obtained by taking a zero field on a radius a. Hence,

$$A=\pm a^2, \tag{62}$$

and consequently,

$$U(b)=\omega_H^2[b\pm(a^2/b)]^2+v_3^2,$$
$$J=4\pi\omega_H^2 v_3[b-(a^4/b^2)]. \tag{63}$$

The relations are reduced to the standard type (39), (40) if we take

$$\alpha=[b\pm(a^2/b)]^2,\quad \beta=[b^2-(a^4/b^2)]^{-1}(1/4\pi), \tag{64}$$

which solves the problem. It should be noted here that the $\pm$ sign introduces a new feature in the solution, namely, the respective orientation of the initial rotation in the beam and of the Larmor rotation. The case of the magnetron corresponds to the minus sign.

To discuss the problem of an electron beam with initial rotation ($A \neq 0$) filling the free space in a coaxial cable, we assume that *both electrodes* are at the *same potential*.

$$U(a)=U(b),\quad A=\pm ab. \tag{65}$$

Hence,

$$U=\omega_H^2(a\pm b)^2+v_3^2,$$

and

$$J=4\pi\omega_H^2 v_3 2(b^2-a^2), \tag{66}$$

which reduces to the standard type with

$$\alpha=(a\pm b)^2,\quad \beta=1/8\pi(b^2-a^2). \tag{67}$$

The corresponding space-charge ρ and angular velocity $\dot{\theta}$ are given by Eq. (52) and Eq. (55). In the case of the minus sign

$$A=-ab,\quad \dot{\theta}=\omega_H[1-(ab/r^2)], \tag{68}$$

one must notice that the angular velocity is positive on the outside of the beam and negative on the inside with a non-rotating layer at $r=(ab)^{\frac{1}{2}}$.

The general conclusion is that, in such problems, Larmor's theorem introduces an additional condition of conservation for either the momentum or the moment of momentum, which has been too often overlooked. If taken into account Larmor's theorem shows that the space-charge density is entirely conditioned and controlled by the magnetic field being proportional to H^2 [Eqs. (37) and (45)]. One should, therefore, be very cautious not to introduce into a discussion separate assumptions about space-charge and magnetic field. It is specially advised never to speak of the behavior of a device under an infinite or arbitrary large magnetic field since this would also mean infinite space-charge density which is a very troublesome factor.

Letters to the Editor

PROMPT publication of brief reports of important discoveries in physics may be secured by addressing them to this department. The closing date for this department is the third of the month. Because of the late closing date for the section no proof can be shown to authors. The Board of Editors does not hold itself responsible for the opinions expressed by the correspondents. Communications should not in general exceed 600 words in length.

Short Range Alpha-Particles from Po

W. Y. CHANG
Palmer Physical Laboratory, Princeton University
February 20, 1945

THE big alpha-ray magnetic spectrograph and the sensitive tracks method of detection, as reported in Chicago's meeting,[1] have been employed to see if there are weak groups of Po alpha-particles. Fine grain alpha-particle plates were used, the width of each plate being inclined at an angle of 30° or 45° to the incident beam. The tracks produced on a plate by the particles, which have been coming from the source, appear parallel to one another, perpendicular to the length of the plate and incident on the plate at about the same angles as expected from the disposition of the photographic plate. Only these tracks were counted with a 430× microscope. The number-energy distribution curve reveals distinctly 12 groups in the low energy region 0.04 to about 2 Mev from the main line (region lower than this was not examined). The first two groups stand out more clearly only on the curve obtained with the weakest source (see below), where the background near the main line is smaller.

Three Po sources of different strengths were used under different magnetic fields. In the various experiments, the chamber-slits were arranged differently, and different materials were used for the source-slits. The distribution curves obtained from these three sources and under the different experimental conditions are very similar to one another. The positions of the corresponding groups in the different curves agree with one another to within about 0.02 Mev. The intensities of any one group in the different curves are about in the same ratio as the relative strengths of the three sources, and the widths depend on that of the main line too. The background due to "stray" alpha-particles from the source decreases continuously and is between ½ and ⅓ of the peak intensities. From blank experiments the background, because of contamination of the chamber, was found to be only between 2 percent of the third group-intensity and zero.

The energies of these groups have been calculated by comparison with the main group, the latter taken as 5.303 Mev. These are summarized in Table I. The energy value of each group in the table represents the average of three corresponding values from three different curves, which were obtained with the three Po sources. The relative intensities were obtained after the general backgrounds were subtracted from the peak intensities, each figure also representing the average of three sources.

TABLE I. Energy of groups of alpha-particles.

Group	Group Energy in Mev	$E_n = \alpha_0 - \alpha_n$ (Mev)	Relative Intensity
α_0	5.303	0	10^6
α_1	5.113 ±0.005	0.190	(250)
α_2	5.065 ±0.005	0.238	(250)
α_3	4.901 ±0.005	0.402	150
α_4	4.838 ±0.005	0.465	110
α_5	4.749 ±0.005	0.554	130
α_6	4.640 ±0.005	0.663	104
α_7	4.449 ±0.005	0.854	116
α_8	4.303 ±0.005	1.000	70
α_9	4.111 ±0.005	1.192	75
α_{10}	4.016 ±0.005	1.287	50
α_{11}	3.890 ±0.005	1.413	40
α_{12}	3.685 ±0.005	1.618	40

If these alpha-particle groups are interpreted in the same way as the ordinary fine structure lines,[2] the differences between the main group energy and the individual group energies will give the corresponding energy levels of Pb^{206} nucleus. These are shown in the third column of Table I. In 1935,[3] Bothe found five gamma-ray lines from Po, two of them being less certain. It is possible to find transitions in our level system which agree approximately with Bothe's gamma-ray lines, but this is rather arbitrary because there are 78 possible transitions between the 13 levels. The average number of quanta, as reported in Bothe's first paper (1930), was about seven in 10^6 of the alpha-particles. Because of the method of detection used, this figure is rather uncertain.

In the high energy region of the main line (from $E_n = 0.01$ to about 2.2 Mev), no indication of any alpha-particle groups could be found. Only an extremely small background decreases continuously to zero. Details will be published elsewhere.

I should like to thank Professors Ladenburg and Dempster for their interest and discussion in this work, Dr. S. Rosenblum for his help, and the former cyclotron group of Princeton for putting some of their apparatus at my disposal. Thanks are also due Dr. Blau for her kindness in preparing some of the sources and to her and Dr. Lampson for their discussion of the tracks method.

[1] W. Y. Chang, Phys. Rev. 67, 58 (1945).
[2] It is to be noted that the intensities of these groups are much smaller than those of the usual fine structure lines, and that most of them have larger energy separations from the main line.
[3] W. Bothe, Zeits. f. Physik 96, 607 (1935).

The Nuclear Excitation of Rhodium

MARCELLUS L. WIEDENBECK
Department of Physics, University of Notre Dame, Notre Dame, Indiana
April 2, 1945

A NEW activity in rhodium has recently been reported by Flammersfeld.[1] This activity was induced by the bombardment of pure rhodium metal with fast neutrons obtained fron the D–D reaction. Since the activity induced was not greatly altered by the presence of small amounts of paraffin, this author suggested that the activity is caused by nuclear isomerism in stable rhodium. A half-life period

of 48±5 minutes was assigned to this activity. The activity observed by placing the sample near a thin-walled aluminum counter consisted entirely of soft γ-radiation.

We have also produced a very strong activity by the direct irradiation of rhodium counters with x-rays produced with the Van de Graaf-Herb electrostatic generator. The decay period of this activity was found to be 45±1 minute. This radioactivity must, therefore, be assigned to a low lying metastable state in rhodium[103] (99.9 percent abundant) produced in the reaction:

$$Rh^{103}+\gamma \rightarrow Rh^{103}$$

The same activity has also been produced by directly irradiating rhodium foils with electrons of energy 2.5 Mev.

Attempts were made to determine the energy of the metastable level by the absorption of the conversion electrons in aluminum foils. Both with 1-mil and ½-mil foils of aluminum between the active rhodium and the counting region, the activity observed was reduced to approximately 1 percent of that observed without the foil as absorber.

Therefore, for the present we can only set the limits of this metastable state as being greater than the binding energy of the rhodium K electrons, since conversion electrons were observed, and less than 30 kev above this value. From the nature of the activity we would estimate that the γ-ray energy is >30 kev and <50 kev. This appears to be the lowest metastable level thus far observed.

Experiments are now in progress to determine more accurately the energy of the metastable level and the higher activation levels which combine with the metastable state.

[1] A. Flammersfeld, Naturwiss. 32, 36 (1944).

Periodic Phenomena at Anodes

J. H. Bartlett
Department of Physics, University of Illinois, Urbana, Illinois
March 20, 1945

If a storage battery is connected through a resistance R to an electrolytic cell, an electric current may be made to flow through the cell. For a certain range of values of R and of the voltage across the cell, the current may oscillate continually and it may show a well-defined period. If the value of the resistance R is small, sustained oscillations are absent in the cells which we have studied, but overshoot phenomena will occur for certain cells. Oscillations were found for Fe in H_2SO_4, $NaHSO_4$, $KHSO_4$; Ni in K_2SO_4 and NaOH; Cu in H_3PO_4, HCl, and KCl; but not for Fe in $FeSO_4$ and Na_2SO_4. (The anode-calomel voltage was varied between -0.7 volt and $+2.0$ volts.)

Wherever slow overshoot is present, if the voltage is changed suddenly with R small, it has been found possible to produce oscillations by increasing R and keeping the voltage at about the same value. The frequency at small amplitude is well-defined, and increases with increasing concentration and with increasing (i.e., becoming more positive) anode-calomel voltage V.

The experimental evidence seems explicable and the picture consistent if one assumes that the anode becomes partially covered with a salt layer, the average amount of which increases with increasing V. Anions diffuse to and are deposited on the anode, while the salt layer may come off either spontaneously or because of action by the anions.

The small amplitude, approximately sinusoidal, oscillations may be regarded as consisting of consecutive overshoots, first in one direction and then in the other. If the overvoltage of the cathode be neglected, then $\Delta V+R\Delta i=0$, where ΔV and Δi are changes of voltage and current. The oscillations take place along a straight line in the $i-V$ plane (as may be demonstrated on the cathode-ray oscillograph) and minimum current implies maximum voltage. If we commence with minimum current, it will increase (a) because of the factor operative at $R=0$, which we interpret as removal of salt by the anions, and (b) because of an additional amount when $R\neq 0$ because the voltage is lowered and with it the stability of the salt layer. When a sufficient amount of anode surface has been laid bare and the anions have diffused up, deposition will become predominant and the current will decrease. This decrease is always accompanied, at high enough V, by an overshoot (attributed above to action on the salt layer by the anions) and the cycle recurs. It is essential, in describing the system mathematically, to notice that the reaction and diffusion rate "constants" are functions of V.

The experimental details and fuller interpretation will appear in the *Transactions of the Electrochemical Society*. The mathematical analysis of the effect of a sudden change of voltage, as well as the criteria for oscillation, will be published elsewhere.

Plant cells and peripheral nerve fibers have been studied by methods somewhat similar[1-3] (except that constant current instead of constant voltage is approximated) and the parallelism between such organic systems and the inorganic ones is great. If $-V$ is plotted against t, the curves obtained for the biological systems resemble very much our i *vs.* t curves (which would be of the same form as $-V$ *vs.* t curves for a finite R).

A detailed discussion of this parallelism as revealed by the results of Blinks,[1] Osterhout,[2] and Arvanitaki[3] will also be published elsewhere. The evidence indicates that processes similar to those in the inorganic systems do occur, and that partial film formation and disruption are of central importance.

[1] L. R. Blinks, J. Gen. Physiol. 19, 633, 867 (1935); 20, 229 (1936).
[2] W. J. V. Osterhout, J. Gen. Physiol. 26, 65 (1943).
[3] A. Arvanitaki, Archiv. Int. de Physiol. 49, 209 (1939).